2/28/96

SANDIA REPORT

SAND94–0015 • UC–610
Unlimited Release
Printed February 1996

Assessment of Cavity Dispersal Correlations for Possible Implementation in the CONTAIN Code

D. C. Williams, R. O. Griffith

Prepared by
Sandia National Laboratories
Albuquerque, New Mexico 87185 and Livermore, California 94550
for the United States Department of Energy
under Contract DE-AC04-94AL85000

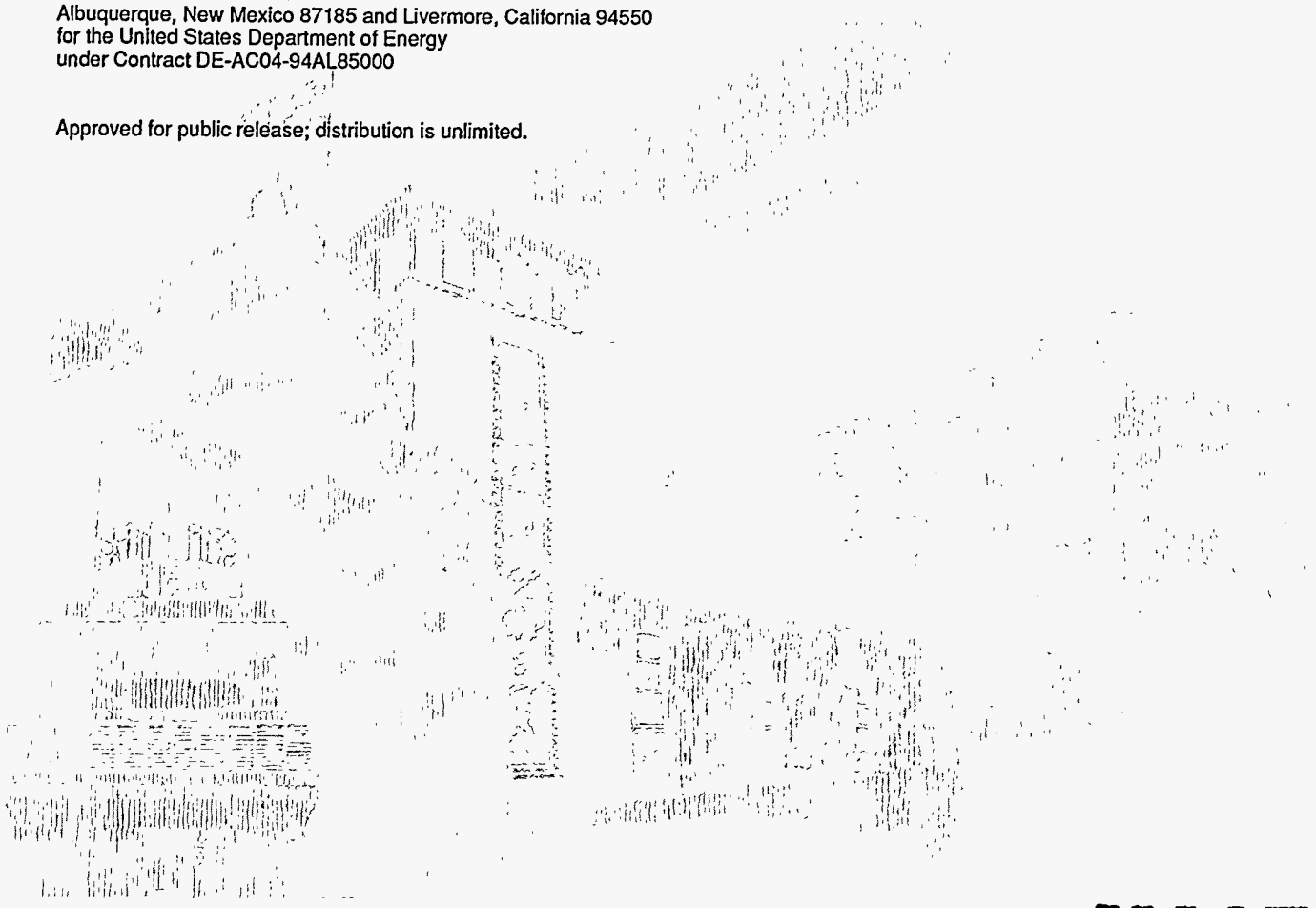

Issued by Sandia National Laboratories, operated for the United States Department of Energy by Sandia Corporation.

Available to DOE and DOE contractors from
Office of Scientific and Technical Information
PO Box 62
Oak Ridge, TN 37831

Prices available from (615) 576-8401, FTS 626-8401

Available to the public from
National Technical Information Service
US Department of Commerce
5285 Port Royal Rd
Springfield, VA 22161

NTIS price codes
Printed copy: A06
Microfiche copy: A01

SAND94-0015
Unlimited Release
Printed February 1996

Distribution
Category UC-610

Assessment of Cavity Dispersal Correlations for Possible Implementation in the CONTAIN Code

D. C. Williams and R. O. Griffith
Containment Modeling
Sandia National Laboratories
Albuquerque, NM 87185

ABSTRACT

Candidate models and correlations describing entrainment and dispersal of core debris from reactor cavities in direct containment heating (DCH) events are assessed against a data base of approximately 600 experiments performed previously at Brookhaven National Laboratory and Sandia National Laboratories in which dispersal of low-temperature corium simulants from scaled models of reactor cavities was studied. Cavity geometries studied are those of the Surry and Zion nuclear power plants and scale factors of 1/42 and 1/10 were studied for both geometries. Other parameters varied in the experiments include gas pressure driving the dispersal, identities of the driving gas and of the simulant fluid, orifice diameter in the pressure vessel, and volume of the gas pressure vessel. Correlations were assessed in terms of their ability to reproduce the observed trends in the fractions dispersed as the experimental parameters were varied. For the fraction of the debris dispersed, the correlations recommended for inclusion in the CONTAIN code are the Tutu-Ginsberg correlations, the integral form of the correlation proposed by Levy and a modified form of the Whalley-Hewitt correlation. For entrainment rates, the recommended correlations are the time-dependent forms of the Levy correlation, a correlation suggested by Tutu, and the modified Whalley-Hewitt correlation.

ACKNOWLEDGEMENTS

The authors acknowledge the U. S. Nuclear Regulatory Commission, Office of Nuclear Regulatory Research, for their support of this work, including specifically the efforts of Al Notafrancesco, project monitor for the CONTAIN code project. We wish to acknowledge the important contributions of M. M. Pilch to the initial phase of this work, which included developing an early version of the computer code used to compare the predictions of correlations with the experimental data base. We also wish to thank R. C. Smith and T. K. Blanchat for their helpful reviews of this work.

CONTENTS

TABLES

ACRONYMS

BNL	=	Brookhaven
SNL	=	Sandia National Laboratories
NPP	=	nuclear power plants
ANL	=	Argonne
IET	=	Integral Effects Tests (p.82)
DCH	=	direct containment heating
PWR	=	pressurized water reactor
RPV	=	reactor pressure vessel
NRC	=	Nuclear Regulatory Commission (U.S.)
RCS	=	reactor coolant system
SD	=	standard deviation
WM	=	Wood's Metal
T-G	=	Tutu-Ginsberg

EXECUTIVE SUMMARY

Introduction. Modeling of direct containment heating (DCH) phenomena in the CONTAIN code is being extended to incorporate models for debris dispersal from the reactor cavity. This report describes work that has been performed to assess various candidate models and correlations for entrainment rates and debris fraction dispersed. The approach used involved comparing the predictions of the correlations with experimental data in which low-temperature melt simulants (principally water and Wood's Metal) were ejected by pressurized gas into scaled models of reactor cavities and then partially dispersed from the cavity by the subsequent gas blowdown. The experimentally measured dispersal was compared with the predictions of the various models being assessed.

Data used in this study include data obtained at Brookhaven National Laboratory (BNL) using 1/42-scale models of the Surry and Zion reactor cavities with water and Wood's Metal as corium simulants, and data taken at Sandia National Laboratories (SNL) using 1/10-scale models of the same two reactor cavities with water as the simulant liquid. In addition to cavity geometry and scale, the experimental parameters varied included the pressure of the driving gas in the pressure vessel, the identity of the driving gas (N_2 and He at BNL, air and He at SNL), identity of the simulant liquid (water and Wood's Metal at BNL, water only at SNL), the diameter of the orifice in the pressure vessel through which liquid is ejected and gas blowdown occurs, the volume of pressurized gas driving the blowdown, and the volume of the liquid (varied in one SNL Zion-geometry series only; in all other experiments, the liquid volume was scaled to a value corresponding approximately to full core melt).

The data base used here includes approximately 600 individual experimental results. These experiments may be grouped into 35 series such that, within each series, the pressure of the driving gas was varied, while all other experimental parameters were held constant. Variations in these other parameters then define the different series.

The DCH experiments which have been performed using high-temperature, chemically reactive melts generated by the iron-oxide/aluminum thermite reaction have not been used in this assessment, even though they are obviously much more nearly prototypic than are the experiments with low-temperature simulants. One reason is that the thermal and chemical interaction between the thermite melts and the blowdown gas will cause large and time-varying changes to the physical variables appearing in the correlations, and it is very difficult to take these effects into account without an integrated treatment that simultaneously evaluates the thermal and chemical processes. Hence, assessment of the correlations against the thermite experiments will be deferred until after the more promising of the correlations (as identified here) have been incorporated into the CONTAIN code, which will permit their performance to be assessed in an integrated analysis context.

Systematization of the Data. As expected, the initial pressure, P_v, of the driving gas in the pressure vessel (which simulates the reactor pressure vessel) was a dominant parameter determining the fraction of debris dispersed from the cavity, F_d. However, a strong dependence upon other experimental parameters was also apparent, with the value of P_v required to achieve a given value of F_d varying by up to an order of magnitude as these other parameters are varied. The dependence of F_d upon P_v was found to be similar, though far from identical, for all the data series. As a result, it was found that all the data series could be brought together reasonably well by plotting F_d against P_v/P_{50}, where P_{50} is the driving pressure required to achieve 50% dispersal in a given data series.

An analytical representation of the data systematics was developed assuming that the dependence of F_d upon the experimental parameters was of the form $f(P_v{}^n X_1{}^{\alpha 1} X_2{}^{\alpha 2}...)$, where the X_i represent the other experimental parameters found to affect the dispersal fractions. The selection of this form was guided in part by the trends of the experimental data and in part by the fact that many of the correlations evaluated could be expressed at least approximately in this form. The data were analyzed to extract values of the pressure exponent n and values of α_i/n. The latter quantity is a measure of the change in driving pressure required to obtain equivalent values of F_d when one of the other parameters is varied. For example, for the pressure vessel orifice diameter d_h, it was found that α/n was approximately unity, which means that F_d increases with increasing d_h and that, if d_h is increased by a given factor, decreasing P_v by the same factor will result in approximately the same value of F_d.

Screening of Candidate Correlations. The analytical representations of the experimental trends are considered to be an important product of the present work because they permit one to make a fairly extensive assessment of many of the correlations considered without performing a direct comparison of the predicted and observed values of F_d for each data point, a process which is somewhat cumbersome. (A few correlations are sufficiently complex that this analytical approach is difficult to apply.) Using these analytical representations of the experimental trends, the candidate correlations were screened to eliminate those which would clearly be unsatisfactory.

After the initial screening, correlations for entrainment rates that remained under consideration were those proposed by Tutu, by Levy, by Ishii, and a modified version of the Whalley-Hewitt correlation. Correlations for dispersed fraction remaining under consideration were the Tutu-Ginsberg set of correlations and the integral forms of the Levy, Ishii, and modified Whalley-Hewitt correlations.

Detailed Assessments. The correlations which passed the initial screening were assessed in greater detail by performing quantitative comparisons between the predicted and the observed values of F_d for each of the approximately 600 experiments in the data set. Results are displayed graphically in various ways. In addition, performance statistics in the form of standard errors of estimate are presented which summarize the results in a concise form.

With some qualifications, all of the correlations considered involve at least one adjustable "cavity coefficient", K_c, whose value is determined by fitting to the data. As was expected, the value of K_c depended upon cavity geometry; different values of K_c were generally required to fit the Surry and the Zion data. A less expected result was that, with one partial exception discussed below, different values of K_c were also required to fit the BNL and the SNL data for the same cavity geometry. If the BNL-SNL differences are interpreted as scale effects, it would mean that F_d tends to decrease with increasing scale, with the effect being weak in the Surry cavity geometry and considerably stronger in the Zion geometry. The correlations examined all predict F_d should either increase with increasing scale or be scale-independent.

Considerable effort was expended trying to understand these results. One difficulty is that the BNL and SNL experiments were scaled counterparts of one another only with respect to the cavity geometries. The geometries of the portions of the experimental apparatus delivering liquid and high-pressure gas to the cavity were different from one another and neither were similar to nuclear power plant primary system geometries. It is possible that these differences distort the comparisons between the two data sets. Analyses were performed which suggest that two-phase discharge effects following gas blowthrough in the SNL experiments did cause systematic variations in gas discharge coefficients in these experiments, and that two-phase discharge effects were likely less in the BNL experiments (the SNL configuration is more nearly prototypic in this respect). However, evidence was also found that these effects were not seriously perturbing the cavity dispersal data.

In summary, no strong reasons were found for rejecting the implications noted above concerning scale effects, but firm conclusions concerning scalability could not be drawn due to the complications acknowledged here. If additional experiments are judged necessary to address the scaling question, it is strongly recommended that the experimental design include proper scaling of all relevant portions of the experimental systems, not just the cavity.

Provided K_c was defined separately for the SNL and BNL data, the Tutu-Ginsberg correlations performed best on the whole (smallest standard errors of estimate). The integrated forms of the Levy, Tutu, and modified Whalley-Hewitt correlations also performed acceptably with standard errors of estimate being only slightly larger than for the Tutu-Ginsberg correlations. The Whalley-Hewitt correlation was noteworthy in that it was the only correlation giving an acceptable fit to the BNL and SNL data for the Surry geometry using the same value of K_c for both data sets. Separate values of K_c were still required to fit the BNL and SNL Zion-geometry data sets.

Recommendations for CONTAIN. The correlations recommended for inclusion in the CONTAIN code are the Tutu-Ginsberg correlations, the integral forms of the Levy and modified Whalley-Hewitt correlations for dispersed fraction, and the time-dependent forms of the Levy, Tutu, and modified Whalley-Hewitt correlations for entrainment rates. These recommendations were based in part upon performance with respect to matching the experimental data and in part upon considerations related to the intended usage within the CONTAIN code.

Assessment of Cavity Dispersal Correlations for Possible Implementation in the CONTAIN Code

D. C. Williams and R. O. Griffith
Sandia National Laboratories

1. Introduction

An important unresolved safety issue in U. S. nuclear power plants (NPP) is whether containment pressurization in direct containment heating (DCH) events can be sufficiently severe to threaten the integrity of the containment. In order to investigate this question, the U.S. Nuclear Regulatory Commission (NRC) has sponsored a substantial experimental program and has also sponsored development of analytical tools for the evaluation of DCH threats. The latter has included the incorporation of DCH modeling into the CONTAIN code, which is the NRC's best-estimate tool for the analysis of containment response in severe accidents [Mur89,Was91].

Past and present DCH modeling in the CONTAIN code has seen considerable use, both for analysis of DCH scenarios in full-scale nuclear power plants (NPPs) and for analysis of the DCH experimental program. However, as they presently stand, the DCH models in CONTAIN involve a number of important limitations. Hence, the NRC is currently funding model development tasks in an effort to mitigate some of these limitations. Phenomena for which modeling efforts are currently underway include single-phase and two-phase debris ejection from the reactor pressure vessel (RPV), ablation of the RPV, entrainment of debris in the cavity and dispersal from the cavity, and the particle size for the dispersed debris.

The purpose of the present report is to summarize work that has been performed to assess various models and correlations which have been considered for calculating the rate at which molten core debris in the cavity may be entrained by blowdown steam from the RPV, and for the total fraction of the corium which might thereby be dispersed from the cavity. The correlations which are identified as being the most promising will then be incorporated into the CONTAIN code.

The overall assessment will actually proceed in two major stages, of which the present report describes only the first. In this stage, candidate correlations will be compared with the results of a large number (~ 600) of cavity dispersal experiments in which low-temperature corium simulants (water or Wood's Metal in most cases) were dispersed from scaled reactor cavities by gas discharged from a pressurized vessel simulating the RPV. These experiments and their results are described in more detail in Section 2 of this report.

Since the corium simulants used in these experiments were neither high temperature nor chemically reactive, their dispersal is governed by hydrodynamic phenomena only, without the heat transfer and chemical reaction effects which are characteristic of DCH events. Hence establishing that a correlation accounts for these experimental results well is not sufficient to establish that it will be adequate for DCH analysis. On the other hand, it does seem reasonable

to believe that, if a correlation does not give an adequate description of these simpler experiments, it will also be inadequate for DCH analysis. Hence, this data base is expected to be very useful for screening out correlations which are clearly unsuitable for DCH analysis.

In addition to this data base involving cold simulants, there is a considerably smaller number of experiments in which high-temperature, chemically-reactive melts generated by thermite-type reactions have been used to provide a much more realistic simulation of DCH phenomena. It has been suggested [Lev91] that, even in these experiments and in actual DCH events, debris entrainment and dispersal is still governed primarily by hydrodynamic effects, and that the effect of the thermal and chemical processes is to alter the relevant hydrodynamic parameters such as gas density, pressure, and flow velocities.

Both the experimental results and calculations with the existing CONTAIN models have shown that the effect of chemical reactions and heat transfer on these hydrodynamic parameters are large and difficult to estimate a priori, in part because they are time-varying and because there may be strong two-way coupling between these processes and the debris entrainment rates. Obtaining an adequate test of entrainment correlations against the thermite experiments therefore requires an integrated treatment in which the heat transfer and chemical processes, as well as the hydrodynamic processes, are modeled simultaneously. Hence, an assessment strategy has been developed which involves the following steps:

1. The experimental data base for the low-temperature simulants has been systematized to establish qualitative and, where possible, quantitative representations of how the dispersal fractions vary as a function of the governing parameters. This step is described in Section 2 of this report.

2. Candidate correlations have been screened against the systematics of the experimental data base in order to eliminate those which do not reproduce the more important trends identified. Correlations screened include those described in the DCH Models and Correlations report [Ost94], correlations described by M. Ishii [Ish91] and S. Levy [Lev91], and the entrainment rate correlation described by N. Tutu [Tut91]; see Section 3 for details.

3. For correlations surviving the screening step, the fraction dispersed predicted by the correlation is compared quantitatively with the experimental results for all the experiments in the data base used (Section 4).

4. Results of the preceding steps have been used to recommend three correlations for entrainment rates and three correlations for total fraction dispersed which will be incorporated into the CONTAIN code. The recommended correlations for entrainment rates are the Levy and Tutu correlations and a modified form of the Whalley-Hewitt correlation, while the recommended correlations for dispersal fractions are the integral form of the Levy correlation, the Tutu-Ginsberg correlations [Tut88, Tut90a, Tut90b], and the integral of the Whalley-Hewitt correlation used for entrainment rates.

5. The correlations selected will be implemented in the CONTAIN code.

6 Once implemented in CONTAIN, the correlations will be further assessed by comparison with the more realistic DCH experiments involving the thermite-generated melts.

Physically, one does not expect entrainment rate correlations and dispersal fraction correlations to be independent; that is, an entrainment rate correlation integrated over the blowdown history should yield a dispersed fraction consistent with that given by a dispersal fraction correlation, if both are valid. Hence, rate correlations and dispersed fraction correlations have been defined in terms of pairs which meet this consistency requirement, insofar as this has proven possible. The CONTAIN implementation will include options in which the user may specify a dispersed fraction correlation and also a rate correlation, and the latter will then be automatically adjusted such that the integral of the rate will equal the dispersed fraction. Discussion of the details of this implementation will be deferred to the appropriate CONTAIN documentation, since it does not directly affect the correlation assessments discussed here.

The present report describes the first four steps of the above process. In Section 5, the important subject of scalability of the correlations is discussed, recommendations are made as to which correlations should be incorporated into the CONTAIN code, and a rationale is offered for these recommendations. Conclusions are briefly summarized in Section 6.

2. Systematization of the Experimental Data

2.1. Description of the Experimental Data Base

The present assessment effort relies primarily upon a series of experiments performed at Brookhaven National Laboratory (BNL) and Sandia National Laboratories (SNL). Measured volumes of liquid representing the corium were placed in a pressurized container and ejected into scaled models of reactor cavities by high-pressure gas. Following liquid ejection, gas blowdown from the pressure vessel entrained a portion of the corium simulant and dispersed it from the cavity. The principal measurement made in each experiment was the fraction of the liquid dispersed. Note that only the integral dispersed fraction was measured, not the dispersal rates; hence correlations for rates may be assessed only by integrating the predicted rates over the blowdown history to obtain the predicted fraction dispersed.

The cavities used were geometrically scaled replicas of the Surry and Zion NPP cavities, with the scale factors being 1/42 in the BNL experiments 1/10 in the SNL experiments. (The BNL experiments also included 1/42-scale replicas of the Watts Bar NPP cavity; however, time did not permit inclusion of these data in the present assessment effort.) In addition to cavity geometry and scale, the experimental parameters varied included the pressure of the driving gas in the pressure vessel, the identity of the driving gas (N_2 and He at BNL, air and He at SNL), identity of the simulant liquid (water and Wood's Metal at BNL, water only at SNL), the diameter of the orifice in the pressure vessel through which liquid is ejected and gas blowdown

occurs, the volume of pressurized gas driving the blowdown, and the volume of the liquid (varied in one SNL Zion-geometry series only; in all other experiments, the liquid volume was scaled to a value corresponding approximately to full core melt). The assessment process is largely based upon determining the degree to which the various candidate correlations can reproduce the experimental trends as a function of these parameters.

In the BNL Surry experiments, three different cavity configurations were used. In the first configuration, no cavity structures were simulated. In the second, the skirt supporting the reactor vessel was simulated, while in the third, all cavity structure (instrument tubes, etc) was simulated. In all the SNL Surry geometry data, the skirt was simulated but other cavity structure was not included. Experiments with thermite-generated melt in which the instrument tube structures were simulated have been performed at SNL, with the result that these structures were quickly failed and ejected from the cavity. Partly for this reason, the BNL data with all cavity structure were not included in the present work. BNL data for both the other configurations were included. These data indicate that the skirt does not have a large effect (see Sections 2.3 and 4.2), although the BNL data with the skirt are very limited and somewhat inconclusive.

Since the BNL and SNL data were obtained at different scales, it would be natural to hope that comparisons of these data would permit conclusions to be drawn concerning the adequacy of the various correlations' abilities to account for scale-dependent effects. However, only the cavities themselves were scaled replicas of one another (or of NPP) in these experiments; the geometries of the high-pressure systems for delivery of liquid and gas to the cavity were rather different. Among other things, these differences likely affected the relative importance of the two-phase discharge stage following gas blowthrough in the BNL versus the SNL tests; Section 4.2 gives additional details. For whatever reason, the SNL versus BNL differences have proven difficult to interpret in terms of scale effects, and any conclusions to be drawn here concerning scale effects must remain quite tentative.

Winfrith Constant-Pressure Tests. In addition to the BNL and SNL tests summarized above, a set of data obtained at Winfrith [Mac85] was also used to some degree in the screening study. In these experiments, the gas driving pressure was held constant for a fixed time (10 seconds) and the fraction dispersed was measured as a function of pressure. Levy [Lev91] found that these constant-pressure tests did behave somewhat differently from the BNL and SNL transient blowdown tests. Since the latter are more nearly representative of NPP accident scenarios, the detailed quantitative comparisons between predicted and measured dispersal fractions therefore did not use the Winfrith data. However, the Winfrith tests made use of a wider variety of fluids than just the water and Wood's Metal used in the BNL tests. These data were therefore used to some extent to assess the dependence upon fluid properties predicted by the various correlations.

2.2. Qualitative Representation of Experimental Trends

Counting only the BNL and SNL tests in Surry and Zion geometries, the data base used here includes approximately 600 individual test results. These tests may be grouped into 35 series such that, within each series, the pressure of the driving gas was varied, while all other experimental parameters were held constant. Variations in these other parameters then define the different series. Although driving pressure is expected to be a very important parameter governing debris dispersal, the fact that other parameters are also important is easily illustrated by plotting the fraction dispersed against the driving pressure for all the data (Figure 2.2-1). It is apparent that the driving pressure required to obtain a given degree of dispersal varies widely, by more than an order of magnitude. Little else is apparent from this figure, other than that it is a mess; clearly, the data must be examined in more detail if the roles of the various experimental parameters are to be clarified.

Within each series, as defined above, there are generally sufficient data points spanning a sufficiently wide range of driving pressures to provide a reasonable definition of the pressure dependence for a given series, although in a few cases this is not true. Plotting the dispersed fraction against driving pressure for each series individually then gives a reasonable picture of this dependence. Comparing such plots for different series also provides insights as to the dependence upon some of the other parameters of interest. This approach is illustrated in Figure 2.2-2 for some selected series of BNL data for the Surry cavity geometry. In this figure, the first series (open squares) gives the results for water as the liquid, N_2 as the driving gas, and a hole diameter, d_h, equal to 0.953 cm (corresponding to 0.4 m at NPP scale). In the second series, parameters were the same as in the first except that the hole diameter was half as great, while the third series parameters are the same as for the second except that helium is the driving gas. Finally, in the fourth series, parameters are the same as in the first except that Wood's Metal rather than water is the liquid used.

From Figure 2.2-2, it is apparent that dispersal increases with increasing hole size, increasing molecular weight, M, of the driving gas, and decreasing density, ρ_d, of the fluid. (These interpretations presuppose that the governing gas property is the molecular weight and that governing liquid property is density; in the latter instance, surface tension probably plays some role also.)

In the initial stages of this work, a large number of comparisons of the type illustrated in Figure 2.2-2 were made and results were summarized as a "trends chart" which is reproduced here as Table 2.2-1. In the trends chart, an entry "increase" means that, as the specified parameter is increased, the dispersed fraction increases, while "decrease" implies that the reverse is true.

Table 2.2-1.

Trends Chart Showing Dependencies of Debris Dispersal on Experimental Variables

Increasing Variable	Observed Change in Dispersal
RCS Parameters	
Vessel hole size, d_h	Increase
Gas molecular weight, M	Increase
Vessel volume, V_v	Increase
Vessel pressure, P_v	Increase
Melt Parameters	
Liquid volume, V_d	Little change
Liquid density, ρ_d	Decrease
Liquid viscosity, μ_d	Decrease (weak)
Cavity Parameters	
Scale	Uncertain
$L_{RCS\text{-}Floor}$	Decrease
Structures	Decrease
Gas density, ρ_g	Unknown
$P_{Containment}$, P_{Cavity}	Unknown
Cavity Geometry, Surry → Zion	Increase

Although qualitative, the trends chart was found to be very useful in understanding the data and in initial screening of the correlations. It also illustrates potential limitations with all the correlations. For example, the trends chart indicates that dispersal decreases with increasing distance of the vessel orifice above the cavity floor ($L_{RCS\text{-}Floor}$). This entry derives from observations made in the Winfrith experimental series. However, none of the correlations considered in this work include any dependence upon this parameter. Furthermore, the available

data would not permit making a good quantitative check of the predictions of any correlation that did include it, since this parameter has not been systematically varied in any of the experiments.

Despite the utility of the qualitative trends chart, a more quantitative representation of the experimental trends was judged desirable. After a certain amount of trial and error, a procedure was developed which appears to be useful, and this procedure will be described next.

2.3. Quantitative Representation of Experimental Trends

For the parameters other than the driving pressure (vessel orifice size, etc.), plotting dispersed fraction against the parameter of interest is not generally useful because only two or at most three separate values of these other parameters were investigated, and even for these it may be difficult to identify matched pairs; i.e., pairs which differ only with respect to the parameter of interest and with all other parameters, including the driving pressure, held constant. From Figure 2.2-2, it is apparent that the dependence upon driving pressure is sufficiently steep that even minor variations in pressure can have a significant effect on F_d. It is also apparent that there is sufficient scatter in the data that it would be risky to base quantitative conclusions upon the comparison of a few well-matched data-point pairs.

What is needed is a means of quantitatively comparing the results for the various series with each series considered as a whole. The shapes of the curves for the different series in Figure 2.2-2 are somewhat similar, though certainly not identical. This suggests that the dominant effect of the parameters distinguishing the different series can be represented as a scale factor applied to the pressure scale (note that the pressure scale is logarithmic in the figure). Hence, one might attempt to represent the effect of these parameters by quantifying their effect upon the driving pressure required to reach equivalent points on F_d versus P curves such as those in the figure.

One characteristic pressure that might, in principle, be used to represent the effects of the experimental variables is the threshold pressure corresponding to the onset of debris dispersal. This concept of a threshold for dispersal has received some attention in the DCH literature [Ish91, Lev91]; see also the Tutu-Ginsberg correlations. However, it has not been adopted here for three reasons:

1. Emphasis on the dispersal threshold reflects an older view of DCH in which only the interactions of airborne debris with steam and gas is considered important. Recent analyses [Wil92] of data from the DCH experiments using the thermite-generated melts have indicated that debris which is not dispersed from the cavity may still undergo reasonably efficient thermal and chemical interaction with the blowdown steam.

2. Even in the older view of DCH, there is no great practical significance in the pressure marking the transition from zero dispersal to some very small fraction dispersed; the threshold would be very important only if the fraction dispersed were to increase almost discontinuously to large values immediately above the threshold, which is not the case.

3. A true threshold turns out to be very difficult to identify in the data analyzed here.

In the approach adopted, the effect of the various parameters defining the different data series was represented by their effect upon P_{50}, which is defined to be the pressure at which 50% of the liquid is dispersed from the cavity. This pressure clearly is of practical importance, since F_d increases from quite small values to large values over a fairly narrow range of driving pressures more or less centered on P_{50}. The steepness of this increase means that the P_{50} value can be useful as a sort of "pseudothreshold" value, even though the data usually indicate that some quite small amount of dispersal can occur at pressures well below the P_{50} value. In addition, the very fact the F_d does increase rapidly with pressure in this portion of the curve facilitates identification of the P_{50} point.

One might attempt to read off P_{50} values directly from plots such as Figure 2.2-2. It seemed preferable, however, to attempt to use a least-squares fitting technique in order to reduce the effect of scatter in the data. For this purpose it was found useful to replot the data in the form of what will be referred to as the "Z-plot", in which the (natural) logarithm of the quantity $Z \equiv F_d/(1-F_d)$ is plotted against the logarithm of the driving pressure. Figure 2.3-1 presents a Z-plot for the data series which were plotted in Figure 2.2-2.

It is obvious that there is considerable departure from linearity in the Z-plot when the full range spanned by the data is considered. However, the region of greatest interest for identifying P_{50} values is the region for which F_d is of the order of 0.5, which corresponds to $Z = 1$ or $\ln(Z) = 0$. In the vicinity of the line corresponding to $\ln(Z) = 0$ in Figure 2.3-1, it is seen that the Z-plots are reasonably linear. Typically, the regime of near linearity includes ln(Z) values ranging from -2 to +1 ($F_d = 0.12$ to 0.73) and is sometimes wider.

In the approach adopted, Z-plots were prepared for each of the 35 data series and the regime of approximately linear behavior was identified by visual inspection. A linear least squares fit was then performed for ln(Z) versus ln(P), excluding data outside the linear regime. The pressure at which the regression line crosses the $\ln(Z) = 0$ line was then taken to be the P_{50} value. Obviously, there is some subjectivity in this procedure associated with deciding the data range for inclusion in the least-squares fit, but it was judged that this subjectivity was probably less than that involved in attempting to read P_{50} values directly off plots such as those in Figure 2.2-2. There were several series for which driving pressures did not extend to sufficiently high pressure for F_d values ≥ 0.5 to be achieved, and some extrapolation was then required in order to estimate P_{50}. In one series, the data were sufficiently erratic that P_{50} was estimated directly without using the least squares procedure.

One test of the utility of the P_{50} approach is provided in Figure 2.3-2, in which a plot of F_d against P/P_{50} is given for the complete BNL-SNL data set. Axis scales and plot symbols are the same as in Figure 2.2-1. Comparison with the latter figure shows that, while hardly perfect, normalizing the driving pressure to the P_{50} value for each series does do a reasonably good job of bringing together the data for the various series. This result supports the concept that, to a first approximation, the problem of cavity dispersal may be decomposed into two parts, with the

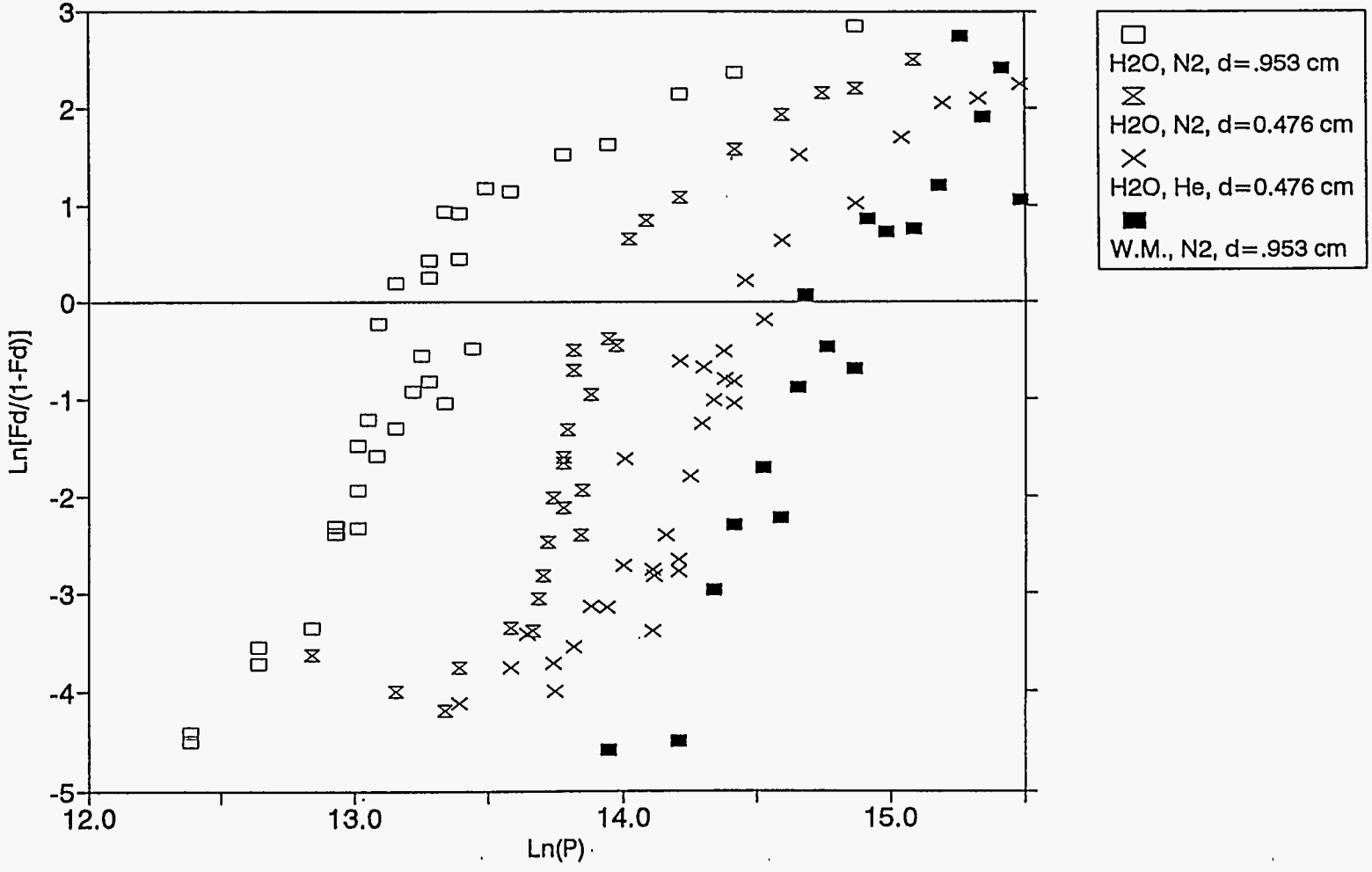

Figure 2.3-1 "Z-plot" ($\ln[F_d/(1-F_d)]$ vs $\ln(P_{o,v})$) for data series of Figure 2.2.2

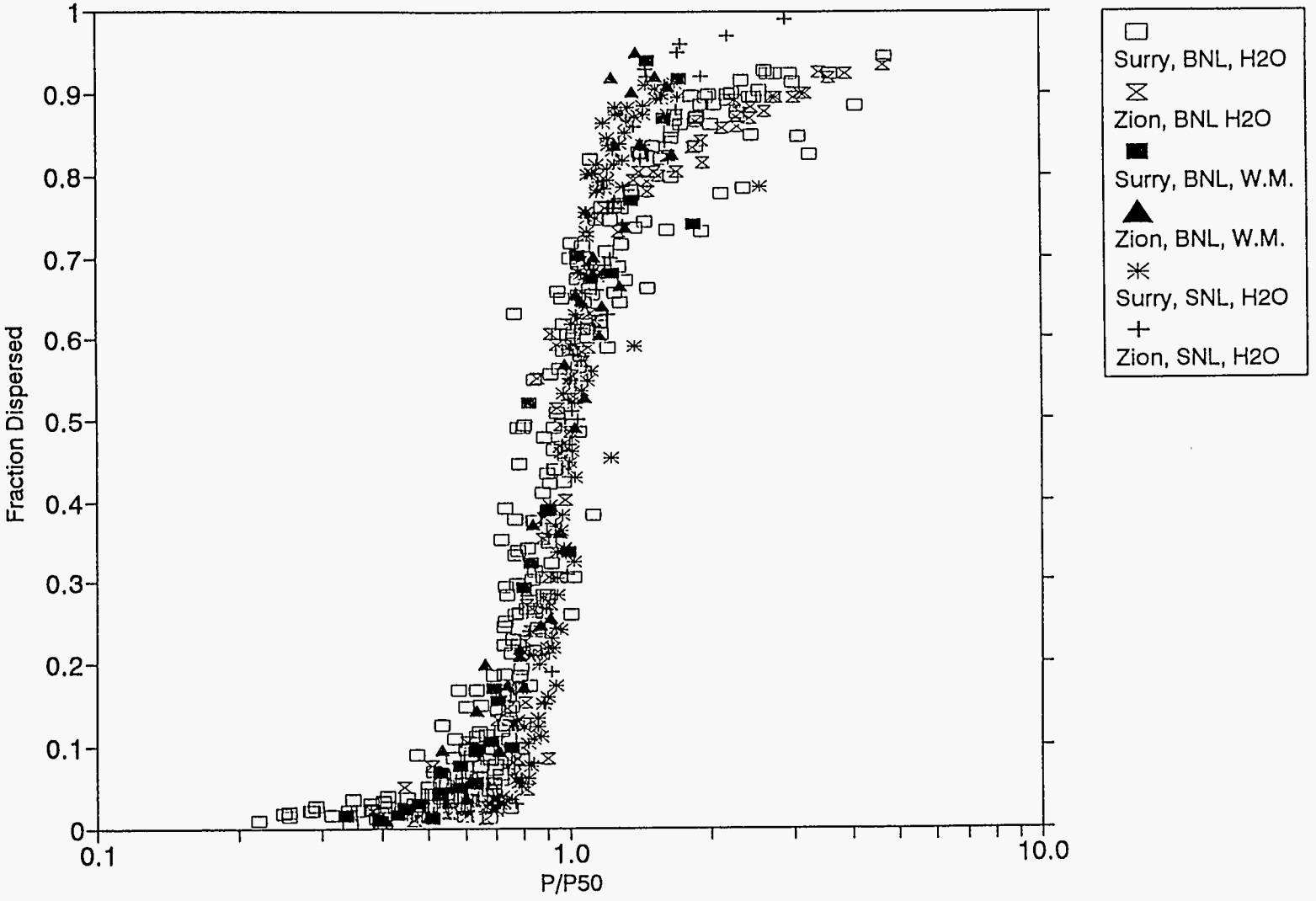

Figure 2.3-2 F_d versus P/P_{50} for the complete data set

first being determining how F_d varies as a function of P/P_{50} and the second being determining how P_{50} varies as a function of the other relevant parameters.

Another interesting way to plot the complete data set is in the form of a Z-plot in which the abscissa is $\ln(P/P_{50})$, rather than $\ln(P)$. This is done in Figure 2.3-3. The trend toward linearity is seen to be quite strong over the range of greatest interest, with substantial departures from linearity developing at high values of Z and somewhat lesser departures at low values. In both instances, the degree of departure from linearity varies considerably among the various data series.

One point of special interest in Figure 2.3-3 is that, in no case, is there any evidence of departures from linearity in the downward direction. If a true dispersal threshold pressure exists, one would expect the Z-plot to turn downward toward $-\infty$ as the driving pressure is reduced toward the threshold value from above. However, the plot provides no evidence of such behavior. It appears, therefore, that if a true threshold for dispersal exists at all, it affects the results only for F_d values and P/P_{50} values too low to be of much practical concern.

Results of the P_{50} analysis for the 35 data series are summarized in Table 2.3-1. The first several columns summarize the pertinent experimental parameters: BNL versus SNL series, Surry or Zion cavity geometry, density of the liquid (ρ_d = 1000 kg/m^3 for water, 9200 kg/m^3 for Wood's Metal), molecular weight of the driving gas, mass of liquid used, volume of the pressurized driving gas. The P_{50} value itself is tabulated in the following column, and the last column gives comments indicating whether extrapolation was required to estimate the P_{50} value, whether the data seemed to be especially irregular, or whether the skirt was simulated in Surry geometry tests.

The next to last column of Table 2.3-1 gives the slope of the Z-plot except in two cases for which the data were too irregular for meaningful values to be extracted. Note that, for small values of F_d, linearity of the Z-plot implies a power-law relationship between F_d and driving pressure, $F_d \propto P^n$; the slope of the Z-plot then corresponds to the exponent n. Although there is considerable variation in the values, there are no obvious trends except that the values of the slopes for the SNL Surry data appear to be higher than for the other cases, including the SNL Zion cases and the BNL Surry cases. This reflects the fact that the dependence of F_d upon driving pressure was even steeper for the SNL Surry data than was the case for the other series. The reason for this difference is not known, but it could be of some importance if it reflects a scale-dependence in the dispersal mechanisms which is different for the Surry and Zion geometries. None of the correlations considered in this work are capable of predicting any such effect, however.

Inspection of Table 2.3-1 shows that the P_{50} values vary as one would expect from the qualitative trends chart; e.g., P_{50} values increase with decreasing hole size, are greater for helium than for nitrogen or air, are substantially greater for Wood's Metal than for water; etc. In order to convert these results into a form more useful for comparison with correlations, we

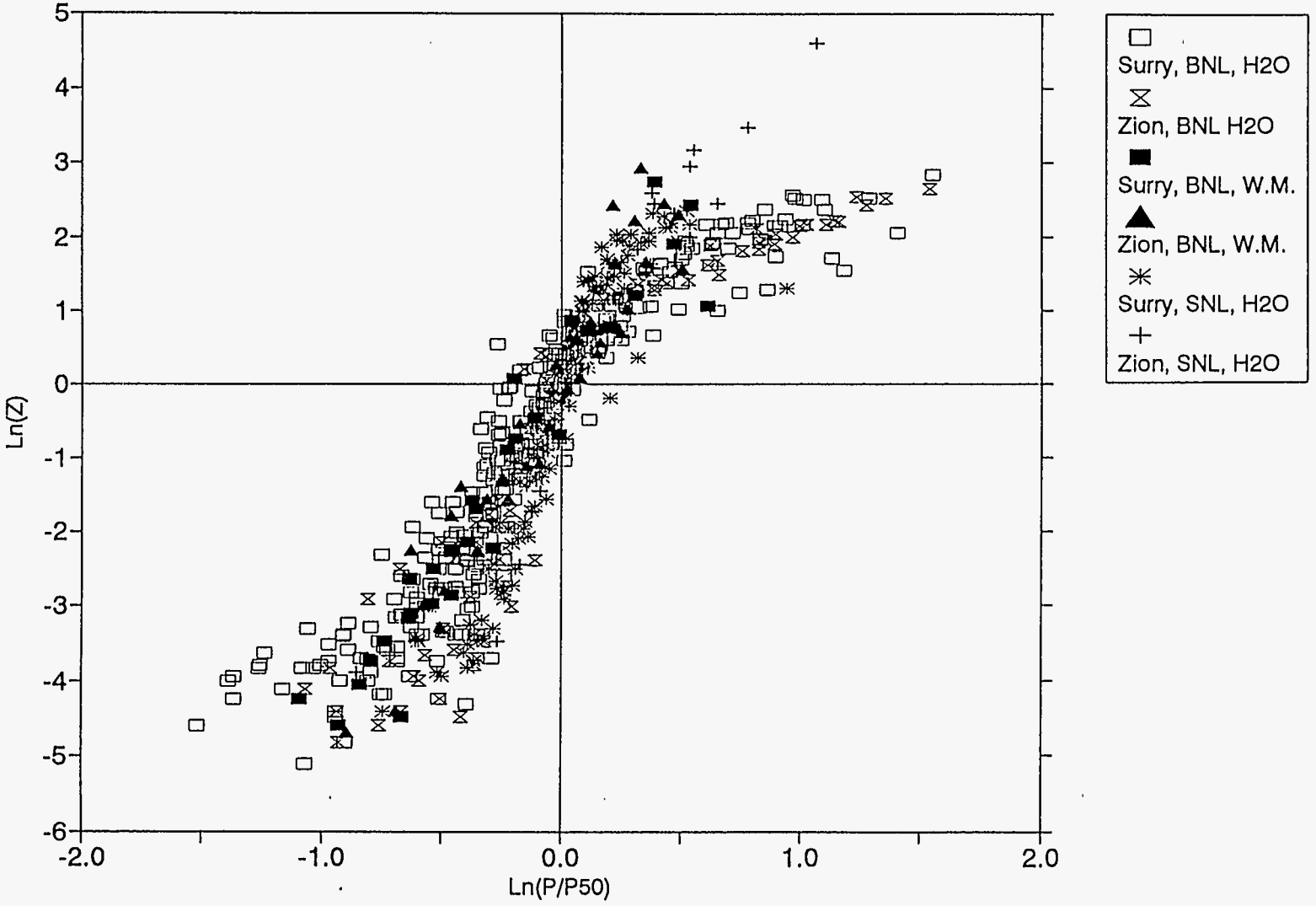

Figure 2.3-3 Z-plot for complete data set with $\ln(P/P_{50})$ as abscissa.

Table 2.3-1
Summary of P-50 Data

Lab	Cavity	Rho-d (kg/m**3)	MW-g	m-d (kg)	V-ves (m**3)	d-hole (cm)	P50 (MPa)	Slope of Z-plot	Comment
BNL	Surry	1000	4	0.19	0.00622	0.4763	2.081	5.07	
BNL	Surry	1000	4	0.19	0.00622	0.6747	1.445	5.12	Extrap.
BNL	Surry	1000	4	0.19	0.00622	0.9525	1.087	3.92	
BNL	Surry	1000	28	0.19	0.00622	0.4763	1.297	5.65	
BNL	Surry	1000	28	0.19	0.00622	0.6747	1.03	4.82	Extrap.
BNL	Surry	1000	28	0.19	0.00622	0.9525	0.612	5.59	
BNL	Surry	1000	28	0.19	0.00929	0.9525	0.458	4.16	
BNL	Surry	1000	28	0.19	0.00929	0.4763	1.098	4.75	
BNL	Surry	1000	28	0.19	0.00319	0.9525	0.798	4.88	
BNL	Surry	1000	28	0.19	0.00319	0.4763	1.747	5.05	
BNL	Surry	1000	28	0.19	0.00622	0.6747	0.777	7.35	Skirt
BNL	Surry	1000	28	0.19	0.00622	0.9525	0.702	3.33	Skirt
BNL	Zion	1000	4	0.194	0.00621	0.4763	0.954	7.63	
BNL	Zion	1000	4	0.194	0.00621	0.6747	0.698	4.35	
BNL	Zion	1000	4	0.194	0.00621	0.9525	0.536	5.34	
BNL	Zion	1000	28	0.194	0.00621	0.4763	0.806	---	Irreg.
BNL	Zion	1000	28	0.194	0.00621	0.6747	0.467	4.45	
BNL	Zion	1000	28	0.194	0.00621	0.9525	0.339	7.44	
BNL	Surry	9200	4	1.75	0.00622	0.6747	6.65	4.97	Extrap.
BNL	Surry	9200	28	1.75	0.00622	0.4763	6.7	---	Extrap.
BNL	Surry	9200	28	1.75	0.00622	0.6747	4.72	4.71	Extrap.
BNL	Surry	9200	28	1.75	0.00622	0.9525	2.886	4.95	
BNL	Zion	9200	4	0.194	0.00621	0.6747	2.779	4.66	
BNL	Zion	9200	4	0.194	0.00621	0.9525	2.018	4.58	
BNL	Zion	9200	28	0.194	0.00621	0.6747	1.854	6.36	
BNL	Zion	9200	28	0.194	0.00621	0.9525	1.314	6	
SNL	Surry	1000	28.96	14	0.0913	2.54	1.867	10.7	
SNL	Surry	1000	28.96	14	0.29	2.54	1.379	7.01	
SNL	Surry	1000	28.96	14	0.29	3.81	0.894	10.5	
SNL	Surry	1000	4	14	0.0913	2.54	2.722	14.65	
SNL	Surry	1000	4	14	0.29	2.54	2.094	13.04	
SNL	Surry	1000	4	14	0.29	3.81	1.655	7.77	
SNL	Zion	1000	28.96	7	0.25	3.81	0.784	3.75	
SNL	Zion	1000	28.96	13.9	0.25	3.81	0.762	5.83	
SNL	Zion	1000	4	13.9	0.25	3.81	1.466	4.41	

Ave. Z-plot slope, SNL Surry Data = 10.6; Std. Dev. = 2.9
Ave. Z-plot slope, All Other Data = 5.15; Std. Dev. = 1.07

note that most of the correlations to be considered can be manipulated such that they can be at least approximately expressed in the form

$$F_d = f(P^n \prod_{i=1}^{N_p} X_i^{\alpha_i}), \tag{1}$$

where N_p is the number of parameters of interest that appear in the correlation, X_i is the ith such parameter, and α_i is a power to which that parameter is raised. That is, the correlations may be expressed as a function of a product of the various parameters raised to various (often fractional) powers. The Tutu correlation for entrainment rates and the Tutu-Ginsberg correlations for dispersed fractions are more complex and reduce to the form of Equation (1) only in certain limiting cases; however, it was not necessary to make extensive use of the development outlined here in assessing those correlations.

In order to screen candidate correlations, it would therefore be convenient to extract information equivalent to experimental values of the α_i. It might be possible to develop an approach for doing this by performing a nonlinear least squares fit to the data of Table 2.3-1, but this was not done here. Instead, it was noted that one could define a number of pairs of series for which the experimental parameters were all held constant except for one parameter, X_i. Let the values of this parameter be $X_{i,1}$ and $X_{i,2}$ for the two series, and let the corresponding values of P_{50} be $P_{50,1}$ and $P_{50,2}$, respectively. Since the value of F_d is, by definition, equal to 0.5 when P is equal to P_{50} in both instances, the value of the argument of the function f must be the same for the two cases; and since all parameter values other than X_i are the same, we have

$$P_{50,1}^n X_{i,1}^{\alpha_i} = P_{50,2}^n X_{i,2}^{\alpha_i}; \text{ hence}$$
$$\frac{\alpha_i}{n} = -\frac{\ln(P_{50,1}/P_{50,2})}{\ln(X_{i,1}/X_{i,2})} \tag{2}$$

As an example, consider the first two series listed in Table 2.3-1. These series differ only in terms of the value of d_h. The ratio of hole sizes for these two cases is equal to 0.4763/0.6747 = 0.706 and the ratio of P_{50} values is 2.081/1.445 = 1.44. Hence, α/n = - ln(1.44)/ln(0.706) = 1.05.

Of course, it would be risky to base conclusions upon a single pair of series. For each experimental parameter which was varied in the complete data base, all possible pairs were identified such that only one parameter was varied, and α/n values were calculated for each such pair. For the hole size, results are given in Table 3.2-2. The values tabulated average close to unity but show a considerable amount of variation, with a standard deviation of 0.33. This variation may simply reflect the uncertainty in analysis (e.g, in extracting P_{50} values from the data), but it may also reflect the fact that the dependence upon one parameter (e.g., hole size in this case) may itself depend upon other parameters involved. (Correlations of the form Equation (1) cannot represent such effects, but there is no reason why they cannot exist in

Table 2.3-2
Dependence of P-50 Upon Hole Diameter

Lab	Cavity	Rho-d (kg/m**3)	MW-g	m-d (kg)	V-ves (m**3)	d-hole(1) (cm)	d-hole(2) (cm)	P50(d1)/ P50(d2)	alpha/n
BNL	Surry	1000	4	0.19	0.00622	0.4763	0.6747	1.440	1.05
BNL	Surry	1000	4	0.19	0.00622	0.6747	0.9525	1.329	0.83
BNL	Surry	1000	28	0.19	0.00622	0.4763	0.6747	1.259	0.66
BNL	Surry	1000	28	0.19	0.00622	0.6747	0.9525	1.683	1.51
BNL	Surry	1000	28	0.19	0.00929	0.4763	0.9525	2.397	1.26
BNL	Surry	1000	28	0.19	0.00319	0.4763	0.9525	2.189	1.13
BNL	Surry**	1000	28	0.19	0.00622	0.6747	0.9525	1.107	0.29*
BNL	Zion	1000	4	0.194	0.00621	0.4763	0.6747	1.367	0.90
BNL	Zion	1000	4	0.194	0.00621	0.6747	0.9525	1.302	0.77
BNL	Zion	1000	28	0.194	0.00621	0.4763	0.6747	1.726	1.57*
BNL	Zion	1000	28	0.194	0.00621	0.6747	0.9525	1.378	0.93
BNL	Surry	9200	28	1.75	0.00622	0.4763	0.6747	1.419	1.01
BNL	Surry	9200	28	1.75	0.00622	0.6747	0.9525	1.635	1.43
BNL	Zion	9200	4	0.194	0.00621	0.6747	0.9525	1.377	0.93
BNL	Zion	9200	28	0.194	0.00621	0.6747	0.9525	1.411	1.00
SNL	Surry	1000	28.96	14	0.29	2.54	3.81	1.543	1.07
SNL	Surry	1000	4	14	0.29	2.54	3.81	1.265	0.58

**With Skirt

Ave. alpha/n for all data = 0.99 Std. Dev. = 0.33

Ave. edited data (* values deleted) = 1.03 Std. Dev. = 0.24

reality.) In the present instance, inspection reveals no very obvious trends in the α/n values as the other parameters are varied.

Also given at the bottom of the table are average and standard deviation values labeled "edited". These were calculated without including the values marked with an asterisk in the table. The reason for excluding these data was not just that they deviated substantially from most other values; inspection of the Z-plots for at least one of the data series involved showed less regular behavior which would cast some doubt upon the P_{50} value extracted for that series, or there were other reasons to doubt the reliability of the P_{50} value.

Results of all the analyses of α/n values are summarized in Table 2.3-3. The first column indicates the experimental variable studied (pressure, hole size, etc.), and the next column shows the symbol used to represent the dependence upon this variable: the Z-plot slope $\underline{n}$ for the pressure dependence, and the values of α_i/n for the others. The next column gives any additional information that may apply to the remaining entries on the same line; e.g., the entry "SNL Surry" on the first line of data indicates that the values apply only to the SNL Surry data set. The next column ("N_{val}") gives the number of values available and the column headed "Avg. $\pm$ S.D." gives the average of the N_{val} values and their standard deviation, where these values are calculated including all available data. The last two columns give equivalent information calculated when the data are edited to eliminate cases judged to be relatively unreliable. The standard deviation values quoted should be understood as simply giving a measure of the amount of variability in the α_i/n values obtained. They do not necessarily represent a valid measure of uncertainty.

The following observations may be made:

Effect of the Skirt in Surry. Returning to Table 2.3-1, the last two entries in the first block of data give the P_{50} values for the only two BNL Surry series in which the skirt was simulated; in all other BNL Surry data series considered, no cavity structure was simulated. Comparing the two cases including the skirt simulated with the analogous two cases without the skirt (fifth and sixth cases of the first data block) is inconclusive: with a 0.9525 cm hole size, the P_{50} value is somewhat higher with the skirt (0.70 MPa) than without it (0.61 MPa), but the reverse trend would be inferred for the 0.6747 cm hole size cases (P_{50} = 0.78 and 1.03 MPa with and without the skirt, respectively). No reason has been identified for believing that changing the hole size by this relatively small amount should result in a qualitative reversal of the effect of the skirt upon dispersal. It is entirely possible that experimental uncertainty is responsible for the differences described. (The effect of the skirt is discussed further in Section 4.2 in connection with the Tutu-Ginsberg correlations, which are the only correlations that distinguish between the cavity configurations with and without the skirt.)

It must be remembered in what follows that the great majority of the BNL Surry data considered here did not include the skirt, while all the SNL Surry data did simulate the skirt. This difference could affect the comparisons between the SNL and BNL data obtained in the Surry geometry. The possibility of this effect generally will be neglected in the present work

Table 2.3-3
Dependence of Dispersal Upon Experimental Parameters

Exper. Parameter	Symbol		All Data		Edited Data	
			N_{val}	Avg. ± S.D.	N_{val}	Avg.S.D.
Driving Pressure	n	SNL Surry	6	10.6 ± 2.9		
		All Others	27	5.15 ± 1.07		
d_h	α_d/n	All	17	0.99 ± 0.33	14	1.030 ± 0.24
M_g	α_M/n	All	13	0.22 ± 0.06	10	0.22 ± 0.04
V_v	α_{Vv}/n	All	6	0.41 ± 0.18		
		BNL			3	0.42 ± 0.024
		SNL	2	0.25 ± 0.03		
V_d	α_{Vd}/n	SNL Zion only	1	0.041		
ρ_d & σ	$(\alpha_\rho+\alpha_\sigma)/n$	Surry	4	-0.703±0.025		
		Zion	4	-0.613±0.012		
μ_d	α_μ/n	Winfrith Air	1	-0.105		
		Winfrith He	1	+0.067		
σ	α_σ/n	Winfrith Air	1	-0.20		
		Winfrith He	1	+0.06		
Scale, S	α_S/n	Surry, BNL α_{Vv}	5	-0.05 ± 0.06		
		Surry, SNL α_{Vv}		-0.12 ± 0.05		
		Zion, BNL α_{Vv}	2	-0.42 ± 0.09		
		Zion, SNL α_{Vv}		-0.50 ± 0.09		

because the data permit no meaningful estimate of its magnitude or even whether it exists, except that the data do indicate that the effect of the skirt is not very large.

Dependence upon Pressure. Values of n for the SNL Surry experiments appear to differ significantly from the other cases, as was noted previously.

Dependence upon Hole Size and Gas Molecular Weight. Values of α/n extracted for these variables showed no consistent trends with the other variables involved.

Dependence upon Vessel Volume, V_v. The data set permitted calculation of six α/n values, four for BNL and two for SNL, with all values being for the Surry geometry. With one BNL value edited out as being dubious, the BNL and SNL values appeared to differ significantly in the sense that the difference between the averages was considerably larger than the standard deviations. However, the small number of data values available renders any such conclusion quite tentative.

Dependence Upon Liquid Volume, V_d. Scaled liquid volume was the same for all the test series except for one SNL Zion series, and hence only one α/n value could be obtained for this variable. This single result indicated that the fraction dispersed depends very little upon the amount of liquid present.

Dependence Upon Liquid Properties: Winfrith Data. Dependence upon liquid density, ρ_d, and surface tension, σ, are lumped together in the next line of the table because the water versus Wood's Metal results do not permit separation of these dependencies. The values tabulated were extracted assuming density to be the governing parameter, but the surface tension ratio for these two liquids is only slightly less than the density ratio and the result for the combined dependence is not sensitive to the assumed split between dependence upon ρ_d versus σ. Note that the dependence is somewhat stronger for the Surry geometry than for the Zion geometry; though the difference may not seem to be great, it will be seen to have clearly observable effects upon the detailed correlation assessments described in Section 4.

Consideration of the Winfrith constant-pressure data was invoked in order to obtain greater understanding of how dispersal may depend upon liquid properties. Potentially relevant properties are assumed to be the density, the surface tension, and the liquid viscosity, μ_d. A Z-plot for the Winfrith data is given in Figure 2.3-4, with the upper half giving results from air-driven tests and the lower half giving results for helium-driven tests. P_{50} values were estimated for each series. Data series from the Winfrith tests are summarized in Table 2.3-4 which gives, for each test, the molecular weight of the driving gas (air or helium), the liquid property values assumed in the analysis, and the P_{50} values obtained; liquid properties and the driving gas were the only parameters varied in this data set. (Liquid properties assumed for Wood's Metal are also included in the table for the sake of completeness, but the Winfrith study did not include any Wood's Metal experiments.)

From the properties listed in Table 2.3-4, it is apparent that any differences between the results for the two silicone oils, 200/5 and 200/10, can reasonably be attributed to the viscosity difference. Values of α_μ/n estimated from the P_{50} values obtained for these two liquids are -0.10 for the air-driven data and +0.07 for the helium-driven data. Judging from Figure 2.3-4, the air-driven data seem somewhat more regular for the two oils and may provide a more reliable value than the helium-driven data; certainly the result derived from the air-driven data (a small

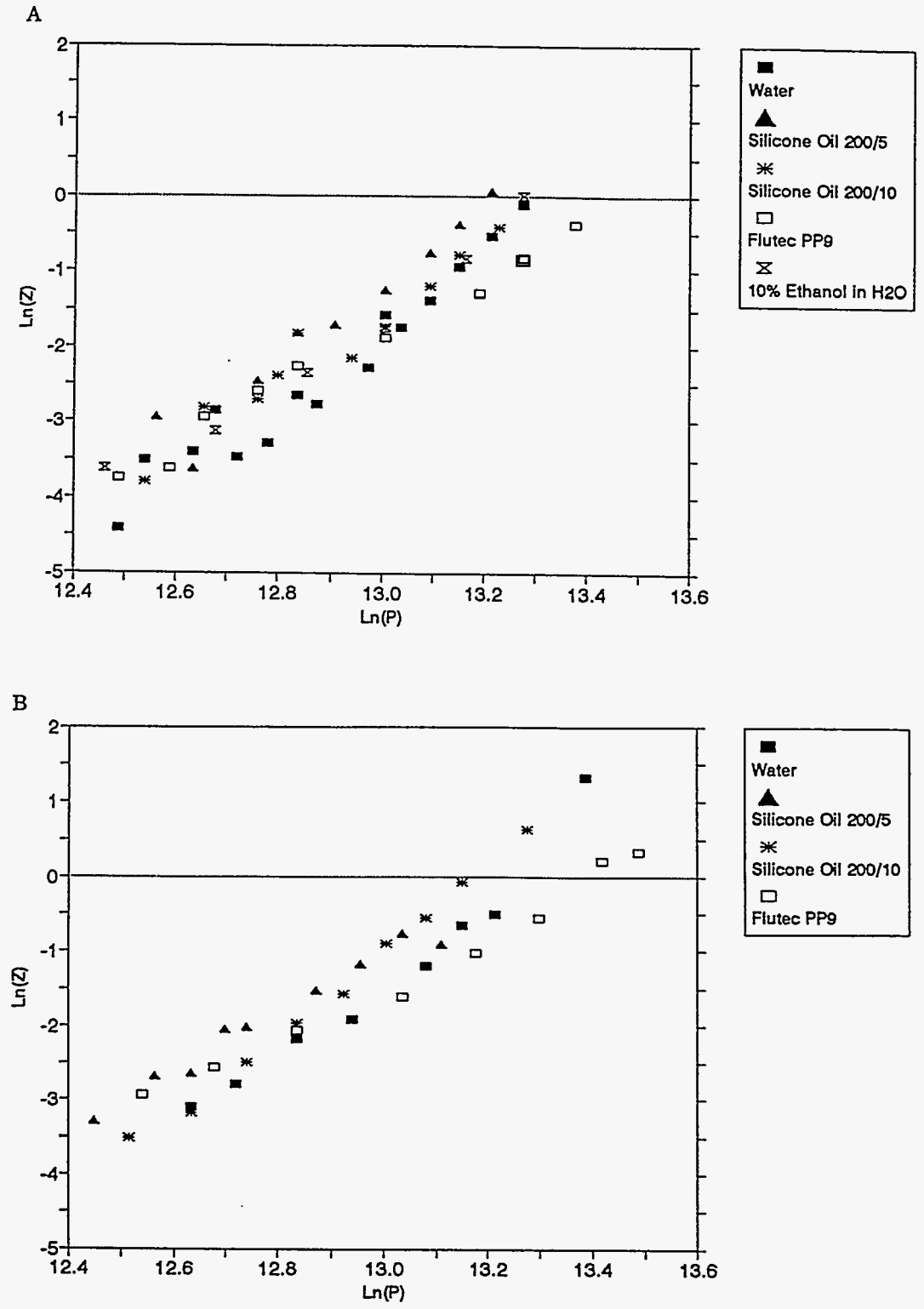

Figure 2.3-4 Z-plots for Winfrith constant-pressure tests. (A), air as blowdown gas; (B), helium as blowdown gas.

negative dependence of dispersal upon viscosity) is more in keeping with physical expectation. All that can really be concluded, however, is that the viscosity effect is quite small.

Table 2.3-4
Fluid Properties and Winfrith Results

Fluid	M_g	μ_d (Pa-s)	σ (N/m)	ρ_d (kg/m^3)	P_{50} (MPa)
Water	28.96	0.001	0.072	1000	0.5987
Si Oil 200/5	28.96	0.0056	0.02	928	0.5435
Si Oil 200/10	28.96	0.0122	0.02	942	0.5897
Flutec PP9	28.96	0.0084	0.019	1988	0.7148
10% Ethanol in H_2O	28.96	0.0016	0.051	980	0.6025
Water	4	0.001	0.072	1000	0.5891
Si 200/5	4	0.0056	0.02	928	0.5551
Si 200/10	4	0.0122	0.02	942	0.5268
Flutec PP9	4	0.0084	0.019	1988	0.6765
Wood's Metal:		0.0016	0.5	9200	

The liquids studied include no pairs which differ only in terms of surface tension; indeed, water and 10% alcohol in water are the only liquids with surface tensions that differ substantially from the others in the Winfrith set. If the viscosity effect is assumed to be zero, comparing the P_{50} data for water and the silicone oils indicates that the surface tension effect is also essentially negligible ($\alpha_\sigma/n \approx -0.04$). If the results for viscosity given above are used to define a range of possible corrections for the viscosity difference between water and the silicone oils, the corresponding range of values for α_σ/n is about -0.20 to +0.06. Again it is difficult to conclude much other than that the effect appears to be rather small. This result suggests that most of the differences between Wood's Metal and water observed in the BNL tests is due to the density difference rather than the surface tension difference, which is again in accord with physical intuition.

Dependence upon Scale. We may attempt to represent the scale-dependence of the dispersal results by defining a nondimensional scale factor S (S = 1 for NPP, S = 0.1 for the SNL tests, S = 1/42 for BNL) and estimating α_s/n values by comparing P_{50} results for analogous SNL and BNL experiments. Unfortunately, these experiments were not completely scaled replicas of one another. In the SNL experiments, both the orifice diameters and the gas volumes differed from the scaled equivalents of any of the BNL tests, and there were other differences in the geometry of the high-pressure parts of the experimental apparatus that could have affected results as well. The SNL Surry experiments included the skirt while most of the BNL Surry data did not, as was noted previously. In what follows, the α_d/n and α_{V_v}/n values obtained previously are used to correct for the fact that orifices and volumes are not scaled replicas of one another, but no correction was attempted for any other differences between the BNL and SNL experimental configurations.

Results are given in the last set of entries in Table 2.3-3. The results depend somewhat upon whether the value of α_{V_v}/n used is that derived from the BNL data or that derived from the SNL data; α_s/n values corresponding to both values of α_{V_v}/n are given. A potentially much more important difference is that the estimated scale effect is quite small, perhaps even zero, for the Surry geometry while it is quite large for Zion. The values of α_s/n given for Zion would imply that driving pressures 2.5 to 3 times as high would be needed to give equivalent degrees of dispersal at NPP scale as is the case at SNL scale (S=0.1). It is also noteworthy that none of the correlations considered in this work predict a negative scale effect upon dispersal (several do predict a significant positive effect), and none predict scale effects to be geometry-dependent except for the Tutu-Ginsberg family of correlations, which in effect define a separate correlation for each cavity geometry.

Much caution is urged in interpreting this result, for several reasons. For example, scaled (S = 0.1 and 0.025) counterpart experiments in the Zion geometry have been performed using thermite melts at SNL and ANL, respectively, with results that appear to be consistent with scale effects being small. Even if the present results represent a valid scale effect in going from S = 1/42 to S = 0.1 with water as the liquid, it may not be valid to extrapolate this effect to actual DCH events in full-scale NPP. In addition, the effect could be an artifact of differences between the experimental configurations used in the SNL and BNL test series, although clear reasons for believing this to be the case have not been identified.

3. Screening of Candidate Correlations

3.1. Approach

The detailed comparisons between candidate correlations and the experimental data base, which are described in Section 4, require a considerable amount of effort. Fortunately, the results of the previous section, summarized in Table 2.3-3, present in a concise form a large amount of information concerning the quantitative dependence of cavity dispersal fractions upon the governing parameters. This information is very useful in screening out unsatisfactory

correlations. The approach involves manipulating the correlation into a form that at least approximates that of Equation (1) and comparing the values of n for the dependence upon driving pressure and the dependence upon α/n for dependence upon other parameters of importance.

Even using this approach, the effort required for a complete evaluation of a correlation may not be trivial, and two additional shortcuts were employed to avoid spending excessive time assessing correlations that really have no chance of being useful. The first shortcut is to note that, according to the results of Section 2.3 and Table 2.3-3, the hole size d_h is a very important parameter governing F_d. Indeed, the fact that α_d/n is of the order of unity means that d_h is as important as the driving pressure in the sense that changing the hole size by a given factor requires a change in the driving pressure by an approximately equal factor (in the opposite direction) in order to obtain an equivalent degree of dispersal, other things being equal. Hence, failure to predict a strong dependence upon d_h will be viewed as fatal, and evaluation of α/n for all parameters will not be needed in such cases, especially in view of the fact that a number of correlations do a good job with respect to d_h.

The other shortcut to be used is based on the fact that several of the correlations to be considered have already been reviewed in the DCH Models and Correlation Document [Ost94], and the physical basis of some of the models and correlations considered there was shown to be unreasonable in several instances. Although no correlation has been rejected solely as a result of the review given in Reference Ost94, considerable use has been made of that work and it is used as additional justification for not performing a full assessment upon correlations which clearly appear to be deficient.

In the next subsection, the approach being used will be illustrated by applying it in some detail to the Whalley-Hewitt correlation. In Section 3.3, results will be summarized for other correlations considered with the presentation being less complete, especially for correlations judged inapplicable.

3.2. Illustrative Example: Screening Assessment of the Whalley-Hewitt Correlation

As given by Whalley and Hewitt [Wha78], the correlation is in the form of a plot of $\epsilon\sigma/\tau\mu_d$ against $\tau\delta/\sigma$, where ϵ is the entrainment rate (kg/s-m^2), σ is the surface tension, τ is the interfacial shear stress, μ_d is the viscosity of the liquid (e.g., the debris), and δ is the thickness of the liquid film. No analytical expression is given; however, it was apparent that the plot levels out with $\epsilon\sigma/\tau\mu_d$ equal to about 5 when $\tau\delta/\sigma$ is greater than about 0.6. This limiting form was shown in Reference Ost94 to be appropriate for most DCH conditions, with some caveats concerning the possibility of overpredicting entrainment when the reactor pressure vessel (RPV) is at relatively low pressure. These caveats were considered to be of only marginal importance in Reference Ost94 and only the limiting form will be discussed in this section, although the full correlation will be briefly examined in Section 4.5.

The interfacial shear stress may be written

$$\tau = \Phi f \rho_g v_g^2/2 \qquad (3)$$
$$f = 0.005$$
$$\Phi = 1 + 360\,\delta/D_c$$

where Φ is the two-phase friction multiplier, f is the single-phase friction factor that would apply for the gas alone if there were no liquid present, ρ_g is the gas density, v_g is the gas velocity, and D_c is the cavity hydraulic diameter. The value of f given in Equation (3), 0.005, was judged in Reference Ost94 to be appropriate for high values of the gas Reynolds number (e.g., $Re_g \geq 10^5$), which should apply for DCH conditions.

As is noted in Reference Ost94, Whalley and Hewitt actually recommend an alternative expression for Φ:

$$\Phi = 1 + 24(\rho_d/\rho_g)^{1/3}\delta/D_c. \qquad (4)$$

This recommendation was based upon the observation that the data base for the correlation in Equation (3) was limited to systems with air at low pressures, and the correlation did not agree well with results for water and high pressure steam, in which the ratio ρ_d/ρ_g was considerably smaller than for water-air data. However, it is the present judgment that the data actually given by Whalley and Hewitt did not appear to support a belief that Equation (4) would give better results when applied to <u>larger</u> values of ρ_d/ρ_g, as are characteristic of DCH conditions. Hence the version given in Equation (3) will be used here. (As was also noted in Reference Ost94, the differences are not large in any case.)

With this value of Φ, the correlation becomes

$$\epsilon = 0.0025 K_c(1 + 360\,\delta/D_c)\,\rho_g v_g^2 \mu_d/\sigma,$$
$$\delta = \frac{V_d}{A_{ww}}. \qquad (5)$$

Here, A_{ww} is the "wetted wall" area assumed to be covered by the liquid film and K_c is a "cavity constant" which is nominally equal to 5 in the limiting form of the correlation as described above (it actually must be "tuned" to give acceptable fits to the data; details will be deferred to Section 4).

At this point, we note that we are interested only in assessing how the correlation depends upon certain experimentally-varied parameters, and will lump all constant numerical factors, physical constants, etc., into a generic constant, C. It is also legitimate to make certain simplifying approximations that keep only leading terms. In this case, we note that $\delta/D_c \geq 0.01$ except when the amount of debris is quite small, and therefore neglect 1 in comparison with $360\delta/D_c$ in Equation (5). The volumetric rate of dispersal of debris then becomes

$$\frac{dV_d}{dt} = -\frac{\epsilon A_{ww}}{\rho_d} \sim -CV_d \frac{\rho_g v_g^2 \mu_d}{\rho_d \sigma D_c}. \qquad (6)$$

Note that, in this approximation, A_{ww} has canceled out, and the Whalley-Hewitt correlation is not very sensitive to what assumptions one makes as to what extent debris is smeared out over cavity surfaces other than the floor.

Next, it is necessary to evaluate $\rho_g v_g^2$ in terms of the experimental parameters. Indeed, since $\rho_g v_g^2$ appears as a very important group in most dispersal and entrainment correlations, its dependence upon relevant parameters is worth keeping in mind.

The gas density in the cavity is equal to MP_c/RT, where M is the gas molecular weight, R is the universal gas constant, T is the temperature, and P_c is the pressure in the cavity. Since $P_v \gg P_c$, where P_v is the vessel pressure, flow out of the vessel is choked and the mean velocity of the gas flowing through the cavity is given by

$$v_g = C_d g(\gamma) \left(\frac{\pi d_h^2/4}{A_c} \right) \frac{P_v}{P_c} \sqrt{\frac{RT}{M}}; \text{ hence}$$

$$\rho_g v_g^2 = \left(\frac{\pi C_d g(\gamma)}{4} \right)^2 \frac{d_h^4}{A_c^2} \frac{P_v^2}{P_c}. \qquad (7)$$

Here C_d is the orifice discharge coefficient for forced flow, A_c is the cavity cross sectional area, and $g(\gamma)$ is a function of the gas specific heat ratio, γ, which actually varies so little with γ that treating it as constant introduces negligible error in conclusions drawn concerning dependence upon the driving gas. With this approximation, it is seen that $\rho_g v_g^2$, and hence the entrainment rate as predicted by the Whalley-Hewitt correlation, does not depend upon either the gas type or the gas temperature. Experimentally, the Winfrith constant-pressure results support this prediction; see Figure 2.3-4, which shows that F_d was virtually the same with air and helium as driving gases, other parameters being equal. (Note that Equation (7) incorporates the assumptions that T and M are the same in both the vessel and the cavity; these assumptions are valid for the experiments with nonreactive low-temperature liquids considered here but neither assumption would be valid in DCH events.)

The quantity $\rho_g v_g^2$ introduces an inverse dependence upon the cavity pressure, P_c. Many of the correlations considered here, including all those assessed in detail in Section 4, share this prediction with the Whalley-Hewitt correlation. This prediction can be very important in DCH analyses, since the cavity is often calculated to pressurize substantially in DCH events, and the latter prediction has been confirmed experimentally. Unfortunately, cavity pressure has not been

varied in any of the experiments which have been performed with low temperature simulants, and the predicted dependence upon P_c has not been verified experimentally.

We next insert Equation (7) in Equation (6), redefine the constant C to include the numerical factors and the function $g(\gamma)$ of Equation (7), and divide through by V_d, which yields

$$\frac{d(lnV_d)}{dt} \approx -C\frac{\mu_d}{\rho_d \sigma D_c}\frac{d_h^4}{A_c^2}\frac{P_v^2}{P_c}. \qquad (8)$$

If we approximate the vessel blowdown as being isothermal, the vessel pressure would decay exponentially, such that P_v would be equal to $P_{0,v}\exp(-t/\tau_b)$, where $P_{0,v}$ is the initial vessel pressure and τ_b is a characteristic time for blowdown given by

$$\tau_b = \frac{V_v}{C_d(\pi d_h^2/4)\, g(\gamma)}\left[\frac{M}{RT}\right]^{1/2}, \qquad (9)$$

where V_v is the vessel volume. Inserting this exponential time-dependence for P_v into Eq. 8 permits integration over the blowdown history to give the fraction dispersed, with the result being of the form

$$F_d \approx 1 - e^{-Y}, \text{ where}$$
$$Y = C\frac{\mu_d}{\rho_d \sigma D_c}\frac{d_h^2}{A_c^2}\frac{P_{0,v}^2}{P_c} V_v\sqrt{\frac{M}{T}}. \qquad (10)$$

Note that the dependence upon gas molecular weight is reintroduced through its effect on the blowdown time, which also introduces the dependence upon gas temperature (not studied experimentally) and upon V_v.

Equation (10) is of the form Equation (1) in Section 2.3 and we may now proceed to make the comparison with the parameter dependencies tabulated in Table 2.3-3.

Pressure Exponent, n. Equation (10) gives n = 2 for Whalley-Hewitt, which is significantly less than the experimental values tabulated in Table 2.3-3. Hence, it will not be expected to predict as steep a dependence of F_d upon P_v as is observed experimentally. Nonetheless, the pressure-dependence is strong enough to be acceptable. (Indeed, the absence of an excessively strong pressure dependence may even prove desirable when calculating entrainment rates at driving pressures much greater than P_{50}; see Section 5.2.)

Dependence upon Orifice Size, d_h. Equation (10) implies $\alpha_d/n = 1$, in excellent agreement with the experimental results.

Dependence upon Gas Molecular Weight. Whalley-Hewitt gives $\alpha_M/n = 0.25$, also in good agreement with the experimental values of about 0.22.

Dependence upon Vessel Volume. The correlation gives $\alpha_{Vv}/n = 0.5$, which is somewhat higher than the value of 0.41 obtained from the BNL experiments and a factor of two higher than the value of 0.25 obtained from the SNL experiments.

Dependence upon Quantity of Debris. Equation (10) indicates that there should be no sensitivity to the amount of debris, in agreement with the single experimental result available.

Dependence upon Liquid Density and Surface Tension. Equation (10) predicts that $\alpha_\rho/n = \alpha_\sigma/n = -0.5$, or $(\alpha_\rho+\alpha_\sigma)/n = -1$, to be compared with the values of -0.6 to -0.7 for the combined density and surface tension effect extracted from the Wood's Metal data with the water data. Thus, Whalley-Hewitt would be expected to overpredict the difference between the water and Wood's Metal results. If the inferences drawn from the analysis of the Winfrith data presented in Section 2.3 are accepted, the problem appears to be that the dependence upon surface tension is overpredicted, while the dependence upon liquid density may be about right.

Dependence upon Liquid Viscosity. Equation (10) implies a substantial positive effect of increased liquid viscosity upon dispersal, ($\alpha_\mu/n = +0.5$), in disagreement with physical expectation and the experimental results, both of which would lead one to expect either a negligible viscosity effect or a small negative effect. This problem will require further consideration if the Whalley-Hewitt correlation is to be used (see Section 4.5).

Dependence upon Geometric Scale. The scale-dependent quantities appearing in Equation (10) are in the form of the group $d_h^2V_v/(D_cA_h^2)$, which is dimensionless. Thus, the correlation predicts no dependence of F_d upon scale. This is in reasonable agreement with the results for Surry geometry, but not the Zion results, if one interprets the SNL-BNL differences in terms of scale effects as described in Section 2.3.

There is, however, one additional complication that requires discussion in interpreting the BNL-SNL differences in terms of scale effects. As we have seen, the Whalley-Hewitt correlation implies a significant negative dependence upon cavity pressure ($\alpha_{Pc}/n = -0.5$). Although P_c was not varied as an experimental parameter, the atmospheric pressure at SNL (0.083 MPa) differs sufficiently from the BNL value (0.1 MPa) that the correlation predicts P_{50} values for SNL experiments should have been about 0.911 times the BNL values, other things being equal. No correction was made for this difference in extracting α_S/n values from the BNL/SNL comparisons in Section 2.3, since no experimental estimates of α_{Pc}/n could be obtained and only experimentally-demonstrated dependencies were used to apply corrections for the differences between the SNL and BNL experimental configurations. Hence, the Whalley-Hewitt correlation predicts that the SNL-BNL comparisons should have yielded a small apparent scale effect, equivalent to $\alpha_S = +0.065$, when the data are analyzed without allowing for the difference in P_c values. This correction slightly worsens the agreement between the correlation and the experiment.

3.3. Summary of Screening Assessment Results.

The approach described above in connection with the Whalley-Hewitt correlation was applied, with varying degrees of completeness, to all the correlations under consideration here (except that the Tutu correlation is not treated for reasons noted below). It must be acknowledged that the development is not always quite as neat as was possible for the Whalley-Hewitt correlation. In the case of the Tutu-Ginsberg correlations, for example, the degree of algebraic simplification needed is greater than in the case of the Whalley-Hewitt correlation (or at least it is less transparent as to when the simplifications will be valid).

For most of the correlations considered, the various parameter dependencies are evaluated and compared to the experimental results of Table 2.3-3 only to the degree needed in order to justify a decision as to which correlations should be considered in detail in Section 4. Some results are given in Table 3.3-1, which recapitulates the experimental results of Section 2.3 and summarizes the predicted dependencies for three correlations (Whalley-Hewitt, Levy, and Ishii) which were evaluated relatively completely.

Note that the next-to-last block in the table, representing scale effects (α_s/n), includes parenthetic entries labeled "apparent". They represent the correction for the SNL-BNL difference in P_c; that is, they are the correlations' predictions as to what the apparent experimental value of α_s should have been when analyzed without taking into account the difference in P_c. If the correlation's predictions as to the effect of cavity pressure are accepted as valid, it would be these "apparent" values of α_s which should be compared to the experimental values. The last block in the table gives the α/n values for cavity pressure P_c predicted by the correlation; there are no experimental values with which to compare for this parameter.

Correlations described in Reference Ost94 are discussed first and are followed by consideration of the Levy, Tutu, and Ishii correlations. For those correlations which survived the screening stage and were assessed in detail, the mathematical form of the correlations are presented in Section 4. The mathematical form of the other correlations is summarized in Reference Ost94, which also gives the original references.

Henry Film Model. This model was based upon the assumption that there are two processes by which molten debris is driven out of the cavity, one involving entrainment and the second involving cavity pressurization forcing the melt out as a relatively coherent mass (film flow). Only the first (entrained) component was assumed to undergo efficient interaction with gas and thereby contribute to DCH. The purpose of the analysis was to estimate the fraction of the debris which could be entrained during the time debris was ejected by film flow, with entrainment (and therefore debris addition to the DCH event) being terminated once melt expulsion was complete.

Table 3.3-1

Comparison of Experimental Parameter Dependencies with Correlation Predictions

Symbol	Experimental Results		Correlations			
	Cases	Ave. ± S.D.	Whalley-Hewitt	Levy	Ishii-Film	Ishii-Entr.
n	SNL Surry	10.6 ± 2.9	2.0	4.6	1/2	2.31
	All Others	5.15 ± 1.07				
α_d/n	All	1.03 ± 0.24	1.0	1.13	0	1.10
α_M/n	All	0.22 ± 0.04	0.25	0.217	1	0.083
α_{Vv}/n	All	0.41 ± 0.18	0.5	0.217	2	0.433
	BNL	0.42 ± 0.024				
	SNL	0.25 ± 0.03				
α_{Vd}/n	SNL Zion	0.041	0.0	(Weak)	-2	0
$(\alpha_\rho+\alpha_\sigma)/n$	Surry	-0.703 ± 0.025	-1.0	-0.543	-1	-0.499
	Zion	-0.613 ± 0.012				
α_μ/n	Winfrith Air	-0.105	+0.5	-0.057	0	-0.08
	Winfrith He	+0.067				
α_σ/n	Winfrith Air	-0.20	-0.5	-0.217	0	-0.400
	Winfrith He	+0.06				
α_S/n	Surry, BNL α_{Vv}	-0.05 ± 0.06	0.0 (+0.065)*	+0.217 (+0.305)*	0 (~0)*	+0.368 (+0.437)
	Surry, SNL α_{Vv}	-0.12 ± 0.05				
	Zion, BNL α_{Vv}	-0.42 ± 0.09				
	Zion, SNL α_{Vv}	-0.50 ± 0.09				
α_{Pc}/n	--- No Data ---		-0.5	-0.674	~0	-0.534

*Apparent value of α_S/n predicted if effect of P_c is ignored in SNL-BNL comparisons.

In the experimental data considered in this work, there is no way to distinguish melt exiting the cavity as a coherent film from melt swept out following entrainment, and both mechanisms should be considered. The entrainment mechanism assumed by Henry was Fauske's application of the Ricou-Spaulding jet entrainment model, which is considered below. Here we consider the film flow ejection mechanism.

For film flow, the model gives a characteristic time for dispersal from the cavity, τ_{disp}, not an expression for F_d or the dispersal rate. It is reasonable to assume that the fraction dispersed by this mechanism will be a function of the ratio τ_b/τ_{disp}, with this function approaching simple proportionality at low values of F_d. In the model, τ_{disp} varies as $P_v^{-1/2}d_h^{-1}$, while τ_b is independent of P and varies as d_h^{-2} as before. Thus, we expect F_d to vary as $P_v^{1/2}d_h^{-1}$. These dependencies correspond to $n = 1/2$ and $\alpha_d/n = -2$. The pressure dependence implied is much too weak to give a reasonable representation of the experimental results, and the strong inverse dependence upon d_h predicted is in gross disagreement with the experimental trends. In addition, Reference Ost94 raised serious questions concerning this model on quite different grounds related to the assumptions used in its derivation. Hence it will not be considered further here.

Ricou-Spaulding Model. As originally described by Ricou and Spaulding, this model treated the entrainment of ambient gas by a gas jet, and was shown to provide a good description of this phenomenon. Fauske adapted it to treat the entrainment of molten corium into a gas flow. Reference Ost94 raised serious questions concerning the validity of this approach, on the grounds that entrainment of liquid into a gas flow would be expected to involve different physical phenomena from the entrainment of another gas into the jet.

Here we note that Reference Ost94 showed that application of this model to the debris entrainment problem predicts that, for a given gas and geometry, the mass rate of liquid entrainment is proportional to the mass flow rate of gas. This implies that the total mass entrained is proportional to the total mass of blowdown gas, independently of the rate of gas delivery and, hence, independently of d_h. Within the ideal gas approximation, total gas mass is proportional to P_v. Hence, we have $n=1$ and $\alpha_d/n = 0$. The inability to reproduce the important dependence upon d_h, together with the criticisms given in Reference Ost94, is sufficient reason to give no further consideration to this model.

Whalley-Hewitt Correlation. The evaluation of this model has already been discussed in Section 3.2, and the resulting dependencies are tabulated in Table 3.3-1. Despite some problem areas, its performance in the screening is seen to be relatively good in comparison with the two models just considered (and several others which follow), and it will therefore be included in the detailed assessments of Section 4.

Kataoka-Ishii Model. The version of this model described in Reference Ost94 was a predecessor to the model referred to as "the Ishii model" in the present work and which is described in Reference Ish91. The latter was developed specifically for application to the cavity dispersal problem while the former was not and, in addition, Reference Ost94 notes that applying the former version to the cavity problem would involve some practical difficulties.

Hence, it is not considered here, and the version of Reference Ish91 is considered instead; it is discussed below.

Entrainment in CORDE. The CORDE models have been included in some earlier versions of CONTAIN, and Reference Ost94 considers the portions related to entrainment and offers some criticisms that cast doubt upon the physical basis of the model. Here we simply add the observation that Reference Ost94 showed that this model, like the model based upon the Ricou-Spaulding jet entrainment model, predicts that entrainment rate will be proportional to the mass flow rate of the gas. Hence, the same conclusions apply; i.e., $n=1$ and $\alpha_d/n = 0$, and this model need not be considered further.

Slip Models. Reference Ost94 considers a family of models designated "slip models" in which it is assumed that dispersal is governed by the rate at which debris moves out of the cavity with a velocity v_d given by $v_d = v_g/\phi$, where ϕ is a slip factor. Reference Ost94 notes that these models also lead to the prediction that dispersed mass will be proportional to gas flow rate, which again leads to the unsatisfactory prediction that $\alpha_d/n = 0$. Slip models will therefore be considered no further.

Kelvin-Helmholtz Model. Like the preceding models, this model also leads to the prediction of entrainment rates proportional to mass flow rate of the gas and, hence, the prediction $\alpha_d/n = 0$, which is viewed as being unacceptable.

Kutateladze Criterion. The Kutateladze criterion is actually a criterion for the onset of entrainment, not a correlation for F_d or dispersal rate. It typically takes the form of assuming that entrainment will begin when the Kutateladze Number, Ku, exceeds some critical value, commonly taken to be about 10. Here, Ku is defined by

$$Ku = \frac{\rho_g v_g^2}{\sqrt{g \rho_d \sigma}}, \qquad (11)$$

where g is the acceleration of gravity. (Some investigators define Ku to be the square root of the quantity defined by Equation (11).)

The Kutateladze Number includes the quantity $\rho_g v_g^2$, which varies as $P_v^2 d_h^4$. This dependence implies $\alpha_d/n = 2$, which is too strong a dependence upon d_h. However, if we assume the dispersed fraction is related to the product of Ku and the blowdown time, $Ku\tau_b$, we may note that

$$Ku\tau_b \propto \frac{P_v^2 d_h^2}{\sqrt{g\rho_d\sigma}} V_r \sqrt{\frac{M}{T}}. \qquad (12)$$

Equation (12) shows a number of promising dependencies, including meeting the important criterion that α_d/n should be of the order of unity. However, Equation (12) does not define a complete correlation for either entrainment rates or F_d and developing one would require additional modeling effort, which would exceed the scope of the present assessment task. Hence it will not be considered further here.

Tutu-Ginsberg Correlations. These correlations (identified as "the BNL correlations" in Reference Ost94) take the form of a relatively complex function, f_{TG}, of an argument X which is itself a function of the experimental variables. Although the function is of the same form for all cavity geometries considered (see Section 4.2), it includes 13 constants which must be determined separately for each geometry by least-squares fitting to the data. The relative complexity of f_{TG} makes it difficult to define a value of the pressure exponent, n, but does not affect the ability to define the α/n, which is determined by how X depends upon pressure and the other parameters. However, X reduces to the form assumed for the argument of f in Equation (1) of Section 2.3 only in certain limiting cases. Some numerical experimentation indicates that the limiting form is generally approached except in one instance that is insensitive to whether it is achieved. Hence, meaningful α/n values might be defined using the limiting forms.

Obtaining the limiting α/n values is somewhat tedious, however, and it has been done only for α_d/n and the scale dependence, α_s/n. For four of the five correlations (Surry with no cavity structure and with the skirt only, Zion, and Watts Bar) α_d/n values range from 0.91 to 1.08, in good agreement with the experimental behavior. For the Surry cavity with all structure present, $\alpha_d/n = 1.37$; this difference is still not large and cannot be considered "disagreement" with the results of Table 2.3-3 in any case, since the latter does not include data for the Surry cavity with all structure.

For the Zion correlation, $\alpha_s/n = 0$ and it is small, 0.041, for Surry with the skirt only, even in the limiting form. (This correlation is one instance in which the limiting form may not be a good approximation, in which case the scale dependence would be even smaller). For Surry with no structure and with all cavity structure, $\alpha_s/n = 0.147$ and 0.135, respectively, and it is equal to 0.112 for Watts Bar. Thus increasing dispersal with increasing scale is predicted. Although the values of α_s/n cited are not large, they can cause significant effects when large extrapolations are made with respect to scale.

The Tutu-Ginsberg correlations were selected for inclusion in the more detailed assessments of Section 4. Their inclusion is based in part upon the results summarized above for α_d/n and α_s/n, and in part upon results reported previously showing these correlations give generally good fits to the dispersal data [Tut90b].

combined film plus entrainment correlation and the entrainment-only version), and the Whalley-Hewitt correlation. The correlations will be considered in the order named. The Levy correlation is discussed in more detail than the others in order to illustrate the methodology and to make some very important points that apply more generally.

4.1. The Levy Correlation

The Levy correlation for the fraction dispersed, F_d, takes the form of a correlation for an "entrainment parameter", Y, which is defined by

$$Y=\ln\left[\frac{\sqrt{1+300\delta_0/D_c}-1}{\sqrt{1+300\delta/D_c}-1}\cdot\frac{\sqrt{1+300\delta/D_c}+1}{\sqrt{1+300\delta_0/D_c}+1}\right],\quad F_d=\frac{\delta}{\delta_0} \tag{13}$$

Here δ is the liquid film thickness and the subscript 0 refers to initial values. In the form assessed here, the correlation for Y is given by

$$Y = K_c f_1 f_2 \frac{0.36 V_v}{A_h\sqrt{RT_0}} Eu_0^{2.3}\left[\frac{2P_c}{\sigma}\right]\sqrt{\frac{2P_c}{\rho_f}}\left[\frac{\mu_g}{\mu_f}\right]^{0.26},\ \textit{where}$$
$$f_1 = \left[\frac{d_{s,h}/S_s}{d_h/S}\right]^2\sqrt{\frac{MT_{0,s}}{M_s T_0}},\ f_2=\frac{\rho_{s,d}}{\rho_d}. \tag{14}$$

Here $A_h = \pi d_h^2/4$, Eu is the Euler Number and is equal to $\rho_g v_g^2/2P_c$, the subscript 0 represents initial values (i.e., at the start of blowdown), and the subscript s denotes values for a standard case defined as discussed below. The cavity coefficient, K_c, is a dimensionless constant whose value is chosen by fitting to experiment and which is expected to be different for different cavity geometries. The correlation does include some explicit dependence upon cavity geometry, since the gas velocity v_g is to be obtained by dividing the volumetric gas flow rate by the cavity cross sectional area, A_c. However, Reference Lev91 implies that this dependence should not be expected to capture all the effects of different cavity geometries, and that K_c would likely have to be determined separately for each geometry of interest.

The factors f_1 and f_2 appearing in Equation (14) deserve some comment. As originally derived by Levy, the correlation did not include these factors. However, it was found that the original form of the correlation overpredicted the hole size effect and underpredicted the dependence upon gas molecular weight. Hence, f_1 was introduced to reduce the dependence upon d_h and strengthen the dependence upon M. These corrections were introduced in the form of a ratio of the actual values to the value assumed in a standard reference case in order to preserve nominal dimensional consistency. Note that in the factor including the diameter ratio in f_1, the intent is to use the ratio of the scaled diameters, and hence the scale factors S and S_s appear. The choice of reference case does not matter except that it affects the value of K_c required to obtain a fit to the experimental data; once defined, changing the standard case would

require a corresponding change to K_c. (In implementing the correlation in CONTAIN, the reference values would be hard-wired while the user would be allowed to specify K_c, with default values being provided.)

Levy compared the correlation (including f_1 but not f_2) with the BNL data for Surry and the SNL data for Zion, but he did not have the BNL Zion data and the SNL Surry data available to him. He also compared the correlation with the BNL data for Watts Bar. With the correction factor f_1 included, he found the correlation did a good job of allowing for the effects of driving pressure, driving gas molecular weight, and orifice size d_h. However, he found that the correlation badly overpredicted the dispersal of Wood's Metal when the value of K_c was based upon fitting to the water data; that is, the difference between the behavior of water and that of Wood's Metal was much greater than predicted by the correlation. (Note that, without f_2, $(\alpha_\rho+\alpha_\sigma)/n$ for the Levy correlation would be -0.326 rather than -0.543 in Table 3.3-1, and substantial underprediction of the difference between water and Wood's Metal would be expected.)

In an attempt to bring the water and Wood's Metal data together, Levy experimented with introducing the correction factor f_2, in order to enhance the dependence upon ρ_d. He found that this procedure gave good results for Watts Bar. For Surry, it improved the fit considerably but there was still a substantial tendency to overpredict the Wood's Metal results, if the K_c values derived from the water data were used. Levy did not endorse use of this ratio and, in most of the work reported in Reference Lev91, the f_2 factor was not used. Instead, separate values of K_c were defined for water and Wood's Metal; e.g., K_c was 0.8 for water and 0.016 for Wood's Metal in the fit to the Surry data set.

It is the present view that it would be undesirable to use a correlation in which the appropriate value of K_c depended strongly upon the fluid, since it is then quite unclear how the user is supposed to decide on what value to use for corium. Hence, the f_2 factor was included in the correlation as it has been evaluated here. Note that this means that the correlation considered is not the standard "Levy correlation" as described in Reference Lev91.

Physically, it should be noted that the need to incorporate "correction factors" such as f_1 and f_2 means that the correlation does not actually provide a complete description of the physics. Note, for example, that the various reference values could actually be incorporated into the constant K_c, which would mean that K_c would no longer be dimensionless. A correlation which requires empirical fitting of a <u>dimensioned</u> constant cannot be complete.

It is the present view that, if this limitation of the Levy correlation were to be considered fatal, applying equal rigor to other correlations would eliminate them all, except for models and correlations that give a very poor fit to the data. Nonetheless, the need to include such empirical "correction factors" does raise a strong caution to the user.

In the present work, the correlation was first evaluated by comparing with the SNL and BNL data for both the Surry and Zion geometries, using the K_c values and standard values ($d_{,,}$

etc.) given in Lev91, and including the f_1 and f_2 factors. At this point, it is necessary to consider the practicalities of how the results should be presented. The simplest and most intuitive approach is to simply plot the predicted and experimentally observed values against F_d, as is done in Figure 4.1-1 for some selected BNL results involving dispersal of water from the Surry geometry cavity. It is apparent that the correlation does a good job of capturing the dependence upon driving pressure, hole size, and identity of the driving gas, as would be expected from the results in Table 3.3-1. One systematic deviation that is apparent is that, as P_v increases to values well above P_{50}, the predicted values of F_d approach unity much more rapidly than do the experimental values. This behavior was common to all the correlations considered here with the exception of the Tutu-Ginsberg correlations.

The problem with the approach to assessment illustrated in Figure 4.1-1 is that one can consider only a few data series at a time, and with 35 data series and five correlations to consider in detail the presentation of results gets a little out of hand. (However, plots of this kind have been generated in a Quattro Pro spreadsheet and examined visually for most of the data series for all the preferred correlations, in order to guard against surprises.)

Another approach is to use a "scatter diagram" in which the observed value of F_d is plotted against the predicted value of F_d. A perfect correlation would result in all values falling on the principal diagonal. In this type of plot, complete success is obvious even when a large number of data series are plotted together; when success is less complete, more detailed evaluation may be needed in order to determine which data series are causing the trouble. When the correlation does a good job of bringing together data from different series, but the shape of the F_d versus P_v curve is not a good fit, the scatter plot presents a nonlinear pattern with points corresponding to different series being close to one another, but not necessarily close to the diagonal.

In Figure 4.1-2, a scatter plot is presented for the same data series in the BNL Surry data set as were plotted in Figure 4.1-1. It is seen that the trend of the data is pretty well along the diagonal, and that points for different data series show little tendency to separate, meaning the parameter variations defining the different series are well accounted for. On the other hand, there would appear to be considerable scatter, perhaps more than one would anticipate from Figure 4.1-1. One reason is that, due to the steepness of the F_d versus P_v curves, scatter plots tend to amplify the deviations, since it is the F_d values that are being compared. This tendency must be kept in mind when using scatter plots to evaluate the quality of the correlation.

When disaster does strike, the scatter plots reveal it very clearly. Figure 4.1-3 provides a scatter plot of the complete data set. The BNL Surry data and the SNL Zion data fall more or less along the diagonal, albeit with considerable scatter. However, the SNL Surry data and the BNL Zion data cling to the borders of the plot. The results show that the SNL Surry data are substantially overpredicted, while the BNL Zion data are underpredicted to an even greater extent. In Figure 4.1-4, these trends are illustrated more directly by comparing the predicted F_d versus P_v curves with the experimental values for a few data series from the SNL Surry and BNL Zion data sets.

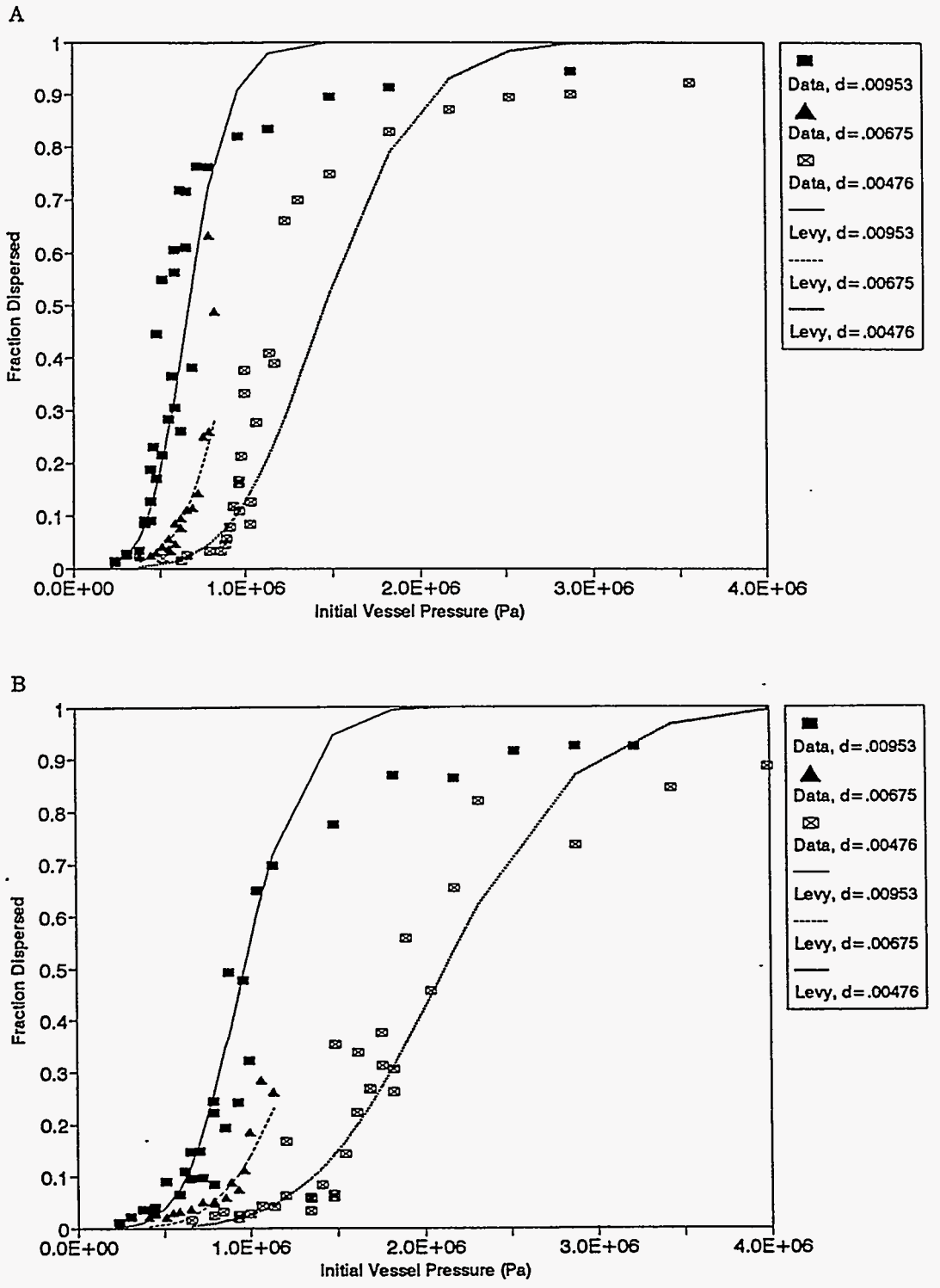

Figure 4.1-1 F_d vs $P_{o,v}$ for Levy correlation and data, BNL, Surry geometry, water as fluid, effect of d_h. (A), air as driving gas; (B) helium.

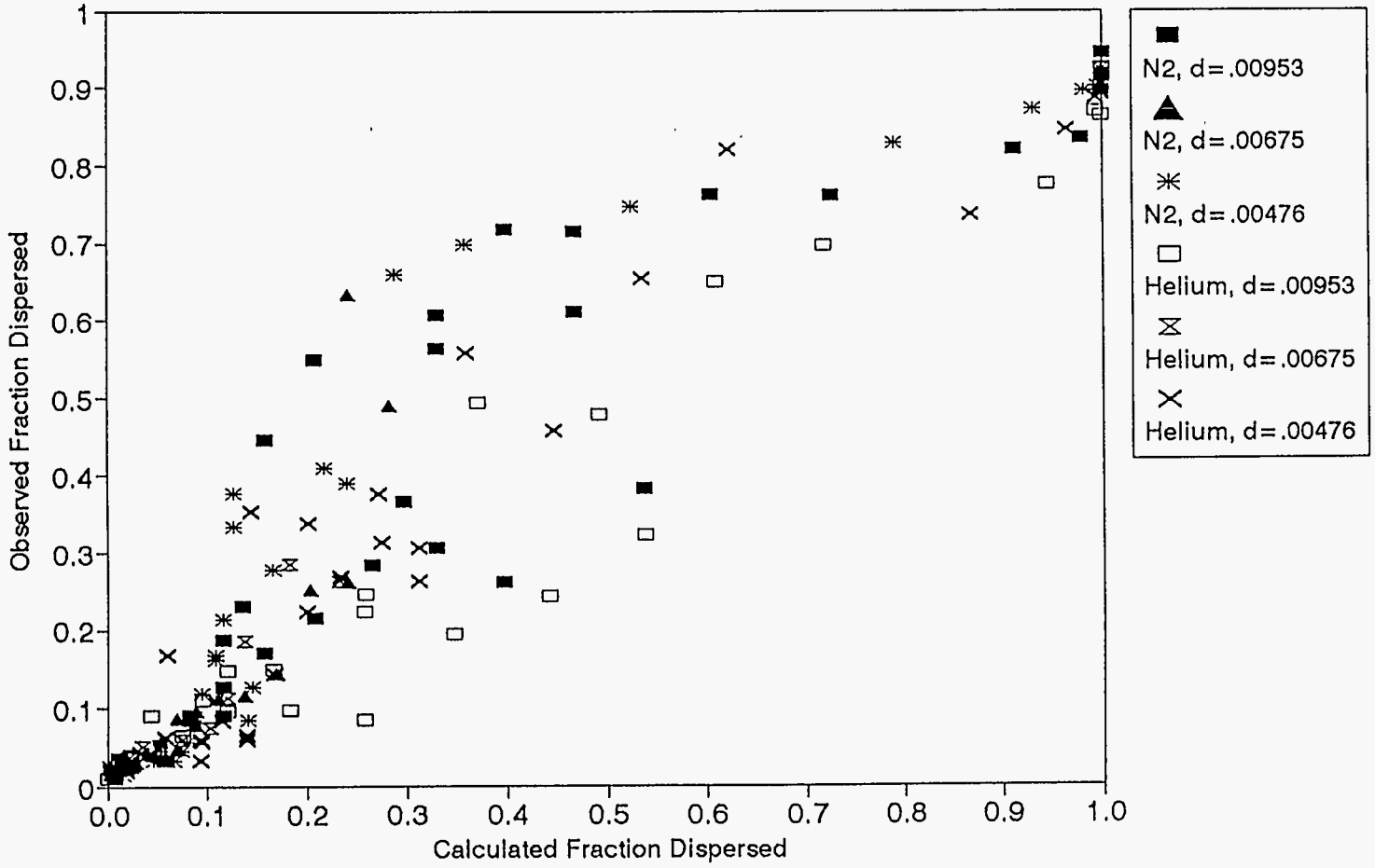

Figure 4.1-2 Scatter plot (i.e., experimental vs predicted values of F_d) for data of Figure 4.1-1

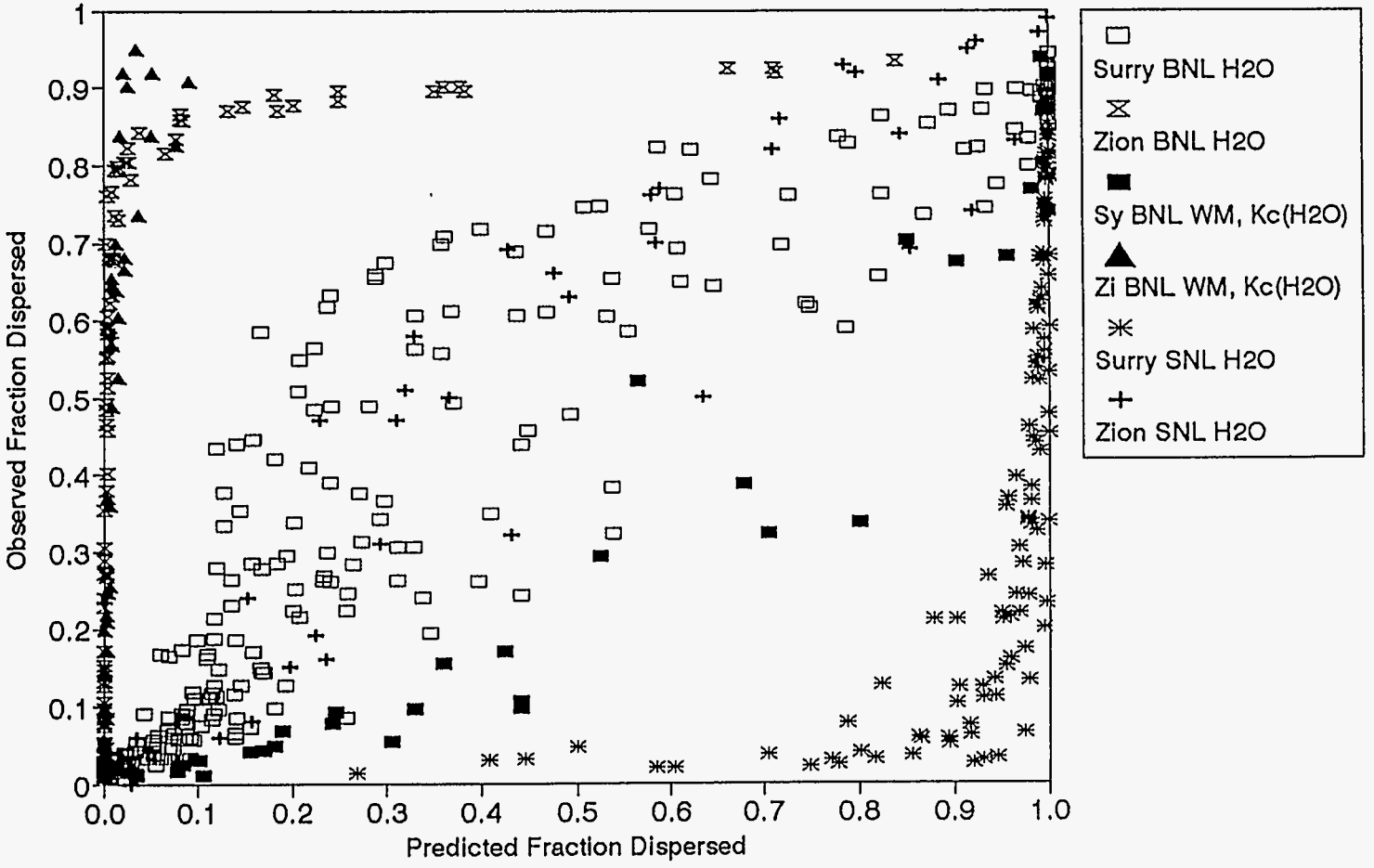

Figure 4.1-3 Levy correlation scatter plot for complete data set

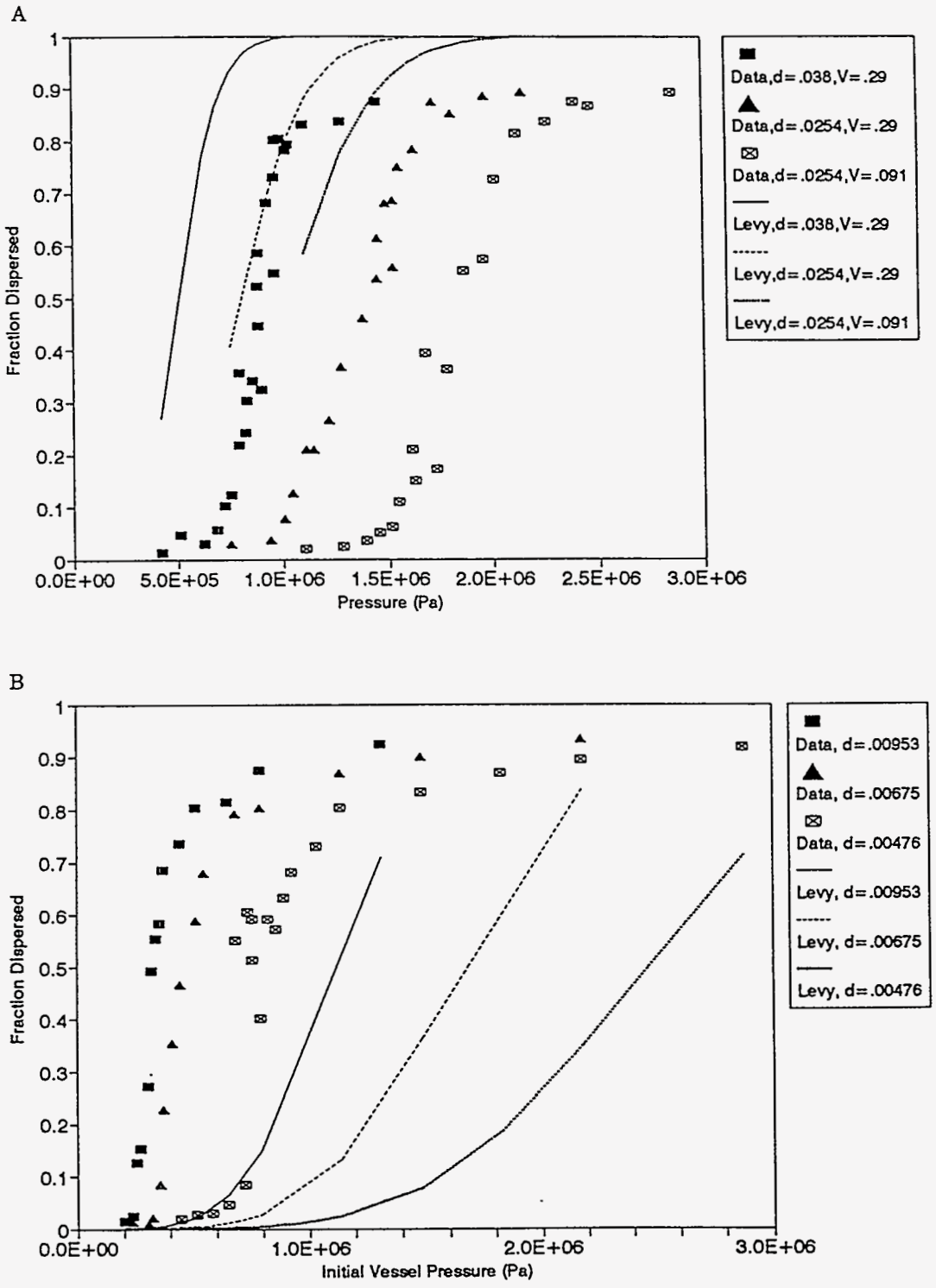

Figure 4.1-4 Levy correlation and data for selected series. (A): SNL, Surry, water, air; (B): BNL, Zion, water, N_2

The explanation for this behavior is quite simple and not very reassuring. The Surry K_c value was determined by fitting to the BNL data while the Zion K_c value was determined by fitting to the SNL data. Thus, it appears that the K_c values determined at BNL are inapplicable to the SNL data in the same geometry, and vice versa. Referring back to Table 3.3-1, we note that the experimental α_s/n values imply a negligible or weakly negative scale effect for Surry and a strongly negative scale effect for Zion, while the Levy correlation implies a fairly significant positive scale effect. Thus, one might expect that fitting the correlation to the BNL data would result in overpredicting the SNL data, while fitting the correlation to the SNL data would underpredict the BNL data, with the errors being larger for Zion than for Surry. Qualitatively, at least, these predictions are well borne out by the results presented here.

Obviously this result is of concern because a fundamental goal of developing correlations of this type is to permit the application of dispersal data obtained at small scales to predict dispersal behavior at NPP scale. If the difference in scale between the BNL and SNL experiments (i.e., a factor of 4.2) is sufficient to derail the correlation, one cannot have much confidence in applying it at NPP scale, no matter how nicely it predicts the results of varying P_v, d_h, etc., at some fixed small scale.

As was discussed in Section 2, there are sufficient differences between the BNL and SNL experiments that it is not clear that scale distortions are responsible for the effects described here. If other factors are responsible, the correlation may still be useful for predicting NPP events. However, it would remain necessary to define an appropriate value of K_c. At present, there appears to be little basis for deciding whether K_c values derived from the BNL or the SNL data sets are more appropriate. In order to proceed further, there seems to be little choice but to fit the correlation separately to the BNL and SNL data sets, even though this may do some violence to the spirit of the correlation.

Of course, one could treat the inability of the correlation to correlate both the BNL and SNL data with the same value of K_c as a fatal error and therefore discard the correlation. Unfortunately, this criterion would require discarding all the correlations considered here with the possible exception of Whalley-Hewitt, which will be seen in Section 4.5 to do a reasonable job of correlating both the SNL Surry data and the BNL Surry data with the same value of K_c. It does not succeed in doing so with the Zion geometry data, however.

Hence the decision was made to define four separate values of K_c; i.e., one each for BNL Surry, BNL Zion, SNL Surry, and SNL Zion. Separate values were not defined for water and Wood's Metal in fitting the BNL data sets. In fitting the BNL data sets, it was noted that there were many more data points for water than for Wood's Metal, and that the latter would have relatively little influence on the overall result if each data point were weighted equally. This result was considered undesirable, since Wood's Metal physical properties more closely resemble those of molten corium than do the physical properties of water. Hence the fitting procedure was modified to assign equal weight to the Wood's Metal data as a whole and the water data as a whole.

A scatter diagram for the complete set is presented in Figure 4.1-5. Although there is more scatter than one might wish, all the data sets now clearly do trend along the diagonal. It is also apparent that, in the BNL data sets, fitting the Wood's Metal data (closed symbols) and the water data (open symbols) introduces some spread in the data, in that the Wood's Metal data tend to fall below the diagonal (overprediction of F_d) and the water data above the diagonal. However the effect is not dramatic. The degree to which the two liquids can be simultaneously correlated is further examined in Figure 4.1-6, which presents F_d versus P_v plots for selected BNL Surry water and Wood's Metal data series. The tendency to underpredict water and overpredict Wood's Metal somewhat is again apparent. However, it is also clear that the correlation captures most of the water-Wood's Metal difference.

Though it is not very apparent in Figure 4.1-5, more detailed study of the results showed that the correlation did a significantly better job of correlating the water and Wood's Metal results in the Zion geometry than it did for the Surry geometry, a trend which is consistent with the α/n data that were summarized in Table 3.3-1. It may be recalled that Levy found that the correlation (with f_2 included) was also successful in correlating water and Wood's Metal data in the Watts Bar geometry. Thus, the inclusion of f_2 yields a correlation which performs well in this regard in two of the three cavity geometries studied, and is only somewhat poorer in the third (i.e., Surry) geometry. Use of the f_2 factor is definitely recommended.

In Figure 4.1-7a, a scatter plot for the Levy correlation as fit to the SNL Surry data is presented. It is seen that the correlation does a very good job of bringing together five of the six data series. The pattern is nonlinear, because the Levy correlation cannot completely reproduce the very steep F_d versus P_v experimental curves of the SNL Surry data. The series with helium as the driving gas and the large (0.038 m) value of d_h does not fall in line with the others. This behavior was observed with all correlations examined; i.e., no correlation was found to bring this data series together with the other five. Some experimental anomaly may be involved, although none has been identified.

Experimental and predicted F_d versus P_v plots are compared in Figure 4.1-7b. It is apparent that neither the failure to fit the exact shape of the curves nor the failure to fit the one "discordant" series is very severe. The steepness of the curves exaggerates the differences in the scatter plot.

In Figure 4.1-8a and -b, scatter plots for the fits to the BNL Zion and SNL Zion data, respectively, are presented. Both data sets trend along the diagonal reasonably well, in contrast to the nonlinear pattern observed for the SNL Surry data set. There definitely do appear to be differences between the response of the Surry and the Zion cavity geometries, at least in the SNL data. Note also that, in the SNL Zion data set, the correlation predicts that F_d depends very little upon the amount of liquid initially present, in agreement with the data.

In Table 4.1-1, a summary is given of data for the standard error of estimate, σ_{est}, which is defined as

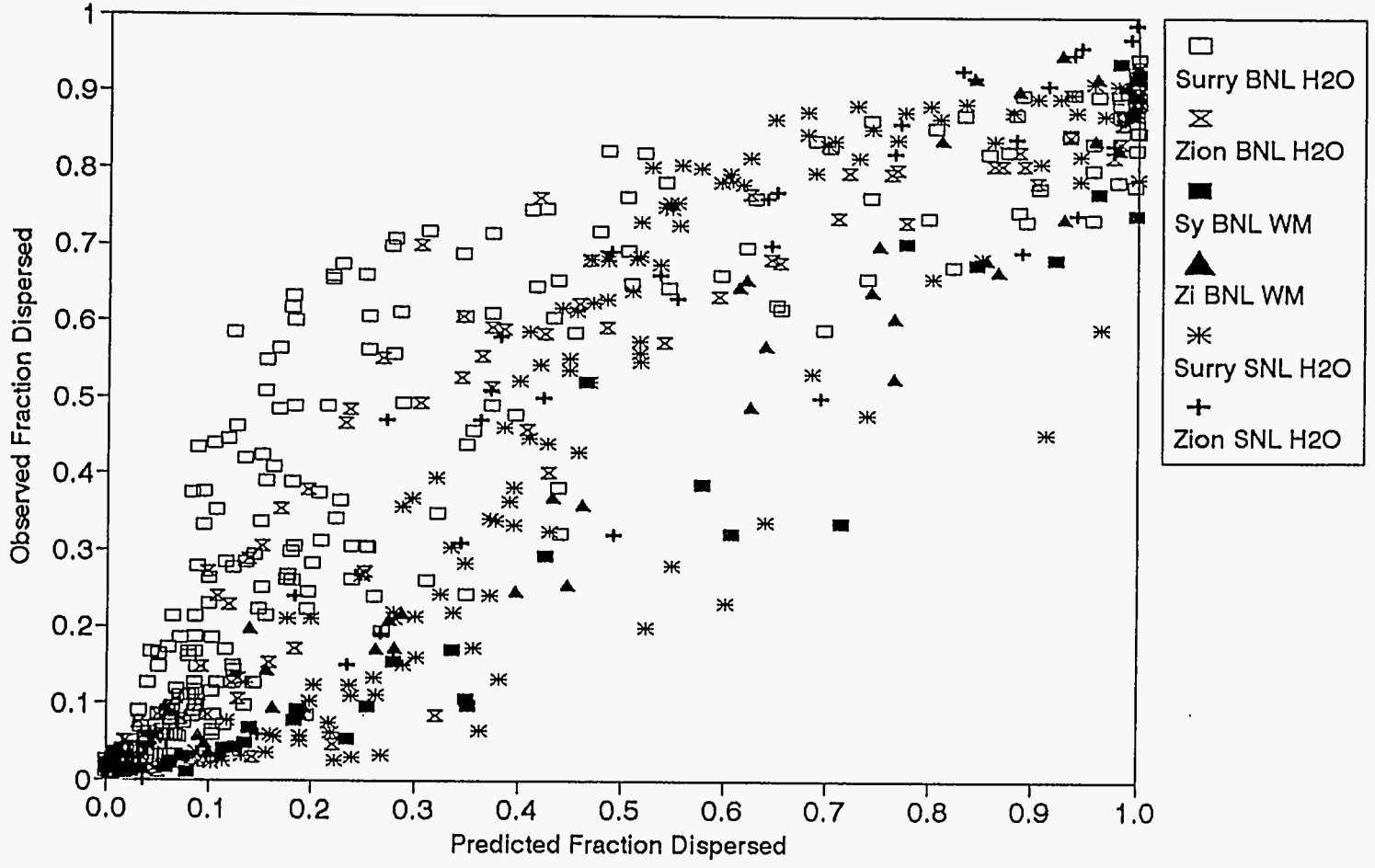

Figure 4.1-5 Scatter plot for Levy correlation, complete data set, K_c fir separately for SNL and BNL data, common K_c for water and Wood's Metal

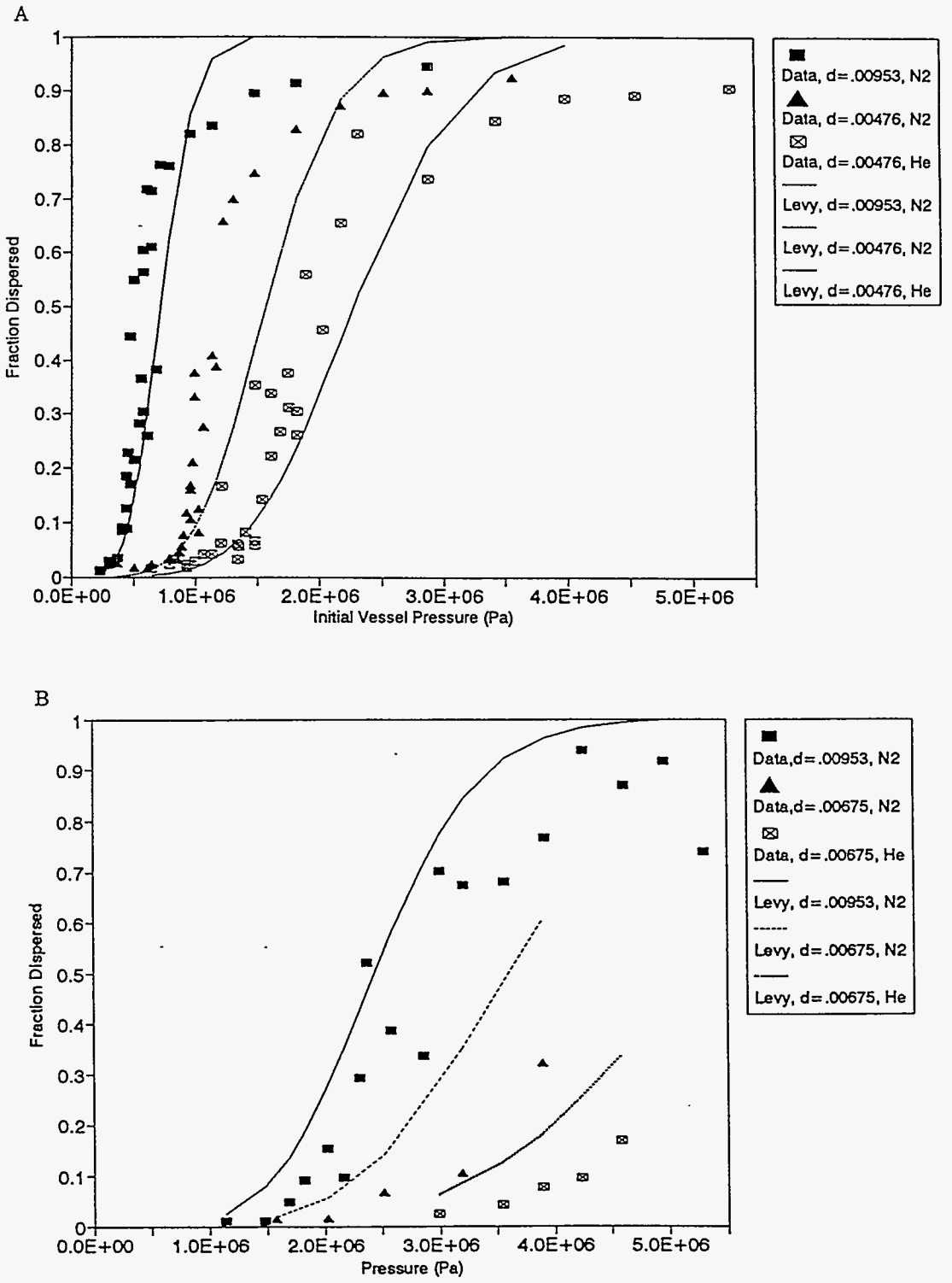

Figure 4.1-6 Levy correlation for selected BNL Surry data series with common K_c for water and Wood's Metal: (A), water; (B), Wood's Metal

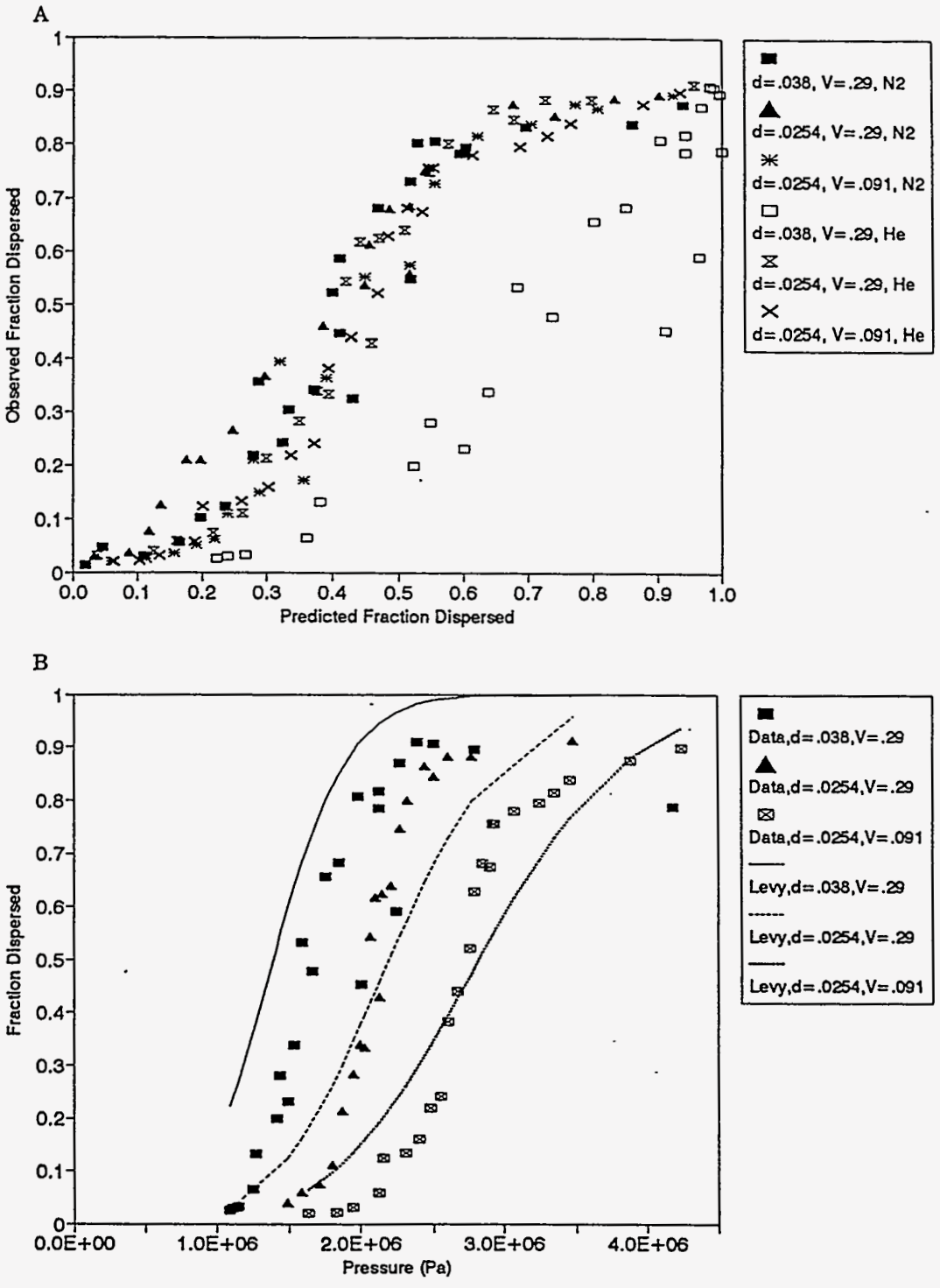

Figure 4.1-7 Levy correlation, SNL Surry data: (A), scatter plot; (B), predicted and experimental F_d versus $P_{0,v}$, with helium as driving gas

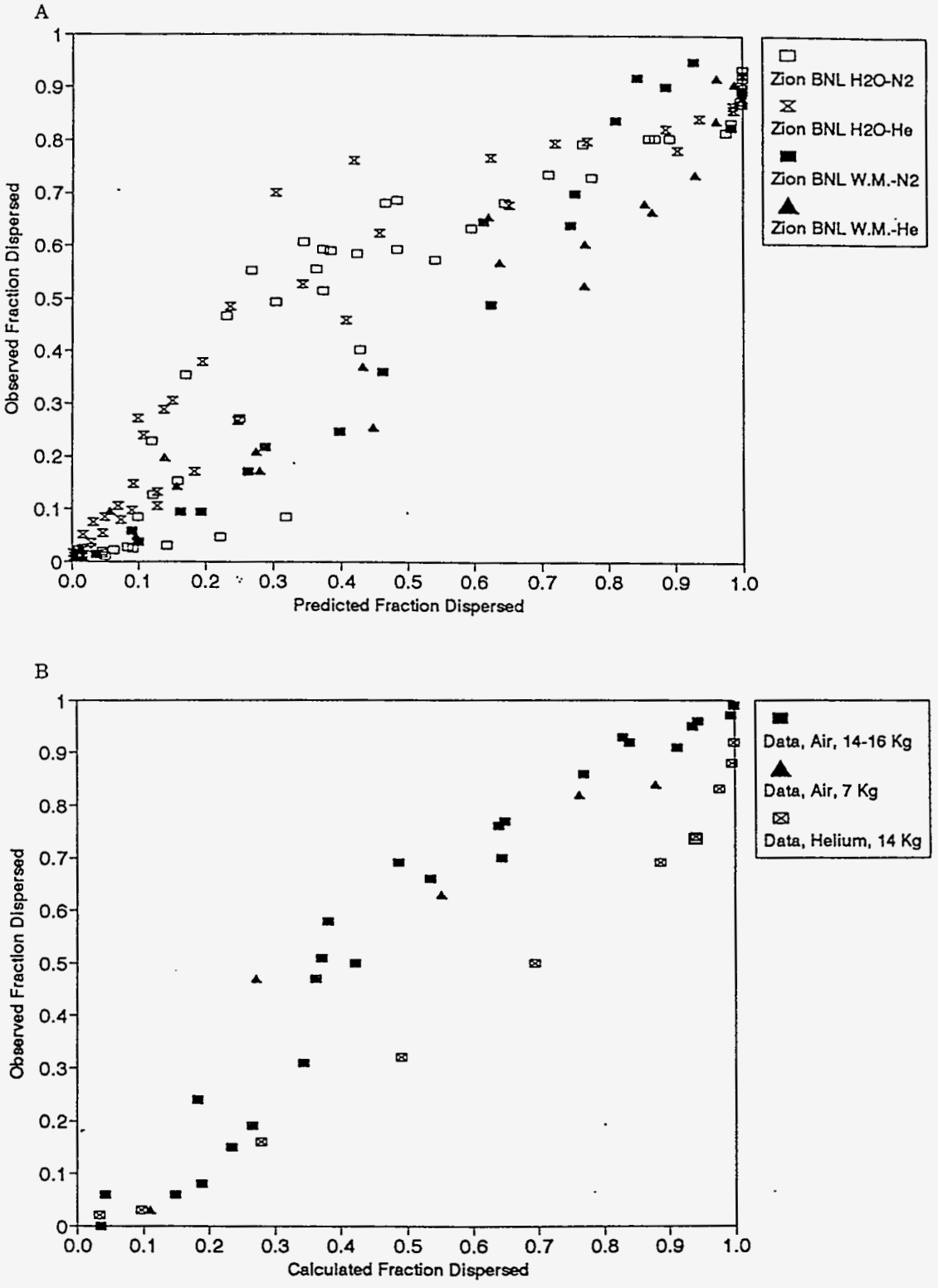

Figure 4.1-8 Levy correlation scatter plots for Zion geometry: (A), BNL data, water and Wood's Metal with common K_c; (B), SNL data

Table 4.1-1
Performance Statistics for Correlations Assessed

Correlation		--- BNL ---			--- SNL ---	
		Surry	Zion		Surry	Zion
Levy, K_c from Ref. Lev91	σ_{est}	0.160	0.537		0.537	0.141
Levy, Separate K_c for BNL and SNL Data	K_c	0.57	0.8		0.048	0.0073
	σ_{est}	0.176	0.125		0.144	0.123
Tutu-Ginsberg, K_c = 1 (All)	σ_{est}	0.102	0.088		0.417	0.472
Tutu-Ginsberg, Separate K_c for BNL and SNL Data	K_c	1	1		0.6	0.47
	σ_{est}	0.102	0.088		0.103	0.153
T-G, Froude No. Replaces Ku	σ_{est}	0.105	0.097		0.142	0.221
Tutu, Separate K_c for BNL and SNL Data	K_c	5.3	16.		1.25	0.4
	σ_{est}	0.115	0.184		0.191	0.103
Tutu, K_c(SNL) = K_c(BNL)	σ_{est}	0.115	0.184		0.409	0.588
Ishii Full Correlation, Separate K_c for BNL and SNL	K_c	0.1	0.21		0.22	0.19
	σ_{est}	0.268	0.293		0.318	0.268
Ishii Entrainment, Separate K_c for BNL and SNL	K_c	20.	28.		6.9	3.2
	σ_{est}	0.198	0.170		0.225	0.184
Ishii Entr., K_c(SNL) = K_c(BNL)	σ_{est}	0.198	0.170		0.381	0.558
Whalley-Hewitt, Separate K_c for BNL and SNL	K_c	100.	130.		118.	43.
	σ_{est}	0.138	0.137		0.208	0.143
W-H, K_c(SNL) = K_c(BNL)	σ_{est}	0.138	0.137		0.213	0.396

$$\sigma_{est} = \sqrt{\frac{\sum_{i=1}^{N_d} (Y_i - X_i)^2}{N_d}}, \qquad (15)$$

where X_i and Y_i are the predicted and experimental values of F_d, respectively, and N_d is the number of data points in the particular set analyzed. Where applicable, K_c values are also given. In assessing the fit to the BNL data set, values of σ_{est} were calculated separately for the water and Wood's Metal data and the value cited is one half the sum of the two. Results are given for all the correlations examined in this work. Table 4.1-1 provides a concise measure of how well the correlations tested do their jobs, albeit at the price of loss of detail.

The first row of results in the table gives σ_{est} values for the Levy correlation using the same K_c values for the BNL and SNL data sets, i.e., values corresponding to the scatter plot of Figure 4.1-3. The failure to correlate the SNL Surry and BNL Zion data is apparent in the large (> 0.5) values of σ_{est} for these cases. The next block of two rows gives the K_c values used to fit the four data sets individually and the σ_{est} values that resulted. These are the results plotted in Figure 4.1-5.

Values of σ_{est} for the BNL Surry and Zion data were also calculated with K_c fit separately to the water and Wood's Metal results. Results were $\sigma_{est} = 0.117$ and 0.10 for Surry and Zion, respectively. These values are significantly smaller than those listed in the table, especially for Surry; evidently, fitting to both liquids simultaneously does increase the correlation error somewhat. However, the effect is not large and it seems to be an acceptable price to pay for the ability to correlate the two liquids with a single value of K_c.

4.2. The Tutu-Ginsberg Correlations

The Tutu-Ginsberg correlations are rather different from the other correlations considered in this work in several respects. In the others, the approach used in developing the correlations involved a combination of physical reasoning and reliance upon existing correlations for entrainment in other situations (e.g., pipe flow), and then adjusting the correlation to a limited degree in order to improve the fit to the experimental data. Although a multiplicative constant is needed in all cases to fit the data adequately, the mathematical form of the correlations was based primarily upon physical reasoning and/or existing correlations and was adjusted to only a limited degree in order to improve the ability to represent the data (e.g., by including the factors f_1 and f_2 in the Levy correlation).

In developing the Tutu-Ginsberg correlations, much greater emphasis was placed upon applying scaling methodologies. The starting point was to formulate a model for debris transport in terms of conservation equations and initial and boundary conditions which was then nondimensionalized. From the nondimensionalized model, 11 dimensionless groups were identified as being potential scaling parameters. Using a combination of physical reasoning and

comparisons to experimental data, five of these scaling groups (discussed below) were judged to be sufficiently important to justify their inclusion in the correlation. The correlations are expressed in terms of a somewhat complex nonlinear function of these dimensionless groups which includes up to 13 constants whose values are determined by nonlinear least-squares fitting to the data. The functional form does not appear to be based upon physical modeling; instead it appears to be chosen to obtain a very flexible fitting function. Thus, the validity of the correlations depends heavily upon the scaling methodology used to identify the nondimensional groups, since physical reasoning is not used to define the functional form of the correlations themselves. (This description includes some simplifications; Reference Tut88 should be consulted for details.)

Since the Tutu-Ginsberg correlations were developed by fitting to the data for integral dispersal fractions, they exist only as correlations for the fraction dispersed; analogous time-dependent correlations for the entrainment rates cannot be defined from this work. Correlations have been defined for five cavity geometries: Surry with no cavity structure, Surry with the skirt in place, Surry with all cavity structure (instrument tubes, etc), Zion, and Watts Bar. For all five, the same basic fitting function is used, but the constants appearing in the fitting function must be determined separately for each cavity geometry considered.

Table 4.2-1 gives the functional form of the fitting function used and the values of the 13 constants reported for each of the five correlations [Tut90a, Tut90b], even though two of the correlations (Surry with all cavity structure and Watts Bar) are not being considered in the present work. The nondimensional scaling groups are introduced through the expression for the quantity x in Table 4.2-1. Two of the groups are the quantities L/d_h and $\rho_{g,R}/\rho_d$, where L is a reference length defined for each cavity geometry and the subscript R means that the indicated quantity is to be evaluated at reference conditions. For present purposes, reference conditions are the initial temperature of the RPV and the initial pressure of the cavity (these must be modified in applying the correlations to NPP and to experiments with hot, reactive debris [Tut88]).

The other three nondimensional groups used in the correlations are denoted N_1, N_4, and N_5 in Table 4.2-1 and these merit some additional discussion.

$N_1 \equiv \sigma\rho_d/(\rho_{g,R}^2 v_{g,R}^2 L)$, where the reference velocity, $v_{g,R}$, is the superficial gas velocity calculated for the cavity at the start of blowdown and assuming the reference values of the gas temperature and pressure. (The superficial gas velocity is defined to be the gas volumetric flow rate divided by the cavity cross section.) The number N_1 is described in the original references [e.g., Tut88] as representing the degree to which the trajectories of molten debris droplets will diverge from the gas flow streamlines. Large values of N_1 were interpreted in that work as implying that the debris will not follow the gas flow closely and, hence, implying that the debris is more likely to strike structures and be de-entrained. It was therefore judged that debris dispersal could only decrease with increasing values of N_1.

Table 4.2-1

The Tutu-Ginsberg Correlations

$$F_d = UF(x-C_1)\,[1 - (FX+FY)]$$

$$x = \log_{10}\left[N_5(L/d_h)^{C_2}(\rho_H/\rho_L)^{C_3}(1+C_4N_4^{C_5})/(1+C_6N_1^{C7})\right]$$

$$FX = \frac{C_8}{1+C_9Z^{C_{10}}},\quad FY = C_{11}e^{-(Z/C_{12})^{C_{13}}},$$

where $Z = |x - C_1|$

$$UF(x-\phi) = 0 \quad x \le \phi$$
$$= 1 \quad x > \phi$$

Cavity	C_1	C_2	C_3	C_4	C_5	C_6	C_7	C_8	C_9	C_{10}	C_{11}	C_{12}	C_{13}
Surry (no structure)	0.136	1.886	0.748	1.248	1.024	1.0	0.630	0.5	0.915	6.4	0.5	2.319	1.8
Surry (skirt)	0.481	1.818	0.652	0.575	0.680	0.350	0.121	0.472	0.688	2.75	0.528	0.958	8.75
Surry (all structure)	0.467	0.601	0.133	0.336	0.992	3.019	0.558	0.777	0.0395	5.0	0.223	4.467	3.0
Zion	0.839	1.512	0.464	2.32	0.324	0.0	0.0	0.296	0.0813	3.6	0.704	1.351	6.6
Watts-Bar	0.263	1.618	0.440	0.273	1.630	3.783	0.522	0.497	0.858	5.0	0.503	3.451	3.0

It is important to note that N_1 is the only parameter entering into the Tutu-Ginsberg correlation that depends upon the geometric scale. If the constants C_6 and C_7 are constrained to be nonnegative, this means that the correlations are incapable of representing scale effects which decrease dispersal with increasing scale, and the correlations can only predict that dispersal is independent of scale or increases with scale. From the values given in Table 4.2-1, it is apparent that the Zion correlation is scale-independent and the Surry correlation with the skirt only is almost scale-independent; the other correlations predict some increase in dispersal with scale.

$N_4 \equiv P_{0,v}V_v^*/P_R$, $V_v^* \equiv V_v/L^3$. N_4 was interpreted in Reference Tut88 as a dimensionless blowdown time, since it is approximately proportional to the actual blowdown time divided by the gas transit time through the cavity under reference conditions. Debris dispersal was expected to increase with increasing values of N_4.

$N_5 \equiv \rho_{g,R}V_{g,R}^2/(g\rho_d\sigma)^{1/2}$, where g is the acceleration of gravity. N_5 is equal to the Kutateladze Number, Ku (equal to Ku^2, in the terminology of the original references). Debris dispersal predicted by the correlations increases with increasing N_5, as would be expected.

Effect of the Skirt in Surry. The large majority of the BNL data for the Surry geometry considered here simulated no cavity structure, with only two data series given for the skirt-only configuration. On the other hand, all the SNL Surry data considered are for the skirt-only configuration. Since there are significant differences between the SNL and the BNL data for a given cavity geometry, as is discussed below, it is of interest to consider to what extent these differences might be related to the skirt in the case of Surry. The Tutu-Ginsberg correlations provide a useful context for examining this question, as they are the only correlations which attempt to distinguish these two configurations.

In the upper half of Figure 4.2-1, F_d data for $d_h = 0.953$ cm and d_h 0.675 cm both with and without the skirt are plotted against driving pressure along with the predictions of the correlation for no cavity structure. Other than the hole size and the presence of the skirt, all other parameters were the same for the four data series plotted. In the lower half of the figure, the same four data series are compared with the correlation for the skirt-only configuration.

Direct comparison of the data with and without the skirt is somewhat inconclusive; for the larger hole size, there may be some tendency of the configuration without the skirt to yield higher values of F_d, but any such trend is not apparent for the smaller hole sizes. Comparison with the correlations is also inconclusive; that is, it is not apparent that it would matter much which correlation is used in comparing with either data set. Indeed, the predictions of the two correlations for these conditions are very similar. (It may be noted that they would be somewhat less similar for the SNL data, because the two correlations have different scale dependencies; however, there are no SNL data without the skirt available for testing these predicted differences.)

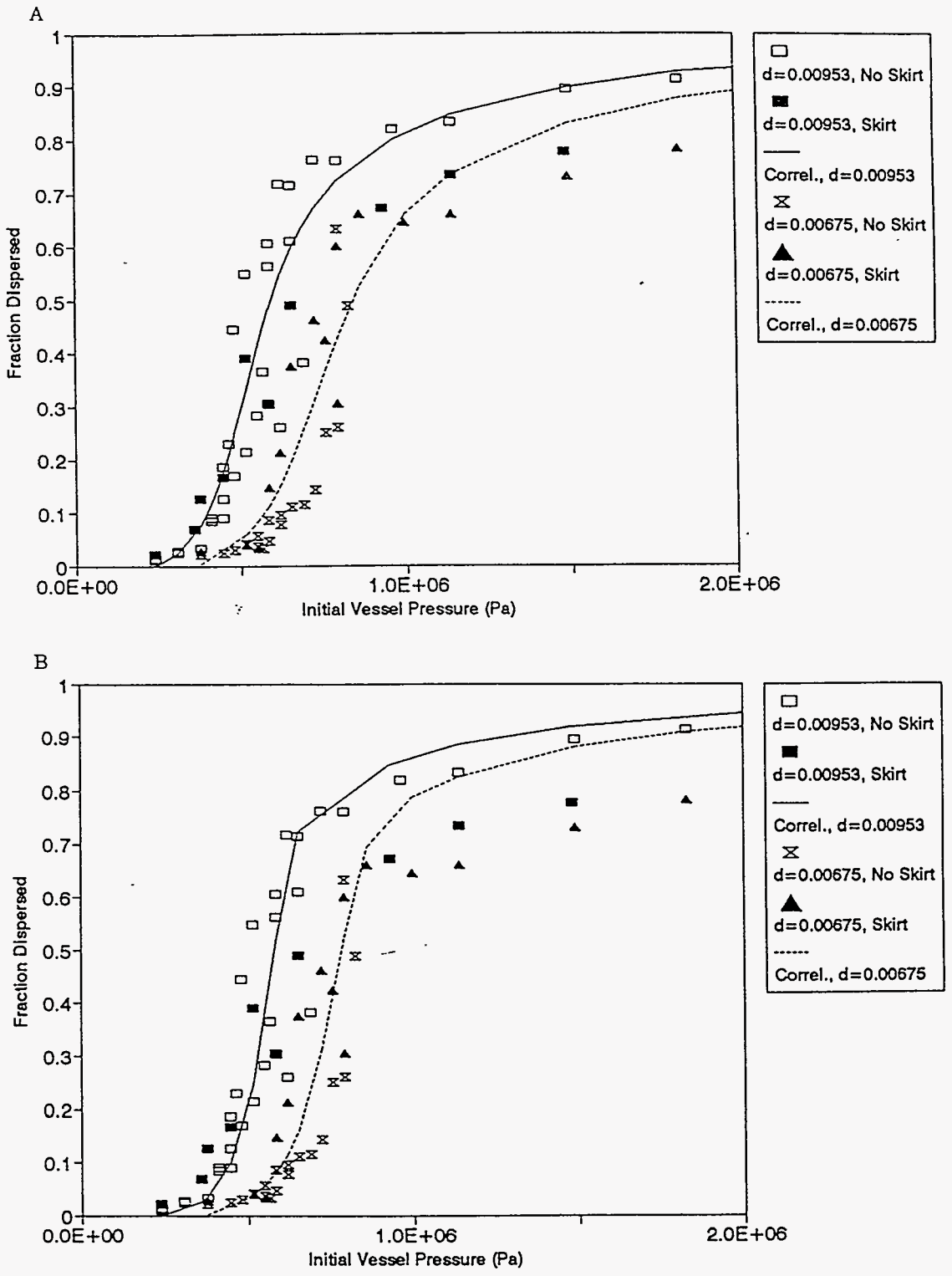

Figure 4.2-1 Tutu-Ginsberg correlations and effect of the skirt in the BNL Surry geometry data. Data are with and without skirt; correlation without skirt in (A) and with skirt in (B)

It appears, therefore, that any effects due to the skirt are within the scatter of the data. This scatter is large enough that moderate effects cannot be ruled out, but the data do support the belief that the effect of the skirt is not very large.

Comparisons with the Data. The predictions of the Tutu-Ginsberg correlations, as given in Table 4.2-1, are compared with the complete data set in the form of a scatter diagram in Figure 4.2-2, while F_d versus $P_{0,v}$ comparisons are given for selected BNL Surry and SNL Surry data series in Figure 4.2-3. It is apparent that the BNL data are in good agreement; indeed, the fit is at least somewhat better than was obtained for any other correlation. However, the fit to the SNL data is poor, with F_d being substantially overpredicted. The problem is somewhat worse for the SNL Zion data than for the Surry data.

In Reference Tut90b, it is argued that the differences between the BNL and SNL data are due to differences in the effective values of the gas discharge coefficients for the SNL and the BNL data, with the SNL values being lower. This conclusion was reached by analyzing the blowdown curves and comparing the actual rate of depressurization with the theoretical value calculated for an isentropic blowdown assuming unit values of the gas discharge coefficient, C_d. The average value of the discharge coefficient cited in Reference Tut90b for the BNL experiments in Surry geometry was 0.614 while the average values obtained for the SNL experiments were stated to be lower than this by factors of 0.6 and 0.47 for the SNL Surry and Zion geometry experiments, respectively. Hence, in analyzing the SNL Surry and Zion data, it was assumed in Reference Tut90b that the reference velocity u_R should be reduced by 0.6 for the SNL Surry data and by 0.47 for the SNL Zion data, and the correlations were fit to the data making these assumptions. (The correlation was fit to the data assuming $C_d(BNL) = 1$; hence, it is the ratio $C_d(SNL)/C_d(BNL)$ that was used in applying this "correction"). Note that, for the tests in a given cavity geometry, the same value of $C_d(SNL)/C_d(BNL)$ was assumed for all the experiments.

When the same assumptions are introduced in the present assessment, the agreement with the SNL data is much improved as is illustrated in Figure 4.2-4; see also the performance statistics summarized in Table 4.1-1. This improvement does not, of course, confirm the validity of the assumptions concerning reduced discharge coefficients in the SNL experiments, since these assumptions were made when the correlation was fit to the data in the first place.

In Reference Tut90b, it was argued that the reason for the differences in discharge coefficients was that, in the SNL experiments, the main volume of pressurized gas was connected to the liquid delivery system by a pipe with substantial flow resistance, which (it was claimed) reduced the blowdown rate. If this hypothesis were valid, it would affect the ability to use the SNL data for comparison with any of the correlations of interest, not just the Tutu-Ginsberg correlations. Hence a considerable amount of effort was expended examining this question in the present work.

Discharge coefficients were estimated for several individual experiments in each of the SNL Surry and Zion data series by analyzing the blowdown curves in the same way as was done in

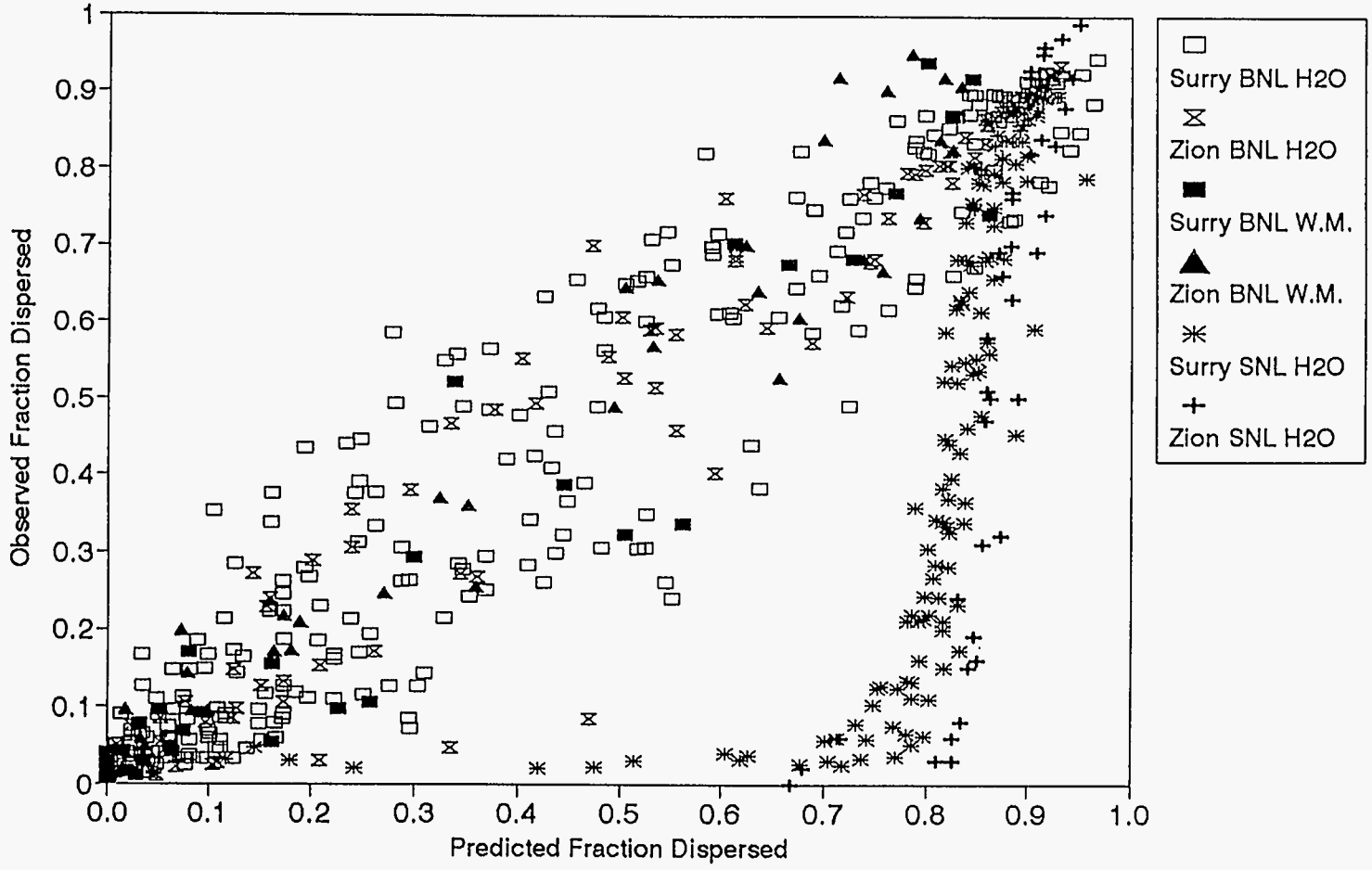

Figure 4.2-2 Scatter plot for Tutu-Ginsberg correlations with no discharge coefficient (C_d) "correction" (K_c = 1, all data)

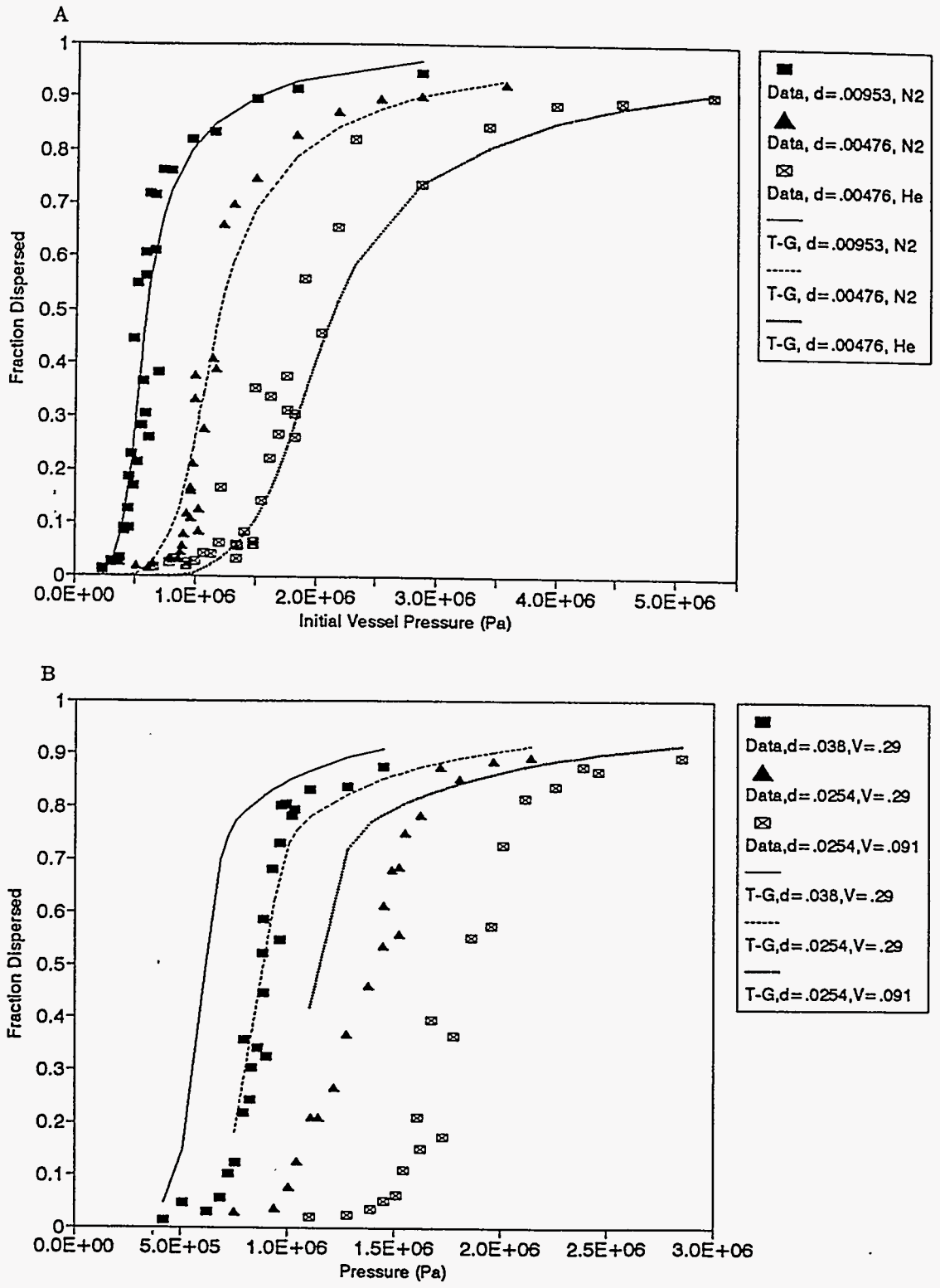

Figure 4.2-3 F_d vs $P_{0,v}$, data and Tutu-Ginsberg predictions for selected Surry geometry data series: (A), BNL data; (B), SNL data without C_d "correction"

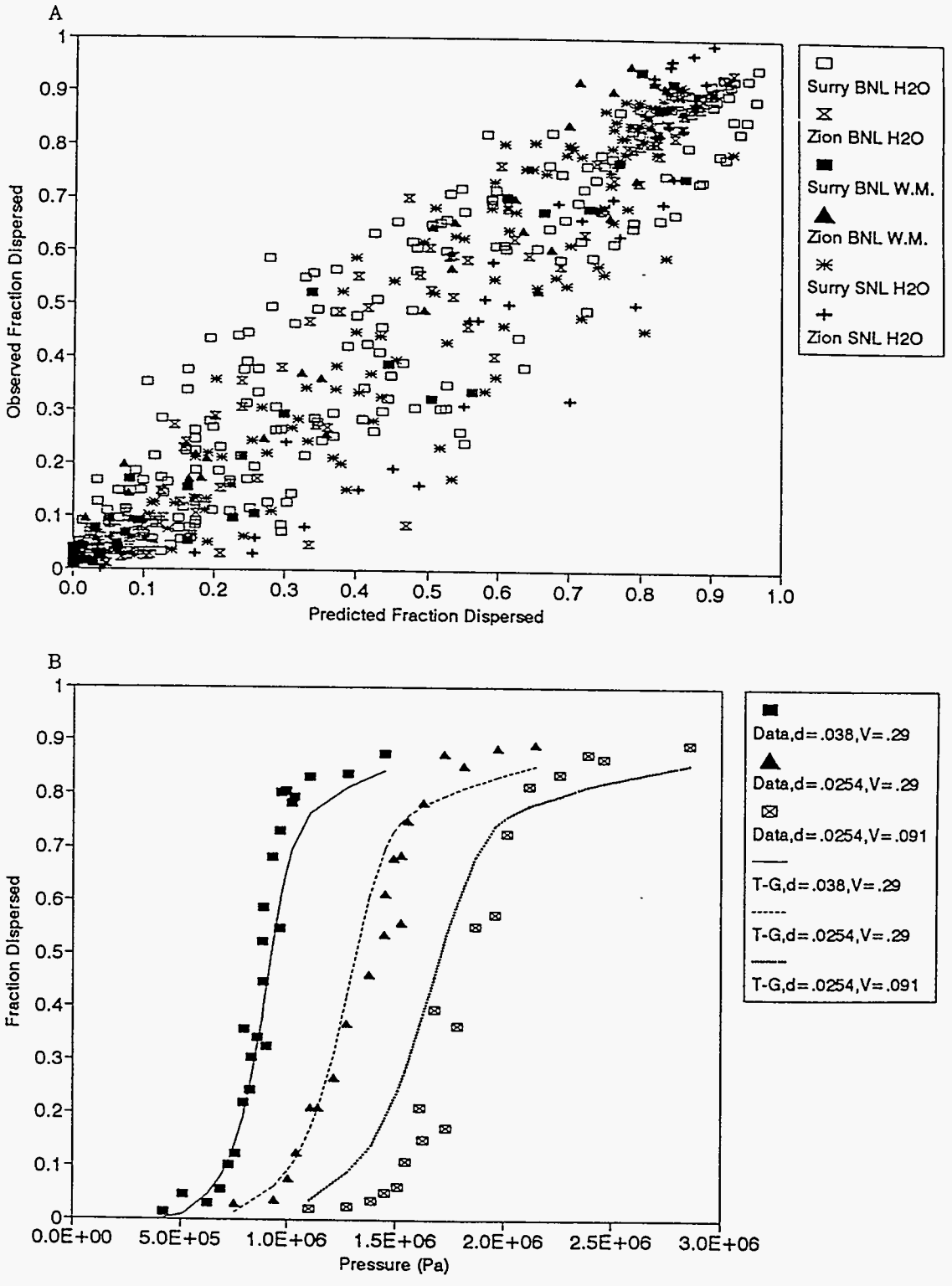

Figure 4.2-4 Tutu-Ginsberg correlations with $K_c = 1$ for BNL data, 0.6 for SNL Surry, 0.47 for SNL Zion: (A), scatter plot for all data; (B), F_d vs $P_{0,v}$ for SNL Surry data, air as driving gas

Reference Tut90b. It was found that there were substantial variations in the C_d values estimated, but that they were far from random*. Instead, they showed a systematic variation with orifice size, pressure vessel volume, driving gas, and driving pressure; some examples are illustrated in Figure 4.2-5a. (Lines drawn through the data are approximate analytical fits with only very limited physical significance.) It is clear that no one value of C_d would be appropriate for all the data series illustrated, and it is also clear that, for some of the data series, the values are not significantly less than those reported in Reference Tut90b for the BNL data.

Additional analysis strongly indicated that the explanation offered in Reference Tut90b for the SNL discharge coefficient results (i.e., flow restrictions in the pipe) was only a secondary contributor to the observed results. For example, a flow analysis was performed which indicated that effects as large as observed should not result from the pipe, and directly-measured experimental pressure drops across the pipe were smaller than required to explain the results (and were in reasonable agreement with the results of the flow analysis). Perhaps most importantly, the restrictive pipe hypothesis does not explain most of the trends in the apparent values of C_d exhibited in Figure 4.2-5a.

It was found that the trends in the discharge coefficient data correlated rather well with an analysis based upon the assumption that two-phase discharge effects following the onset of gas blowthrough were the primary factor involved.* The results for the SNL Surry data are illustrated in Figure 4.2-5b, in which the values of C_d obtained by analyzing the depressurization rates are plotted against the ratio of the blowdown time (τ_b; designated "Tau-gas" in the figure) to a parameter "$\tau_{2\phi}$" which is an approximate measure of the duration of the two-phase discharge as estimated using a simple model based upon separated flow. If two-phase flow effects are reducing the gas blowdown rates, one would expect this effect to decrease as $\tau_b/\tau_{2\phi}$ increases; hence C_d should increase with increasing $\tau_b/\tau_{2\phi}$, approaching the value for single-phase gas discharge as a limit.

It is apparent from the figure that C_d does correlate reasonably well with $\tau_b/\tau_{2\phi}$, and that the trends are as expected. This explanation was also in agreement with the larger values of C_d reported for the BNL experiments in Reference Tut90b, since the geometry of the liquid delivery system in the latter experiments was such as to minimize the amount of liquid remaining after the onset of gas blowthrough and, hence, minimize the two-phase discharge effects. (Values of $\tau_b/\tau_{2\phi}$ calculated for the BNL experiments were always considerably larger than any displayed in Figure 4.2-5b.) Note that this difference does not necessarily argue against the validity of the SNL data versus the BNL data; in NPP events, two-phase discharge effects following gas blowthrough will undoubtedly be present and the SNL tests might be more nearly prototypic in a qualitative sense. However, the geometry of the liquid delivery system was not prototypic in either system.

---

*Additional details are given in D. C. Williams, "Discharge Coefficients and the Use of the Experimental Data Base on Cavity Dispersal," DRAFT Letter Report to the USNRC, Sandia National Laboratories, September 8 1992.

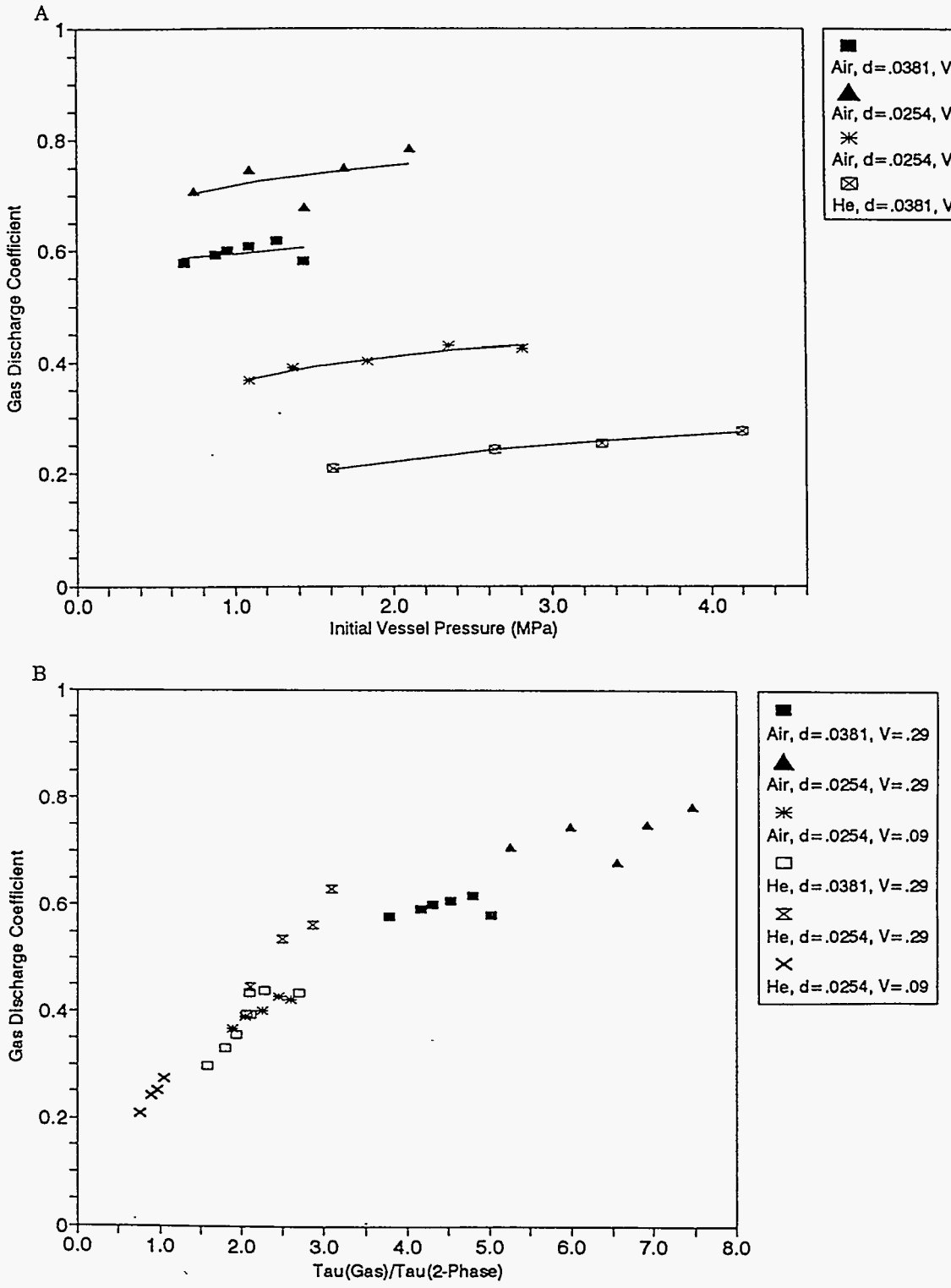

Figure 4.2-5 Apparent values of discharge coefficient C_d in the SNL Surry data: (A), as function of $P_{0,v}$, d_h, vessel volume, and gas type; (B), correlation with two-phase flow parameter

It remains necessary to consider whether the discharge coefficient variations displayed in Figure 4.2-5 should be taken into account when comparing correlations with the data and/or comparing BNL and SNL data, or whether such comparisons should be made at all. It was previously noted that the Levy correlation did a good job of reproducing the trends of the BNL data and also did a good job of bringing together five of the six SNL Surry data series (Figure 4.1-7a). The SNL Surry data were reanalyzed with the Levy correlation evaluated using values of C_d that, for each data point, were obtained from the analytical fits illustrated in Figure 4.2-5a. As before, the value of K_c assumed was tuned to optimize the fit to the SNL Surry data as a whole. A scatter diagram for the results is given in Figure 4.2-6. It is apparent that the ability of the Levy correlation to bring together the SNL Surry data series is largely destroyed when the C_d "correction" is introduced.

It may be noted that this result was not entirely unanticipated. If the effect of two-phase discharge upon depressurization rates is as large as implied by the C_d data, there must be substantial departure from separated flow conditions during the two-phase discharge period, which in turn implies considerable momentum transfer to the liquid. This liquid momentum could play a role in dispersing liquid from the cavity. The discharge coefficient "corrections" considered here implicitly assume separated flow and therefore neglect the momentum transferred to the liquid.

To summarize, the reduction in C_d (as obtained from the blowdown curves) is minor in some of the SNL data series but large in others; trends exhibited by the data series with small C_d values are nonetheless in line with trends exhibited by those with large values and with trends exhibited by the BNL data; and variations in the C_d values do not appear to alter the ability of otherwise-successful correlations to bring together the data. Hence, the SNL data will be used in this work without making any "corrections" for differences in the discharge coefficients.

It remains true that the Tutu-Ginsberg correlations give good agreement with the SNL data only if the reference velocity $v_{g,R}$ is reduced by factors of about 0.6 for Surry and 0.47 for Zion. These reduction factors will be treated here as empirical "cavity coefficients" (K_c values) as was done for the Levy and other correlations considered. They enter the Tutu-Ginsberg correlations as multipliers to the reference velocity.

Before leaving the subject of the Tutu-Ginsberg correlations, one other feature of these correlations should be noted. It was noted in Section 4.1 that, as $P_{0,v}$ is increased to values substantially greater than P_{50}, the F_d values predicted by the Levy correlation approach unity much more rapidly than do the experimental results. The same will be found to be true of the remaining correlations assessed below. However, this is not true of the Tutu-Ginsberg correlations; as can be seen from Figures 4.2-1 through 4.1-4, their behavior as a function of $P_{0,v}$ at large values of $P_{0,v}/P_{50}$ is in much better agreement with the data. This result may be a tribute to the flexibility of the fitting functions used more than it is due to capturing any fundamental physics omitted by the other correlations. Whatever the reasons, it has beneficial practical implications for some of the implementation options planned for the CONTAIN code; see Section 5.2.

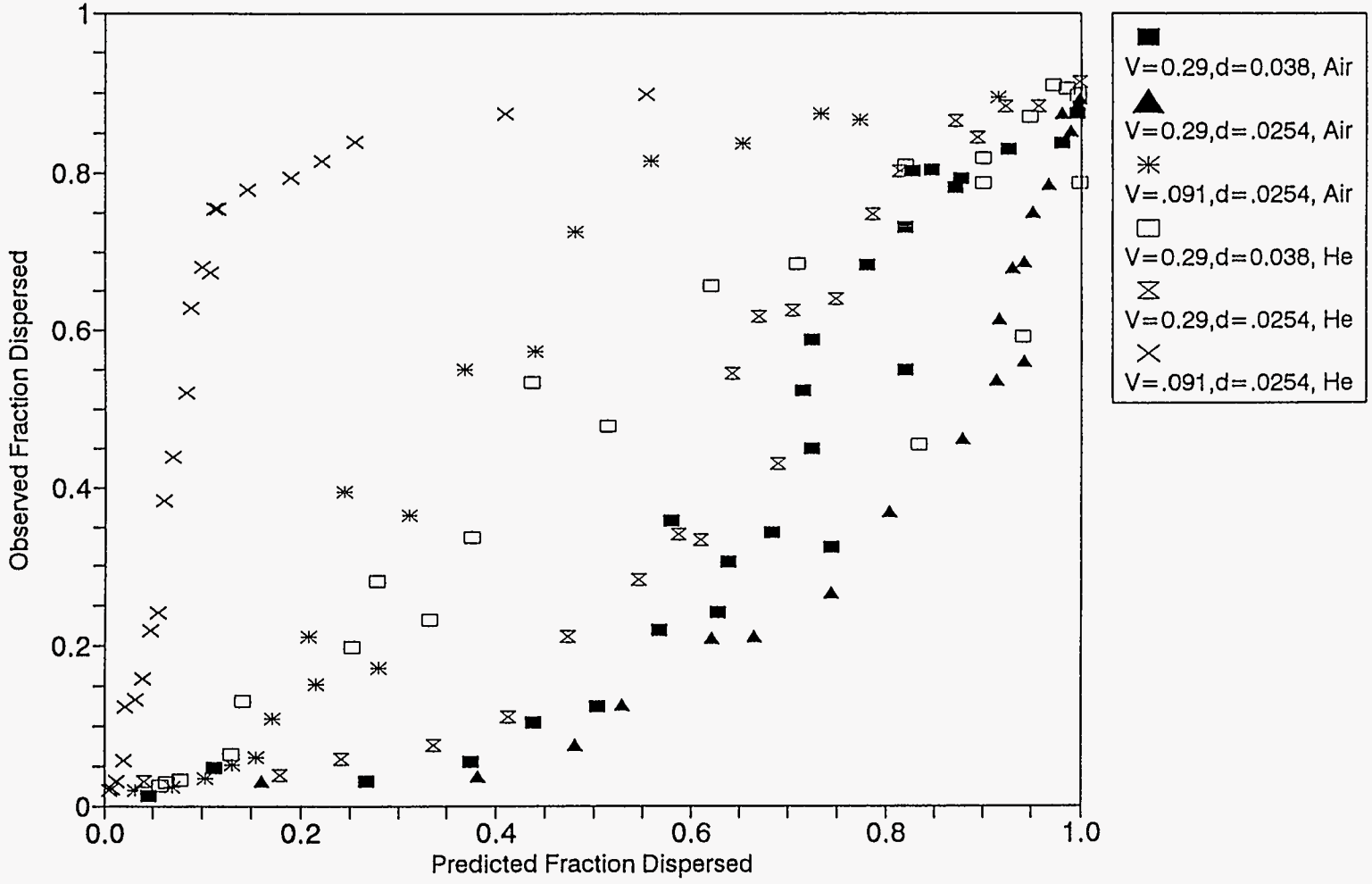

Figure 4.2-6 Scatter plot for Levy correlation and SNL Surry data with C_d "correction" applied illustrating adverse effect of the "correction"; compare with Figure 4.1-7(A)

4.3. The Tutu Entrainment Rate Correlation

The Tutu correlation for entrainment rates [Tut91] was developed to provide time-dependent dispersal rates which could be used in conjunction with the Tutu-Ginsberg correlations for the fraction dispersed. The correlation is somewhat complex and a detailed description will not be given here; see Reference Tut91 for details.

The correlation is derived, in part, by treating the cavity in terms of an "equivalent one-dimensional duct". This equivalent duct is defined to have a wetted wall area equal to that estimated for the actual cavity, but it has a reduced cross section defined in such a way as to take into account, approximately, the fact that velocity profiles measured experimentally are highly nonuniform, with the highest velocities concentrated along the cavity floor and walls. Hence the superficial velocity calculated for the duct is considerably higher than that which would be calculated using the actual cavity cross section. Calculated rates of entrainment and dispersal are therefore higher than what one would calculate if one used the actual cavity cross section in estimating gas velocities.

As in the Levy correlation, a considerable amount of physical reasoning was used in developing the correlation. However, its derivation required use of some physical assumptions which are unvalidated and could prove inaccurate; furthermore, the functional form of the correlation initially obtained was subsequently modified to obtain improved agreement with the experimental data. In addition, the correlation includes an empirical constant ("cavity constant", K_c, in the present terminology) whose value must be determined by fitting to the data, with different values likely being needed for different cavity geometries. Like the other correlations discussed here, the justification for the Tutu correlation must be considered largely empirical; its theoretical foundation is not judged to be distinctly superior or inferior to that of the other correlations.

Reference Tut90b compared dispersed fractions calculated by integrating the rate correlation with the BNL dispersed fraction data for the Surry data set with no cavity structure, and also compared predictions with those of the Tutu-Ginsberg correlation for NPP events in the Surry no-structure geometry. Comparisons for other cavity geometries were not given.

In the present work, comparisons were made for the standard data set used here. The fraction dispersed was calculated by numerically integrating the predicted entrainment rate over the blowdown history. The blowdown was assumed to be isentropic and a discharge coefficient, C_d, of 0.74 was used, as was done in Reference Tut91. The value of K_c was chosen to optimize the fit to the data in the same manner as was done for the Levy correlation, with separate values of K_c being needed for the Surry and Zion geometries and for the BNL and the SNL data (four K_c values in all).

Results are presented in Figure 4.3-1 in the form of a scatter plot, while Figure 4.3-2 gives comparisons between calculated and experimental F_d versus $P_{0,v}$ plots for some individual data series. Table 4.1-1 summarizes the performance statistics (σ_{cst} values) and also gives the K_c

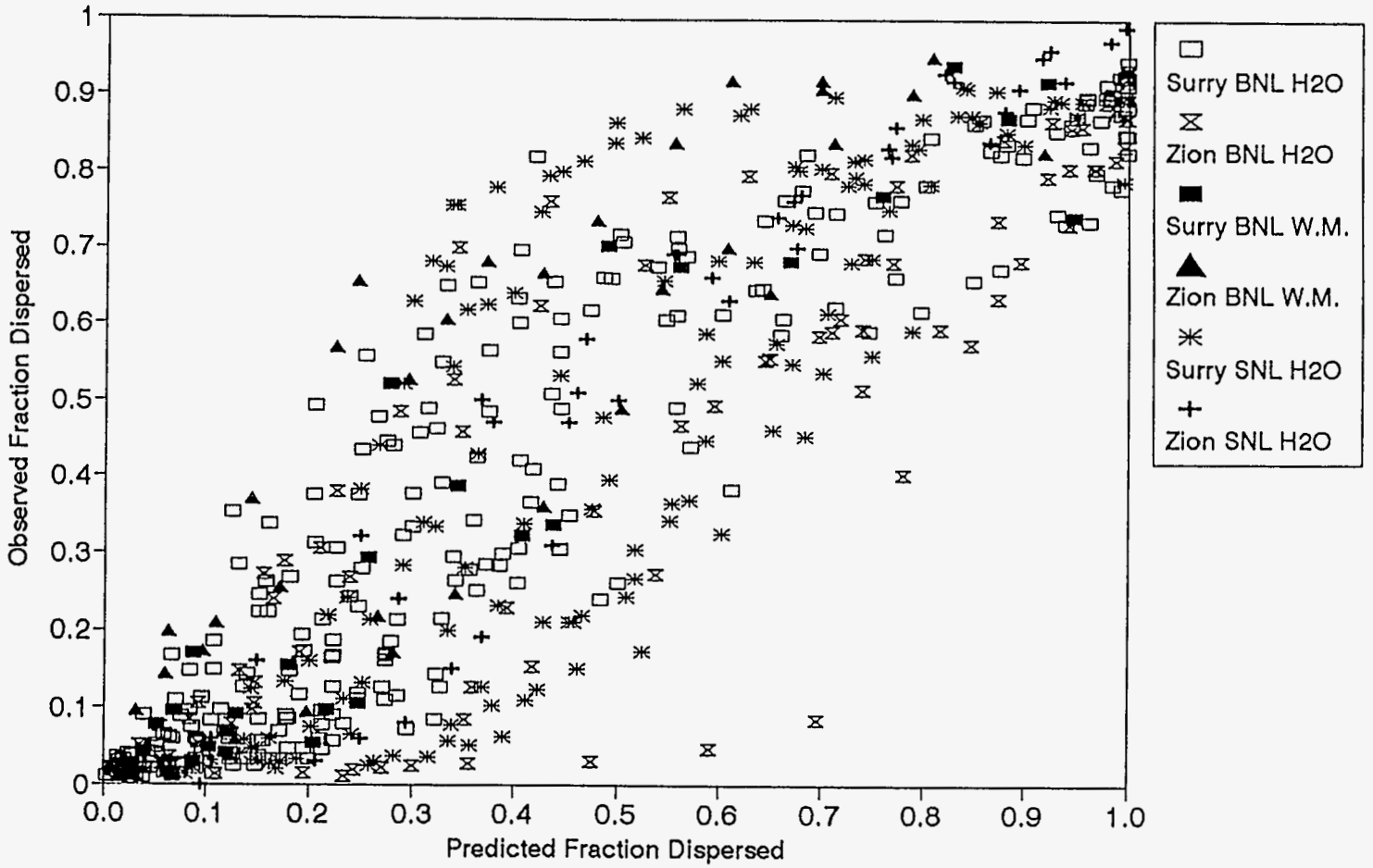

Figure 4.3-1 Scatter plot for the Tutu correlation, K_c fit separately for SNL and BNL data

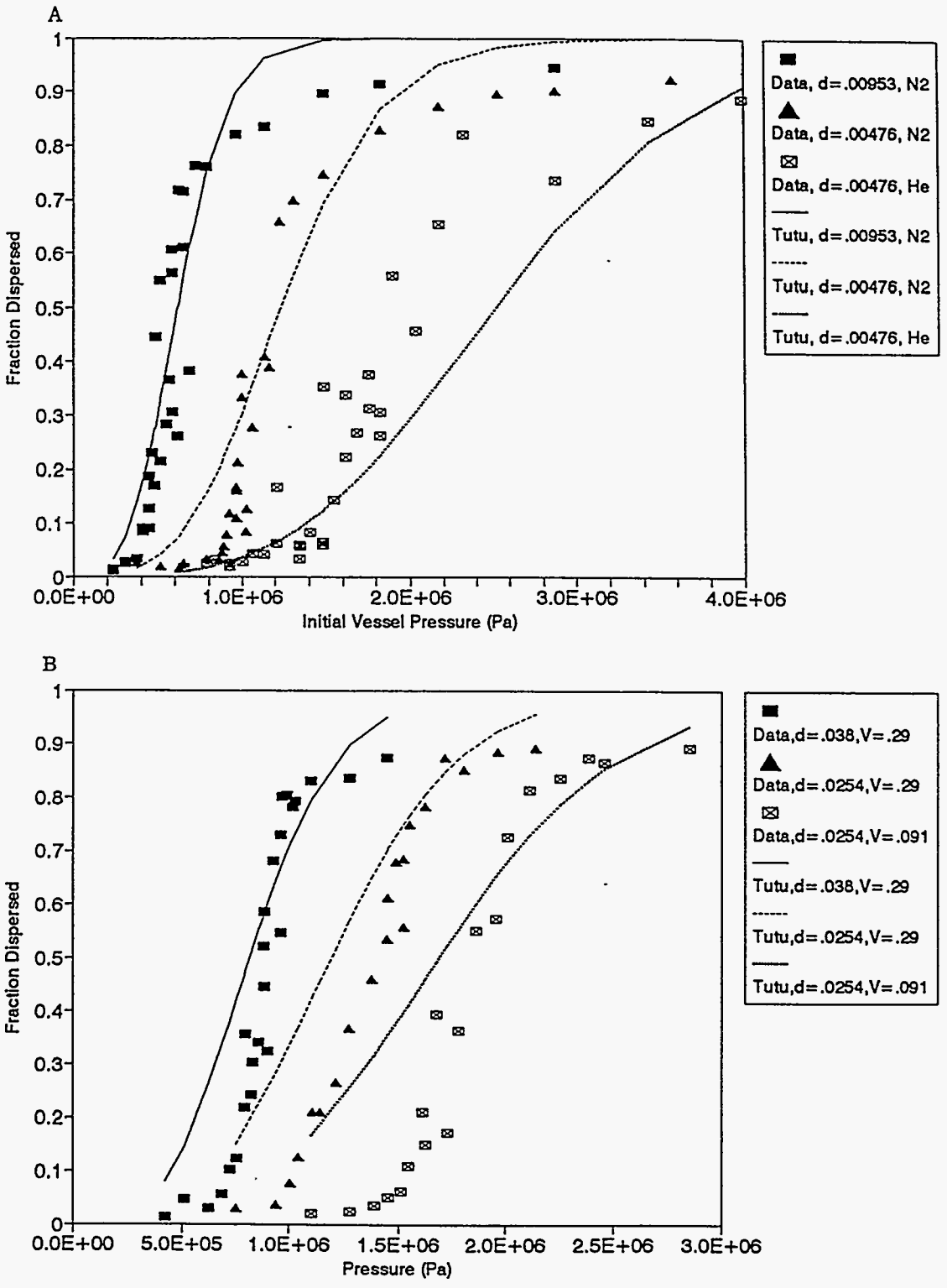

Figure 4.3-2 F_d vs $P_{0,v}$ experimental data and Tutu correlation predictions, Surry geometry, water as fluid: (A), selected BNL data; (B), SNL dat a with air as driving gas

values. The K_c value obtained for the BNL Surry data set (5.3) is in reasonably good agreement with the value of 4.6 cited in Reference Tut91.

Overall, the agreement between the data and the correlation is about as good as that obtained for the Levy correlation, but the pattern of strengths and weaknesses is somewhat different. The Tutu correlation gives somewhat better results for the BNL Surry data set and the SNL Zion data set than does the Levy correlation, while the reverse is true for the BNL Zion and the SNL Surry data sets.

The comparison between the Tutu correlation and the complete data set was also run using the same K_c values for the SNL experiments as were used for the BNL experiments. Performance statistics (σ_{est} values) are also given for this case in Table 4.1-1. It is apparent that agreement with the SNL data is very poor when the values of K_c derived from the BNL are used. Examining the results in more detail showed that the correlation substantially overpredicted dispersal for the SNL data, much as did the Levy correlation when the BNL values of K_c were used. In part, this result is due to the significant positive dependence of dispersal upon scale in the Tutu correlation, while the data indicate scale effects are either small (Surry) or negative (Zion), if one interprets the SNL-BNL differences as representing scale effects.

4.4 The Ishii Correlation

The Ishii correlation consists of two parts, a model for liquid transport out of the cavity by film flow and a model for entrainment of liquid into the gas stream. The intended purpose of the development given in Reference Ish91 was to consider scaling issues, not develop a full dispersal correlation, and there are some ambiguities concerning how to estimate F_d from what is given in the reference. The present approach is based upon estimating characteristic times for dispersal, τ_{disp}, and comparing them with the characteristic blowdown time, τ_b. It is possible to defend assumptions other than those made here, but they would not improve the overall agreement. Since the experimentally determined values of F_d represent the net effect of all transport mechanisms, one should compare the experimental data with the predictions of the full model; i.e., film flow plus entrainment. For various reasons, it is also of interest to compare with the predictions of just the entrainment model. Both approaches will be used here.

Transport by Film Flow. In the models described in Reference Ish91, it is assumed that corium is ejected from the RPV as a jet with a diameter which is assumed to be equal to the diameter of the orifice, d_h, formed by the failure of the vessel head. The liquid jet velocity, v_{dJ}, is given by

$$v_{dJ} = \sqrt{\frac{2\Delta P}{\rho_d}}, \tag{16}$$

where $\Delta P = P_v - P_c$. In the model, it is assumed that, when the jet impacts the cavity floor, it spreads out with an initial film thickness, δ_i, equal to $d_h/4$. The film is then assumed to flow down the cavity and out the exit chute with a velocity given by continuity. Thus, it is assumed that the rate of flow of liquid within the film is equal to the rate at which liquid is ejected from the vessel. These assumptions lead to

$$v_{df} = \frac{d_h^2 v_{dJ}}{4 D_c \delta}, \tag{17}$$

where v_{df} is the flow velocity within the film of thickness δ, and D_c is the hydraulic diameter of the cavity.

Reference Ish91 gives several possible choices for estimating δ; here we assume $\delta = \delta_i$, which is the choice made in the examples discussed in Reference Ish91. With this assumption, v_{df} is given by

$$v_{df} = \frac{d_h v_{dJ}}{D_c}. \tag{18}$$

In Reference Ish91, the characteristic time for film flow to transport the corium out of the cavity, τ_f, is taken to be v_f/L_c, where L_c is the cavity length. However, we note that v_{df} varies only linearly with d_h, implying $\tau_b/\tau_f \propto 1/d_h$; i.e., that F_d will <u>decrease</u> with increasing d_h. This result is unrealistic and this definition of the dispersal time will not be used here. Instead, τ_f will be taken to be the ratio of the total corium mass to the rate of mass transport by film flow. The latter is, in turn, just the rate of ejection from the vessel, in this model.

<u>Corium Entrainment</u>. In Reference Ish91, the rate of entrainment ϵ, in kg/m^2-s, is taken to be

$$\frac{\epsilon D_c}{\mu_d} = 6.6 \times 10^{-7} (Re_f We)^{0.925} \left[\frac{\mu_g}{\mu_d}\right]^{0.26}, \tag{19}$$

where

$$Re_f = \frac{\rho_d j_f D_c}{\mu_d}, \quad We = \frac{\rho_g j_g^2 D_c}{\sigma}\left[\frac{\Delta\rho}{\rho_g}\right]^{1/3}. \tag{20}$$

Here, Re_f is the film Reynolds number, j_f is the film superficial velocity (film volumetric transport rate divided by the cavity cross section, with the latter taken to be $\pi D_c^2/4$), and j_g is the superficial velocity for gas flow through the cavity.

Following Reference Ish91, we take the characteristic time for entrainment, τ_e, to be equal to $\delta_f \rho_f / \epsilon$.

Estimation of Dispersed Fraction. We next assume that the two processes, film flow and entrainment, act in parallel and that the total dispersal rate is therefore the sum of the two. The overall time constant for dispersal, τ_{disp}, is then given by

$$\tau_{disp} = \frac{1}{\frac{1}{\tau_f} + \frac{1}{\tau_e}} = \frac{\tau_f \tau_e}{\tau_f + \tau_e} \qquad (21)$$

F_d is then assumed to be given by

$$F_d = 1 - e^{-\tau_b / \tau_{disp}}. \qquad (22)$$

When the entrainment-only version of the correlation is to be evaluated, τ_{disp} is equated to τ_e.

Comparison with the Data. As given in Reference Ish91, the correlation includes no empirical constants to be specified by fitting to the experimental data. However, experience with other correlations indicated that useful fits to the data would not be obtained without some parameter fitting, and preliminary evaluations of the correlation confirmed this expectation. Hence, the dispersal rates calculated by the correlation were multiplied by a cavity constant, K_c, and F_d was then calculated from

$$F_d = 1 - e^{-K_c \tau_b / \tau_{disp}}. \qquad (23)$$

As before, K_c values were fit separately to the data sets for BNL Surry, BNL Zion, SNL Surry, and SNL Zion.

A scatter plot for the full correlation is given in Figure 4.4-1a, with unencouraging results. The σ_{cst} values tabulated in Table 4.1-1 are also rather large for all four data sets, indicating a poor fit. Detailed comparison between the model and the experimental results is given for a few selected BNL Surry data series in Figure 4.4-1b. It is seen that the predicted F_d versus P_v curve is much too flat, the dependence upon d_h is virtually unacknowledged, and there is an extreme sensitivity to the gas type. These results follow from the results tabulated in Table 3.3-1 plus the fact that the total dispersal calculated is heavily dominated by the film flow contribution. This version of the model need not be considered further.

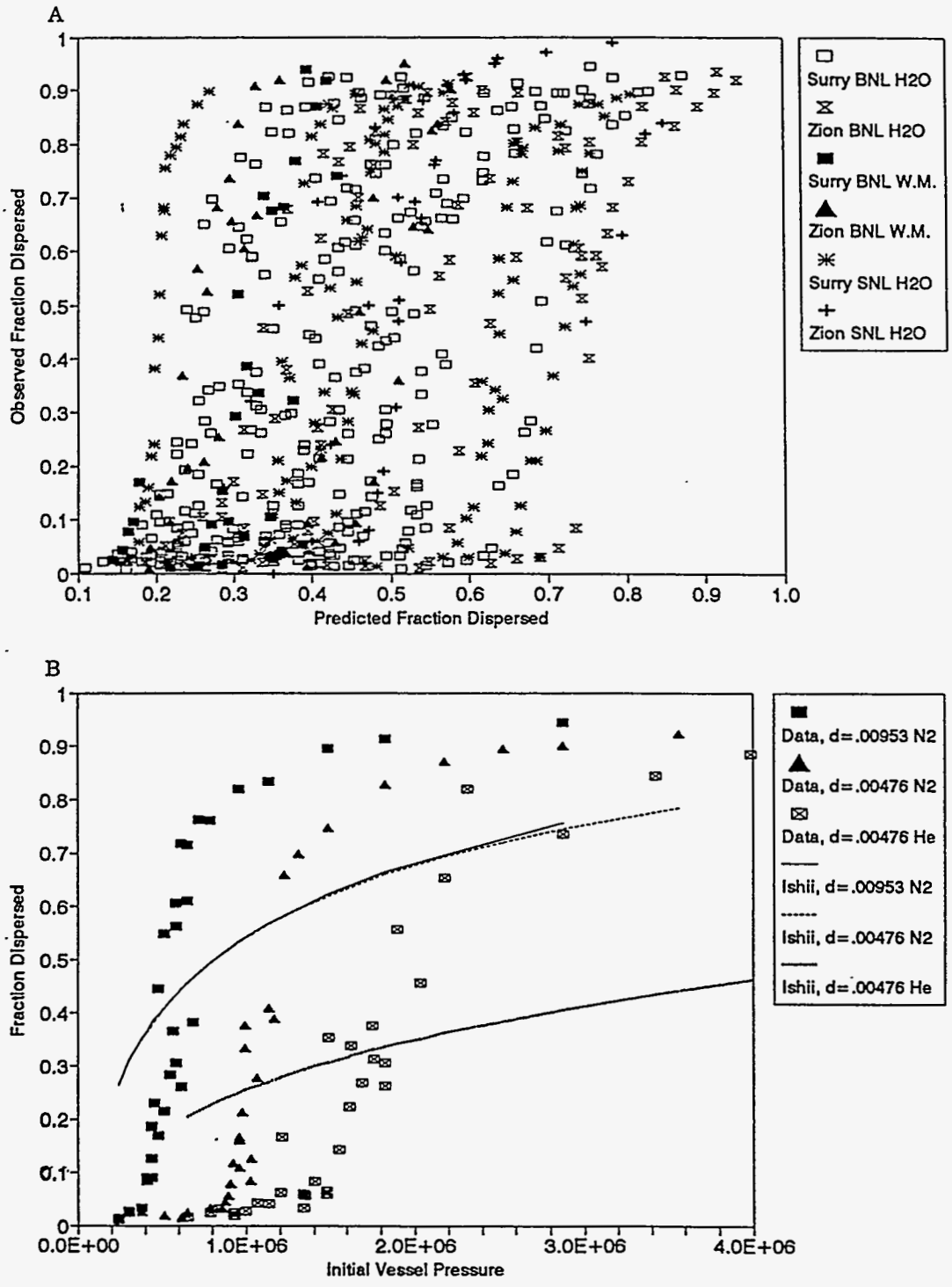

Figure 4.4-1 Full Ishii correlation: (A), scatter diagram for full data set; (B), F_d vs $P_{0,v}$, data and correlation for selected BNL Suorry data with water as fluid

Equivalent results calculated assuming the entrainment correlation only are plotted in Figure 4.4-2. Though the spread in the scatter plot is still rather broad, there is certainly more of a trend toward the diagonal than was observed for the full correlation. Figure 4.4-2b shows that the steepness of the F_d versus P_v curve is still underpredicted somewhat, but not to an unacceptable degree. The dependence upon d_h is reproduced and may, in fact, be overpredicted. The dependence upon gas type is substantially underpredicted, as was anticipated from Table 3.3-1. Also as expected, the correlation underpredicts the difference between water and Wood's Metal somewhat. Note, however, that the data do not provide a direct test of the model's prediction that the dominant difference between these liquids is due to surface tension effects, not density effects. Other trends were found to be consistent with predictions based upon Table 3.3-1.

Values of σ_{est} tabulated in Table 4.1-1 for the Ishii entrainment model represent considerable improvement over the full model results, but they are still poorer than was obtained for the models considered previously. The model was also run with K_c values for the SNL data set equal to the corresponding values used for the BNL data. Resulting values of σ_{est} were 0.38 and 0.56 for the SNL Surry and Zion data, respectively. Clearly, it is not possible to fit the BNL and SNL data for equivalent cavity geometries with a single value of K_c . This result was no surprise, given the α_s/n values in Table 3.3-1.

4.5. The Modified Whalley-Hewitt Correlation.

The Whalley-Hewitt correlation was presented in some detail in Section 3.2. The screening assessment given there was generally favorable, but it was noted that the substantial positive dependence of F_d upon liquid viscosity posed a problem, since it is not in accord with either physical expectation or experimental data such as the Winfrith data discussed in Section 2.3. Indeed, if such a dependence were valid, it would pose an almost hopeless practical problem, because liquid viscosities, unlike most other liquid properties, can vary by large factors over relatively moderate temperature ranges, and it would be difficult to define the correct value of viscosity for a complex liquid of uncertain temperature and composition such as corium in DCH events. Fortunately, there is no evidence that cavity dispersal phenomena have any strong dependence upon liquid viscosity, within wide limits.

Following Levy's approach, one could modify the dependence upon viscosity by introducing a factor of $(\mu_{s,d}/\mu_d)^x$, where $\mu_{s,d}$ is the viscosity of some standard substance such as water and x is an appropriate fractional power. (Of course, the need to impose such a modification is equivalent to acknowledging that the correlation cannot represent a complete physical description, as was noted previously in connection with other correlations.) However, there seems to be little basis for deciding what the viscosity dependence should be, other than it should be small. Hence, in the present assessment, the correlation was evaluated with the viscosity hard-wired to a value of 10^{-3} Pa-s, the value for water.

In Section 3.2, it was noted that the combined dependence of the correlation upon liquid density and surface tension was larger than that inferred from the experimental data, and that

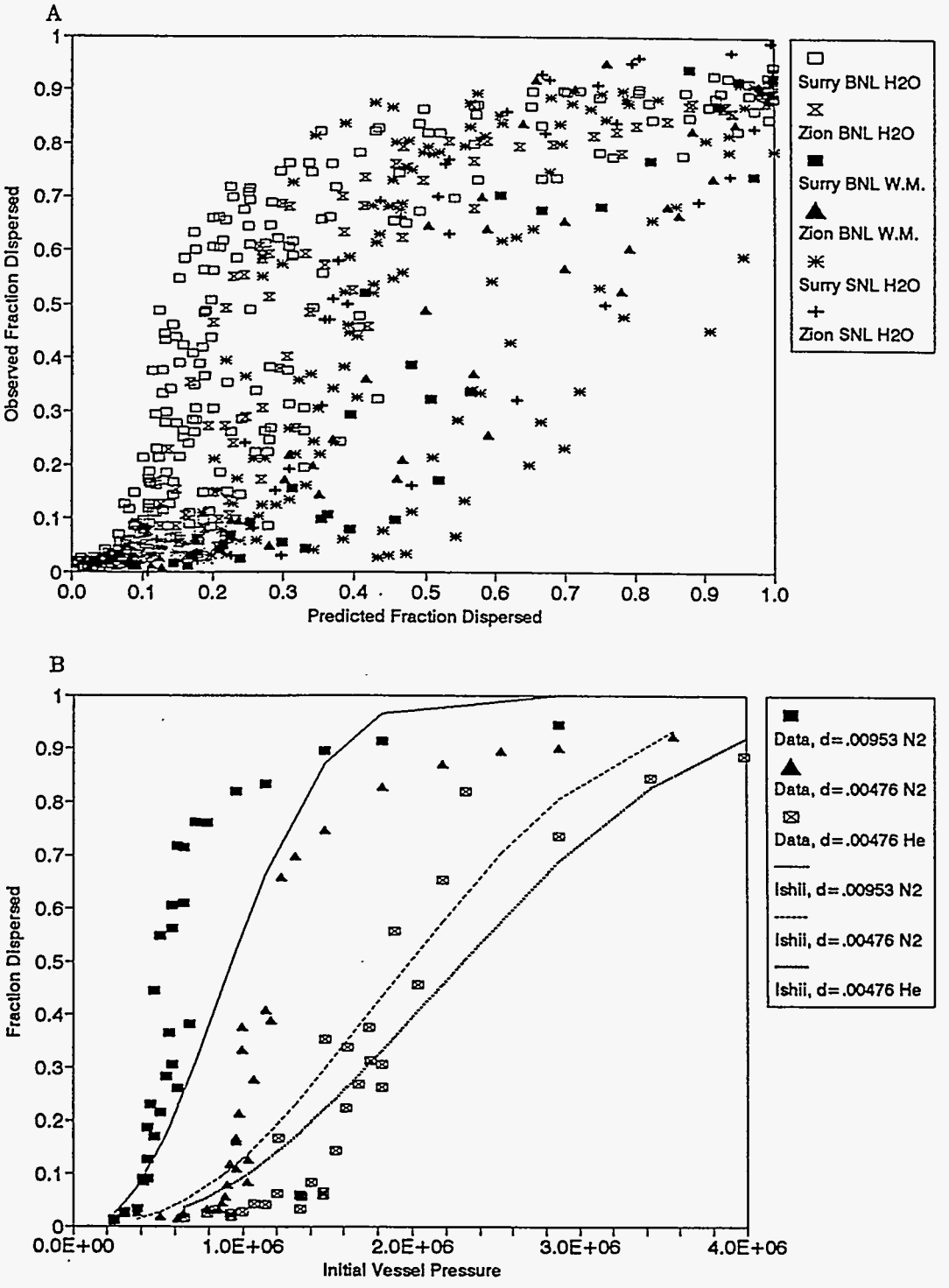

Figure 4.4-2 Ishii correlation (entrainment correlation only): (A), scatter diagram for full data set; (B), F_d vs $P_{0,v}$, data and correlation for selected BNL Surry data with water as fluid

it was likely that the dependence upon surface tension was being overpredicted. Not surprisingly, the initial assessment indicated that the difference between water dispersal and Wood's Metal dispersal was being overpredicted, even for the BNL Surry results. Hence a factor of the form $(\sigma_s/\sigma)^x$ was incorporated in order to reduce the dependence upon σ, with σ_s taken to be 0.072 J/m^2 (the value for water).

In Section 2.3, an attempt was made to estimate α_σ/n from the Winfrith data for water and silicone oils. Results ranged from -0.20 to +0.06, primarily due to the uncertainty in the correction for the viscosity difference between water and the silicone oils. If the value of α_μ/n implied by the Levy correlation, -0.057, is used to apply the viscosity correction, the result obtained for α_σ/n is about -0.11. Since n = 2 for the Whalley-Hewitt correlation, this value implies α_μ = -0.22, or x = 1-α_μ = 0.78. This value of x was adopted for assessing the correlation. (The exact value of x used was 0.7826. Strictly speaking, there is some inconsistency between what is done here and the previous decision to delete all dependence upon the viscosity. However, the practical difference between the latter and the use of α_μ/n = -0.057 are very minor and certainly less than the experimental uncertainties involved.)

One other variation to the Whalley-Hewitt correlation was also considered. As was discussed at the beginning of Section 3.2, Whalley and Hewitt [Wha78] gave the correlation in the form of a data plot of $\epsilon\sigma/\tau\mu_d$ against $\tau\delta/\sigma$, with no analytical expression for the dependence upon $\tau\delta/\sigma$. For values of $\tau\delta/\sigma$ greater than about 0.6, $\epsilon\sigma/\tau\mu_d$ was essentially independent of $\tau\delta/\sigma$, but $\epsilon\sigma/\tau\mu_d$ declines as $\tau\delta/\sigma$ decreases below 0.6 and goes to zero for sufficiently small values of $\tau\delta/\sigma$. The correlation discussed in Section 3.2-2 is based upon the limiting form of the correlation obtained at large values of $\tau\delta/\sigma$. The limiting form should apply to NPP [Ost94], but numerical evaluation suggested that the region of the downturn at low values of $\tau\delta/\sigma$ might be more significant in the small-scale experiments. Hence an approximate representation of the full curve was defined and assessed. It was found to have some marginally attractive features, such as reducing somewhat the tendency to overpredict the rate at which F_d approaches unity at high values of P_v/P_{50}. On the whole, however, the approximation to the full correlation did not improve agreement with experiment, and even worsened agreement in some instances. Hence it was abandoned as introducing unjustified complications, and will not be discussed further here.

The modified Whalley-Hewitt correlation assessed in the present work, then, takes the form

$$\epsilon = 0.0025 K_c (1 + 360\,\delta/D_c)\,\rho_g V_g^2 \mu_{s,d} \sigma^{-1} \left(\frac{\sigma}{\sigma_s}\right)^{0.7826}, \qquad \delta = \frac{V_d}{A_{ww}}. \tag{24}$$

Here the subscript s refers to the properties of the standard substance (water). The total mass entrained per unit time is equal to ϵ multiplied by the wetted wall area, A_{ww}, which was taken to be the same as was assumed in assessing the Tutu correlation. F_d was calculated as was done for the Tutu correlation assessment, i.e., by numerically integrating the entrainment rate over

a blowdown history based upon Tutu's isentropic blowdown model with a discharge coefficient of 0.74 (Section 4.3).

A scatter diagram for the modified Whalley-Hewitt correlation is given in Figure 4.5-1a, while predicted and experimental F_d versus P_v curves are compared for three selected Surry BNL data series in Figure 4.5-1b. The scatter diagram suggests a tighter correlation than the Ishii entrainment correlation but not as tight (or at least not as linear) a pattern as the more complex correlations considered in Sections 4.1-4.3. The correlation does a good job of bringing together the water and Wood's Metal results, which is not very surprising in view of the rationale used in defining the $(\sigma/\sigma_s)^x$ described above. The fact that the correlation is fairly successful in this regard for both the Surry and Zion geometries is worth noting, however.

Figure 4.5-1b indicates that, like the Ishii entrainment correlation, the modified Whalley-Hewitt correlation underpredicts the steepness of the F_d versus P_v curves and gives a reasonable representation of the effect of d_h. Unlike the Ishii entrainment correlation, it also represents the effect of gas type well.

Though it is not very obvious from Figure 4.5-1a, examining more detailed scatter plots showed that the pattern for the BNL data is actually fairly tight (though not very linear), and much of the breadth of the pattern in Figure 4.5-1a is produced by the SNL Surry data. The reasons are illustrated in Figure 4.5-2. Evidently, the spread comes from both the tendency to overpredict the dependence upon vessel volume V_v and the inability to represent the very steep F_d versus P_v curves for this data set. It is interesting to note that, in the BNL Surry data set, the correlation did not conspicuously overpredict the volume effect, and these results are in accord with the α_{V_v}/n values given in Table 3.3-1.

The summary statistics in Table 4.1-1 also clearly reflect the fact that the correlation has the hardest time with the SNL Surry data. In general, the σ_{est} values tabulated show that the modified Whalley-Hewitt correlation does about as well as any of the others (and better than some) with the partial exception of the Tutu-Ginsberg family with their very flexible fitting functions.

One of the most important features of the Whalley-Hewitt results is that the value of K_c obtained from fitting to the BNL Surry data (100) differs relatively little from that obtained by fitting to the SNL Surry data (118). Hence, when the correlation was run for the SNL data using K_c values derived by fitting to the BNL data, results for the SNL Surry data were changed very little; note, however, that the fit to the SNL Zion data was still very unsatisfactory, when the BNL value of K_c was used. It is concluded, therefore, that alone of all the correlations considered, the modified Whalley-Hewitt correlation can simultaneously fit both the BNL and the SNL Surry data, without significantly degrading the quality of the fit to either data set. This capability is unrelated to the modifications introduced because only water was used in the SNL experiments, and the modification has no effect for water, since water is the "standard substance".

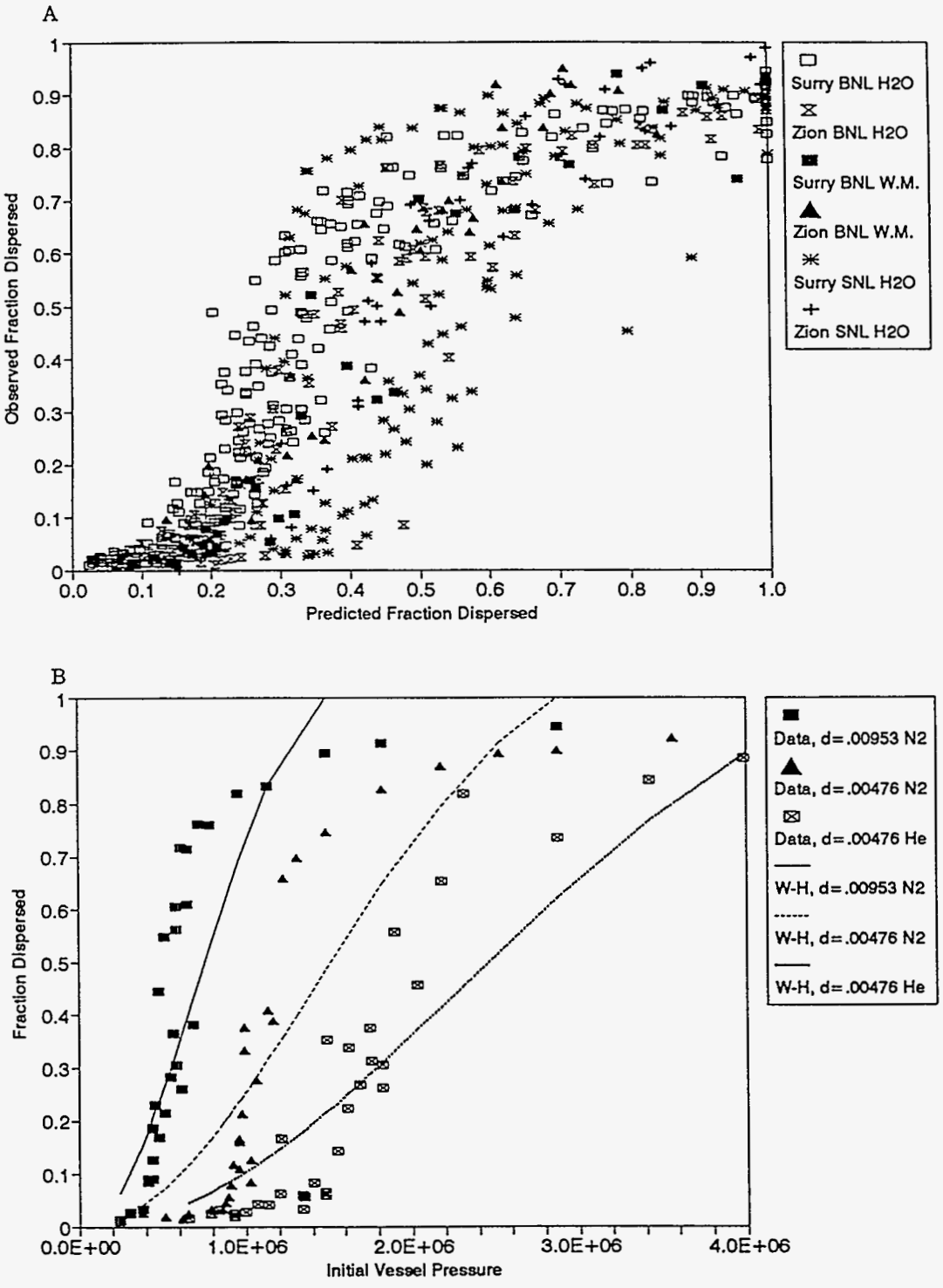

Figure 4.5-1 Modified Whalley-Hewitt correlation: (A), scatter diagram for full data set; (B) F_d vs $P_{0,v}$, data and correlation for selected BNL Surry data with water as fluid

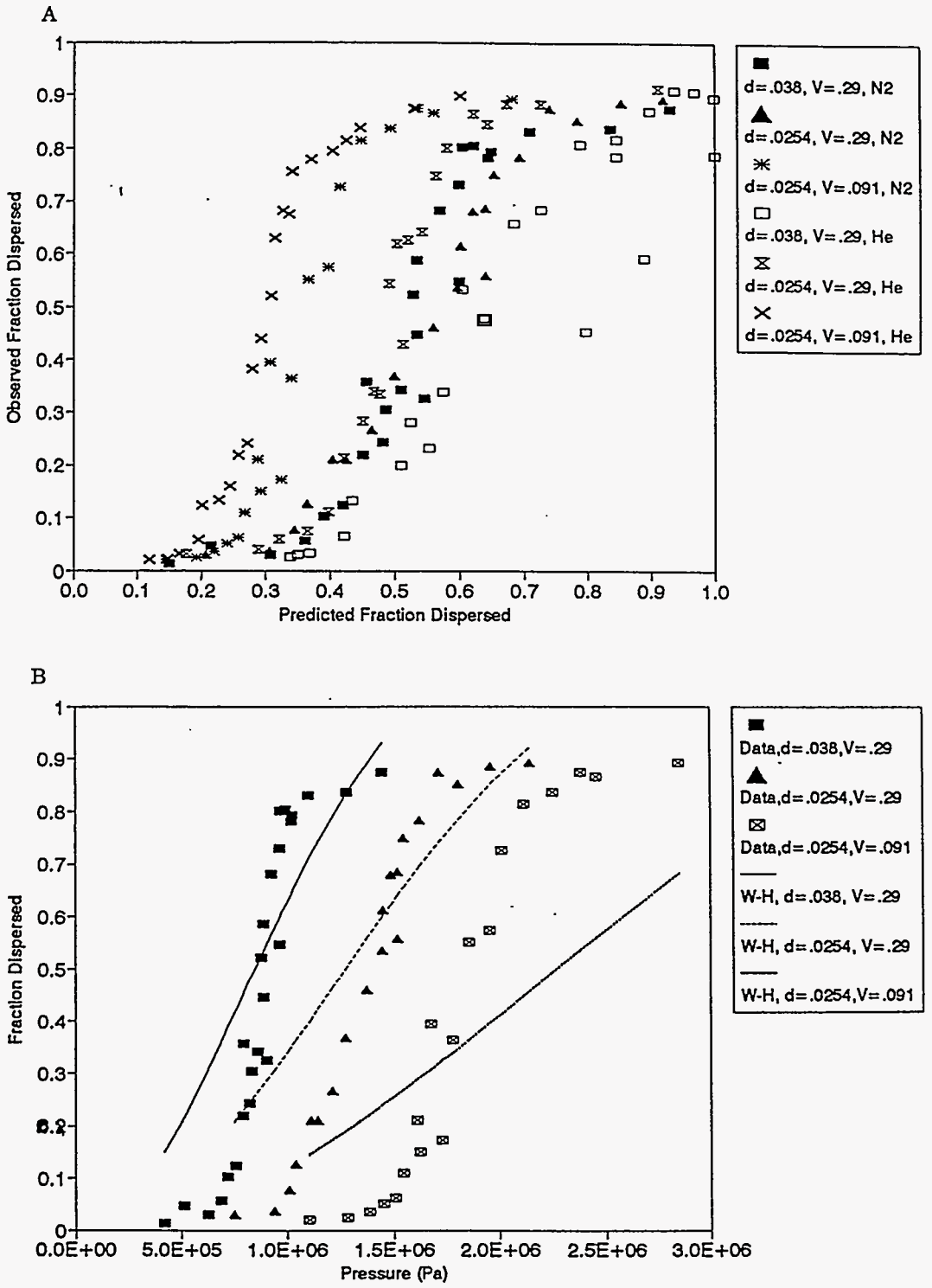

Figure 4.5-2 Modified Whalley-Hewitt correlation, SNL Surry data: (A), scatter plot; (B), F_d vs $P_{0,v}$, for data with air as driving gas

Based upon the α_s/n values of Section 3.2 and Table 3.3-1, this result may not seem entirely surprising, since Whalley-Hewitt is not predicted to have a significant scale effect. However, this line of reasoning failed in the case of the Tutu-Ginsberg correlations, since only the Surry skirt correlation and the Zion correlation are involved in the fit to the SNL data. Neither of these correlations has a significant scale effect, yet they failed to fit both the BNL and SNL data without redefining an empirical constant.

5. Discussion and Recommendations

5.1. Observations on Scalability

At the outset of the present work, major goals included using comparisons between the BNL and SNL data with equivalent cavity geometries to draw conclusions concerning the scalability of the various correlations. Unfortunately, this may be difficult to do because the experiments were designed under the assumption that geometric scaling was needed only in the cavity, and that details of the high-pressure parts of the system (other than such gross parameters as the volume, driving pressure, driving gas) would not matter. It now appears that some of these details may matter, as was discussed in connection with the Tutu-Ginsberg correlations in Section 4.2. The fact these experiments are not scaled counterparts of each other (or of NPP) outside the cavity region renders any conclusions as to scalability rather ambiguous.

This limitation is important here because it is the present view that the similarity approach to scaling is difficult to apply here, due to the lack of an adequate understanding of the dominant physics. In similarity analysis, any of a number of possible approaches are used to identify nondimensional groups governing the physical behavior, and relations are sought between these groups. When the relationship is established by means of empirical correlation, validity is assessed by showing that the nondimensional groups for the scenario of interest fall within the regime studied experimentally. When this condition is met, the (sometimes overly optimistic) presumption is that the correlation is valid, even though the individual physical (i.e., dimensioned) parameters of the scenario of interest may be far outside the range studied experimentally.

Approaches based upon similarity work well when the underlying physics is understood sufficiently well that there can be confidence that the governing nondimensional groups have been properly identified. Thus, in many problems involving turbulence in fluid flow in simple geometries, it is well established that the ratio of inertial forces to viscous forces as represented by the Reynolds Number is the dominant parameter. In simple applications, correlating with the Reynolds Number alone may prove adequate.

Unfortunately, this is not the case in the present situation. Cavity dispersal is a complex transient phenomenon involving two-phase flow in a complex three-dimensional geometry with many potential complications not considered in any of the models and correlations assessed. Hence, it is uncertain as to what dimensionless groups should be used in the correlations, and

it is even uncertain as to how a given group should be evaluated (e.g., what gas velocity should be used in a group containing v_g).

Consider, for example, the dependence of dispersed fraction upon driving pressure, which is the dominant and best characterized of the dependencies upon the various experimental parameters. In the correlations considered in detail in Section 4, this dependence arises primarily through a dependence upon $\rho_g v_g^2$. Physically, this is certainly reasonable because this quantity is equal to the momentum flux in the gas flow; it is also equal to twice the kinetic energy per unit volume of the gas.

Hence it is not surprising that dispersal data have been widely correlated with dimensionless groups containing the quantity $\rho_g v_g^2$. However, there is no consensus as to what these groups should be. Dimensionless groups which have been used include:

- Kutateladze Number, $Ku = \rho_g v_g^2/(g\rho_l\sigma)^{1/2}$;
- Euler Number, $Eu = \rho_g v_g^2/2P_c$;
- Entrainment Weber Number, $We = (\rho_g v_g^2 L/\sigma)(\Delta\rho/\rho_g)^{1/3}$ [Ish91], where L is a characteristic dimension of the cavity; and
- Dispersal Froude Number, $Fr_{disp}=\rho_g v_g^2/g\rho_d L$.

It is typical that the supporting data bases for the correlations proposed provide considerable support for the postulated dependence upon $\rho_g v_g^2$. However, there is generally much less direct experimental support of the implied dependencies upon the other parameters that must be introduced in order to obtain the nondimensional group containing $\rho_g v_g^2$. (Indeed, even all aspects of the dependence upon $\rho_g v_g^2$ are typically incompletely established experimentally; for example, the correlations' dependence upon $\rho_g v_g^2$ is generally such as to imply an inverse dependence upon the cavity pressure P_c which has not been tested.)

Of all the correlations considered in this work, the Tutu-Ginsberg correlations make by far the most sophisticated use of similarity principles and scaling methodology, and for just this reason they can be used to illustrate the difficulties inherent in attempting to deduce scaling behavior from applying similarity principles to experiments performed at just one scale. In Section 4.2, it was judged that explanations offered in Reference Tut90b for the differences between the SNL and the BNL data were inadequate, and the possibility that these differences might represent genuine scale effects with dispersal decreasing with increasing scale was therefore considered. Since the Surry skirt-only and the Zion versions of the Tutu-Ginsberg correlations predict little and no scale effect, respectively, the tendency of the correlations to overpredict dispersal in the SNL experiments (see Figures 4.2-2 and 4.2-3) would then be explained if the actual scale effect were to be negative.

Such trends would be expected if the dispersal Froude Number, Fr_{disp}, were to play an important role. A rationale for its role can be constructed by noting that Fr_{disp} is a measure of the ratio of the available kinetic energy per unit volume of gas to the energy required to disperse a unit volume of the debris. This ratio decreases with increasing scale because the available energy density is scale-invariant while the energy for dispersal increases as the distances and elevations involved increase, i.e., with increasing scale.

This concept was tested by replacing Ku (i.e., N_5) in the Tutu-Ginsberg correlation with the a multiple of the Froude Number chosen to give the same numerical value at the scale (1/42) of the BNL experiments. An exact match cannot be obtained for both water and Wood's Metal because the ratio Ku/Fr_{disp} are not quite the same for the two liquids, but the differences are rather slight. The comparison with the experimental data was then rerun, without introducing any C_d "corrections" or other adjustments when comparing with the SNL data. A scatter plot is given in Figure 5.1-1, and plots of selected individual data series are compared with the correlation in Figure 5.1-2. Performance statistics (σ_{est} values) for this case are also included in Table 4.1-1.

It is apparent from the results that there is a negligible impact upon the fit to the BNL data. Hence, one could not possibly distinguish between these two formulations on the basis of experiments performed at a single scale, at least with the two liquids used here. The differences between the response of Ku and the response of Fr_{disp} in going from water to Wood's Metal is too small to provide a test, and the predictions of dependence upon all other experimental parameters for the two formulations is exactly the same. Yet the differences in the implications for events at NPP scale are profound: the Froude version predicts that, at full scale, the driving pressure required to obtain a given degree of dispersal is three to four times as great as the required pressure predicted by the standard form. This difference is illustrated in Figure 5.1-3 in which the predictions of the two versions are compared at both 1/42 scale and for full scale using the correlation for the Surry geometry including the skirt, and with $d_h = 0.28$ m (full scale). It is seen that the full-scale curve for the Froude version is shifted far to the right, while the other three curves are virtually on top of one another because there is almost no difference between the two versions at 1/42 scale and because the standard form of this correlation predicts almost no scale dependence.

Comparing the two versions with the SNL data, it is found that the Froude version gives substantially better agreement than does the standard form without specifying a different value of K_c for the SNL data (i.e., without the "C_d correction" used in Reference Tut90b). It is only somewhat poorer than the standard version with separate K_c values specified for the SNL data. Indeed, of all the correlations considered here, the Tutu-Ginsberg correlations with Fr_{disp} replacing Ku come the closest to fitting the complete data set without making any adjustments for the SNL data. This result is obtained despite the fact that Ku in the standard form was simply replaced with Fr_{disp}, without making any other alterations. Even better results might be obtained if the entire least-squares fitting process were to be repeated using Fr_{disp}.

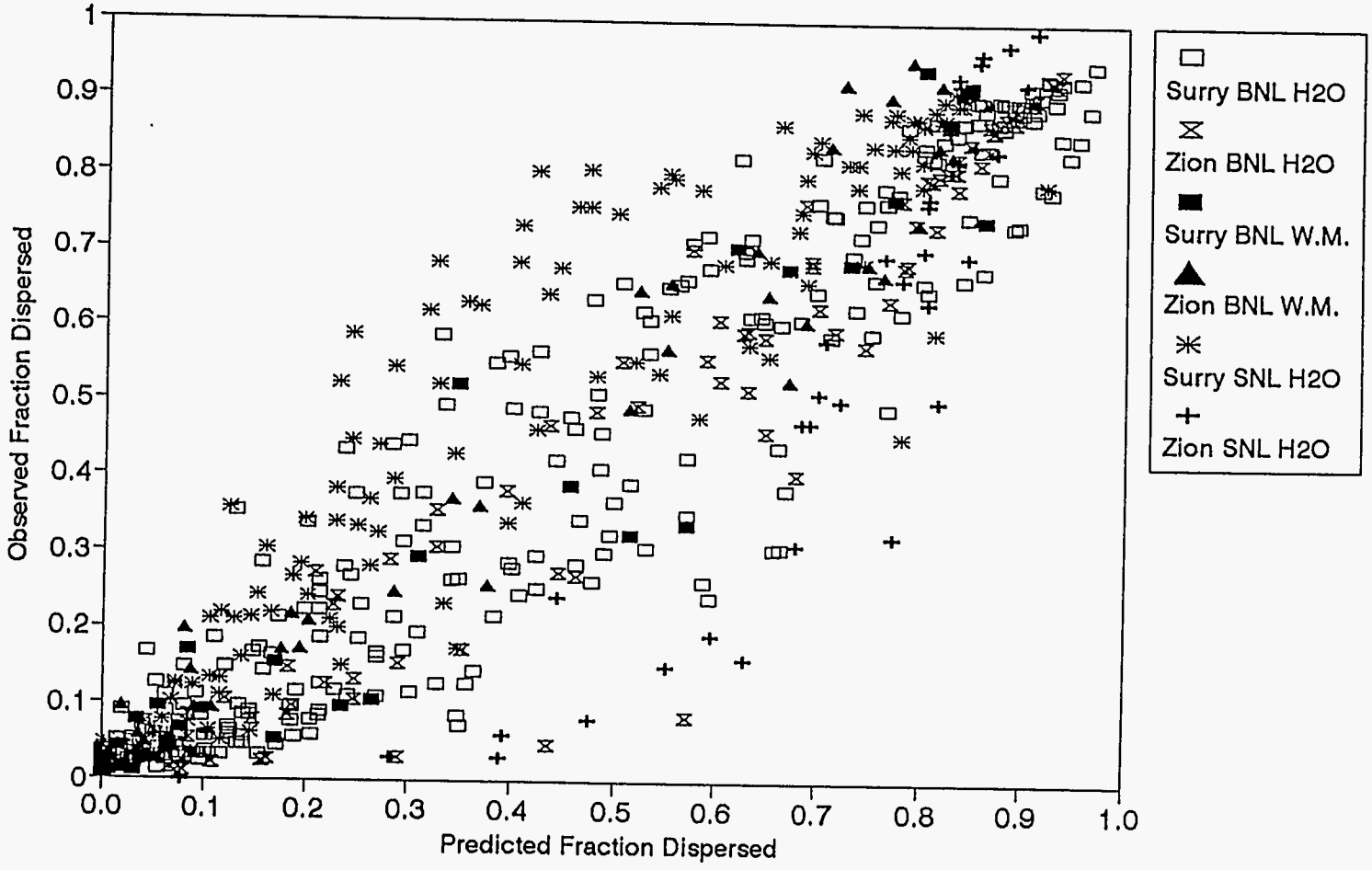

Figure 5.1-1 Scatter plot for Tutu-Ginsberg correlations with Froude scaling (Fr_{disp} replaces Ku)

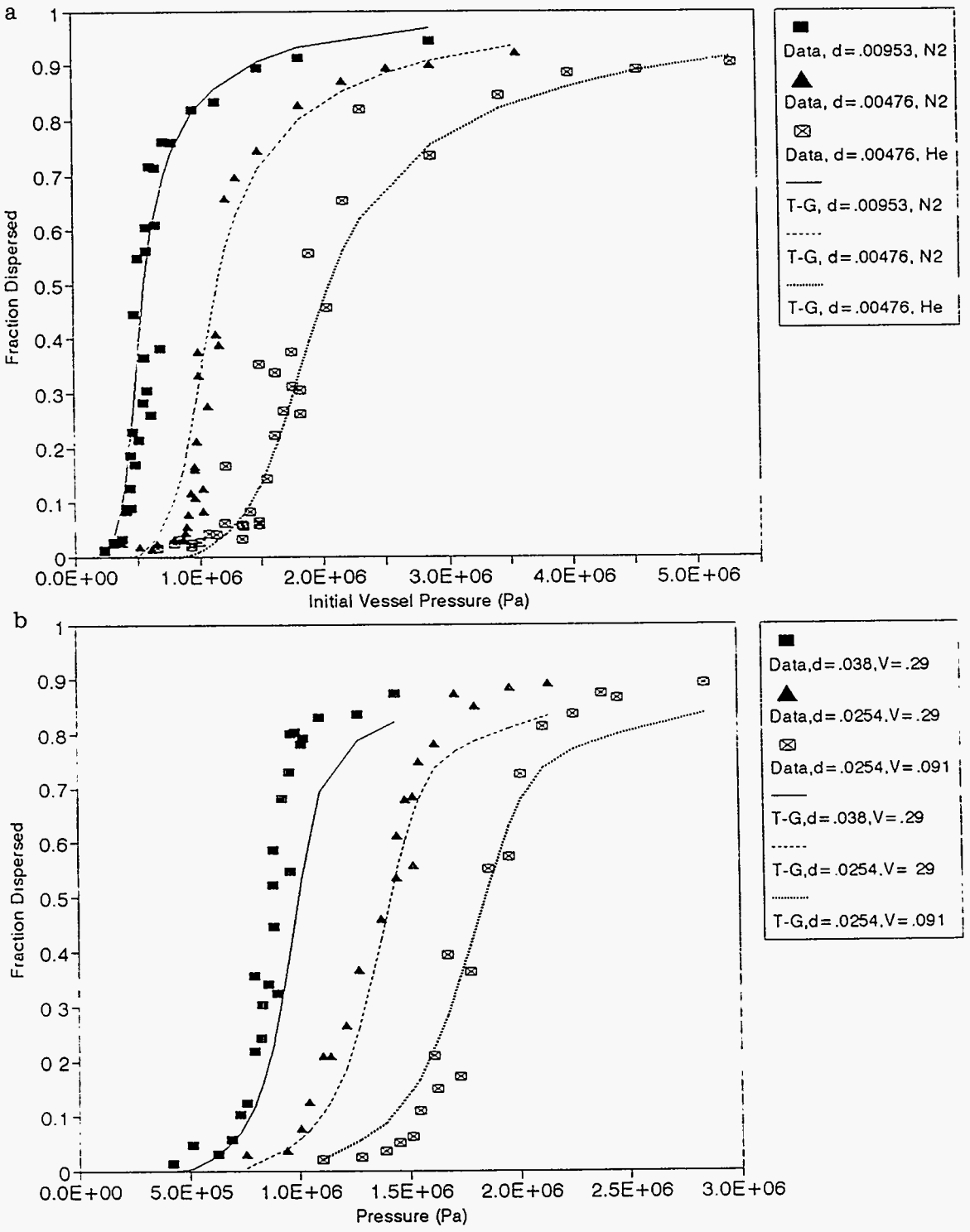

Figure 5.1-2 F_d vs $P_{0,v}$ data and Tutu-Ginsberg correlation with Froude scaling (Fr_{disp} replaces Ku), Surry geometry, water as fluid. (a), selected BNL data; (b) SNL, air as driving gas.

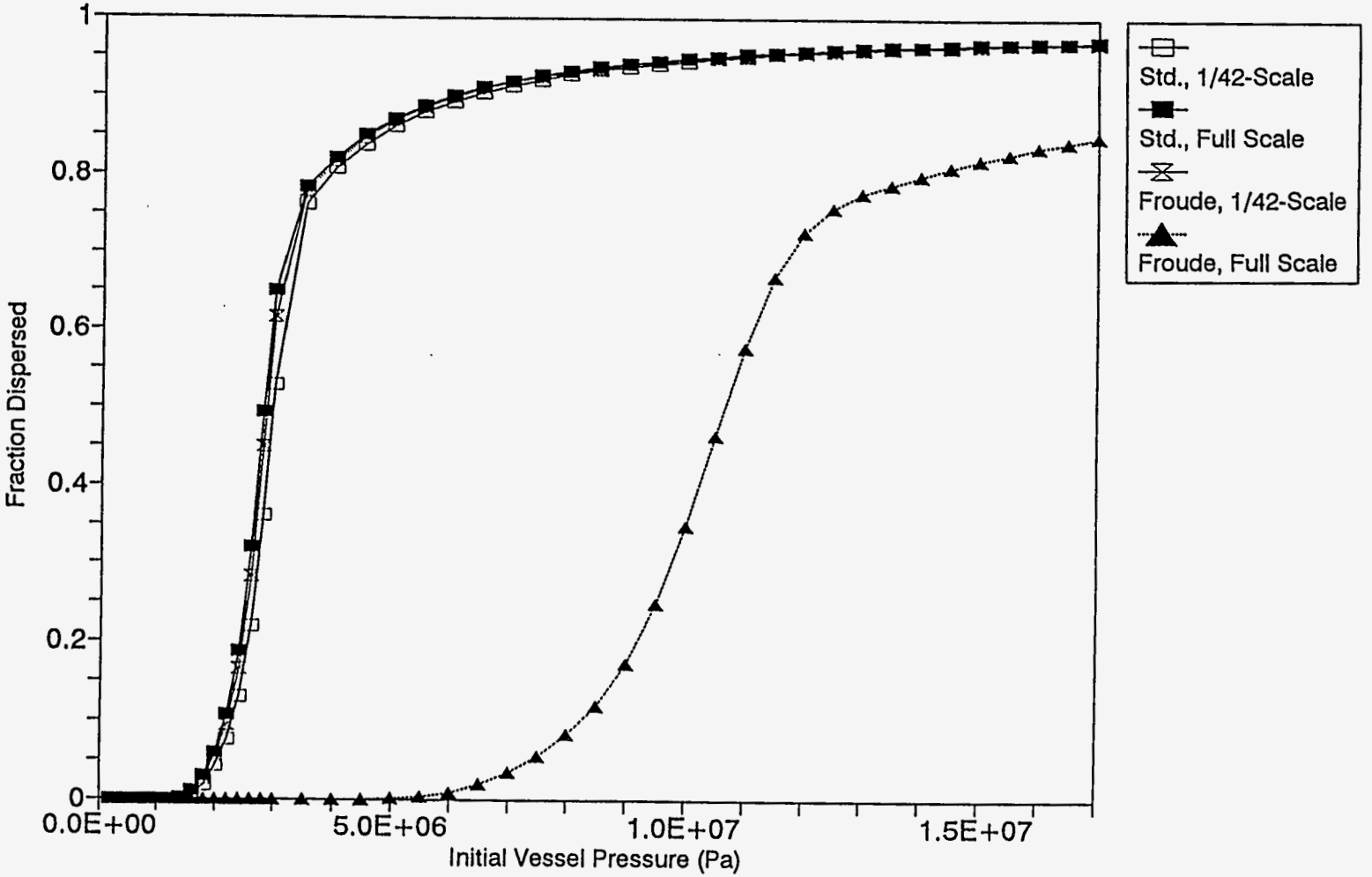

Figure 5.1-3 Effect of Froude scaling on extrapolation to NPP scale, Tutu-Ginsberg correlations for dispersal of corium from the Surry cavity (with skirt)

At an earlier stage of this work, the possibility that there might be a substantial negative scale dependence, as would be implied by identification of the Froude Number as a dominant scaling group, was seriously considered. However, the weight of the evidence is now considered to be against this possibility for the following reasons:

- The analysis of the systematics of the experimental data in Section 2.3 does not indicate that a strong scale effect exists for Surry, although the data are consistent with such an effect in Zion.

- The Whalley-Hewitt correlation, which is almost scale-invariant in the form adopted here, nonetheless does a reasonably good job of matching both the BNL and the SNL Surry data without fitting K_c separately for the latter. (The same is not true for the Zion data, however.)

- There exist other experimental data [Mac85, Chu91] on dispersal of low-temperature simulants from scaled reactor cavities which imply scale effects are either small or positive.

Despite the preceding, the rationale given above for a possible role for Fr_{disp} in scale effects still seems valid, in principle; that is, at some sufficiently large scale, dispersal must decrease with scale for the reasons given. However, if one quantitatively compares the energy available in the pressure vessel with the energy required to remove debris from the cavity, the former still greatly exceeds the latter even at NPP scale. Hence it may be that Froude scaling does not apply at any scales of practical interest.

It is tentatively concluded that scale effects are minor in the Surry geometry, while the situation is uncertain for Zion. If interpreted at face value, the data do imply a significant negative scale effect for Zion. However there may be confounding factors (e.g., differences between the SNL and BNL test configurations in the high pressure and melt delivery portions of the systems). Furthermore, qualitative comparisons of the ANL and SNL Integral Effects Tests (IET) in the Zion configuration give no obvious indications of strong scale effects. It is intended to perform a more quantitative comparison between the correlations selected for the CONTAIN code and the IET test results once the correlations are implemented in the code, and it is possible that these comparisons will provide additional insights concerning scaling.

5.2. Recommended Correlations for the CONTAIN Code

The immediate objective of the present work is to select three correlations for entrainment rates and three for dispersed fraction which will be implemented in the CONTAIN code. Before making the specific recommendations, it is well to keep in mind some desirable features for the correlations to be selected, both for each individual correlation and for the set as a whole. These features include:

Goodness of Fit to the Data. This is the obvious criterion, but not the only criterion or even the most important criterion when differences in performance are not overwhelming.

Intended Usage in CONTAIN. Current plans are to allow the user to specify the dispersed fraction or specify a correlation for dispersed fraction, and specify a correlation for entrainment rates which the code will automatically tune to reproduce the dispersed fraction prediction. (Some simplifications and approximations will be required to achieve this; these approximations need not be considered here.) Among other things, this means that, for each dispersed fraction correlation considered, there should be a rate correlation consistent with it; i.e., the rate correlation should integrate to the dispersed fraction given equivalent input. Though there can be reasons for using an "inconsistent" rate correlation, doing so should not be required.

"Conservative" Versus "Nonconservative" Behavior. Intuitively, one might suppose that it would always be conservative to choose correlations which maximize debris dispersal. However, this will often not be the case. Both experimental results and CONTAIN calculations indicate that most of the dispersed debris will be trapped in the subcompartments not too far from the cavity exit in many instances, without being transported to the large volumes of the upper dome. Under these conditions, total debris-gas interactions may be dominated by interactions with the blowdown steam, not interactions with the containment atmosphere. When this is the case, very rapid dispersal limits the amount of steam the debris can interact with and thus mitigates the DCH event, and a correlation that overpredicts entrainment rates can be nonconservative. CONTAIN calculations have long shown this effect [Wil88]; experimentally, a definitive test is difficult to come by but the experimental results are certainly consistent with this concept and generally tend to support it.

Note that this effect can introduce a (possibly unexpected) sensitivity to dispersal fractions as F_d approaches unity. Intuitively, one might suppose that it would make little difference whether a dispersed fraction correlation predicted $F_d = 0.95$ or $F_d = 0.99999....$ However, an entrainment correlation automatically adjusted to match the latter value would blast the debris out much more rapidly than it would if it were matching the former value. Hence, the dispersal fraction correlation predicting $F_d = 0.95$ would likely be more conservative, in this example.

Applicability to Large Values of $P_{0,v}/P_{50}$. The data base used in this work includes only integrated dispersal fractions; no information on dispersal rates is available. One consequence is that the assessment methodology necessarily places heavy emphasis on matching behavior in the vicinity of $P_{0,v}/P_{50} \sim 1$. At much higher values of $P_{0,v}/P_{50}$, F_d values are close to unity and show relatively little sensitivity to the parameters of interest; furthermore, the amount of liquid remaining under these conditions is likely governed by different phenomena (e.g., films adhering to structures) than those governing rates of dispersal of the main mass of liquid.

In applications to DCH events in NPP, however, it now appears that events with $P_{0,v}/P_{50} \sim 1$ are unlikely to be very threatening, at least in PWR large dry containments. Both experimental results and CONTAIN calculations indicate that debris transport to the main volumes of the upper containment is likely to be quite limited under these conditions, and the blowdown steam supply is too limited for interactions of debris with this steam to pose a severe threat. Hence, interest is expected to be focussed on driving pressures substantially greater than P_{50}. Under these conditions, the exact value of F_d is of less interest than the rate at which the debris is

dispersed, for reasons discussed above. However, it is not certain that the physical processes which govern the dependence of debris dispersal fractions upon driving pressure in the vicinity of P_{50} are necessarily those which determine how rapidly the debris is dispersed when $P_{0,v}$ is much greater than P_{50}. These possibilities should be kept in mind when selecting correlations for possible implementation in the CONTAIN code.

Diversity in Behavior. It is desirable that the correlations chosen permit a wide variety of behaviors to be simulated. One reason is the effect just discussed; i.e., the difficulty of predicting a priori just what behavior will be "conservative". Another reason is that correlation assessment will continue by comparing integrated CONTAIN calculations using the various correlations with the experimental results of the thermite tests. It is not currently clear which behaviors will prove the most realistic, and the most promising case may be missed if all the correlations selected behave similarly.

Among other things, this means that there should be variety in the scale effects predicted by the correlations. The experiments with low-temperature simulants have proven disappointingly inconclusive concerning scale effects. One possible reason is that they were not really designed to be well-scaled counterparts of one another, except for the cavity geometries themselves. In addition to being intrinsically more realistic, the recent and current IET tests with thermite have been more carefully designed to include scaled counterpart tests. These tests may permit distinguishing between the different scale responses predicted by the various correlations, but only if the correlations chosen do include a range of responses.

With these points in mind, the following recommendations are offered for correlations to be included in the CONTAIN code:

1. The Levy Correlation, for both dispersal fractions and entrainment rates. The dispersed fraction correlation is simply the integral of the rate correlation under the assumption of an exponential blowdown, so that the consistency requirement is readily satisfied. Performance is generally good (with the qualifications stated in Section 4.1) and the correlation has been widely presented and considered by the DCH technical community. Reference Lev91 presents additional comparisons between the correlation and experimental data which tend to complement those presented here.

2a. The Tutu-Ginsberg Correlations for dispersed fraction. Of all the correlations considered, these give the best fit to the BNL data. They fit the SNL Surry data well with the qualifications discussed in Section 4.2. These correlations have also been widely considered by the DCH technical community. In the context of the criteria discussed above, it is viewed as being very significant that these are probably the only correlations which will not predict that F_d converges rapidly to unity as P_v/P_{50} ratios become large.

2b. The Tutu Rate Correlation. This correlation is the natural companion correlation for the Tutu-Ginsberg dispersed fraction correlations. It performs about as well as the Levy correlation on the whole.

3. The Modified Whalley-Hewitt Correlation, for both rates and dispersed fraction, with the dispersed fraction to be obtained by numerically integrating the rate correlation. It is the only correlation which permits simultaneously matching of the BNL and SNL Surry data, which is considered to be significant even though this correlation still fails to simultaneously match the BNL and SNL Zion data (as do all the others). It is also the only rate correlation which is predicted to be scale-independent: the others all predict dispersal to increase with increasing scale, which is not supported by the experimental results. The fact that the pressure-dependence exponent (n=2) is smaller than for the others appears to be a disadvantage in the performance test of Section 4.5, but it could turn out to be favorable under some conditions.

The Ishii correlation is not recommended for inclusion at this time for several reasons. First, the full Ishii correlation that includes the film transport model is clearly ruled out on performance grounds alone. The entrainment model by itself is more nearly acceptable (though distinctly second to the modified Whalley-Hewitt), but it has other limitations. Like the other rate correlations, the Ishii entrainment model has a positive scale dependence (in fact it is the strongest of those considered) and thus does not contribute to "diversity" with respect to scale-dependence.

One important limitation was glossed over in the discussion of the model given in Section 4.4. Debris ejection from the RPV and RPV blowdown can be divided into three stages: a stage of single-phase liquid ejection prior to gas blowthrough, a two-phase stage following gas blowthrough and prior to complete debris ejection, and a single-phase gas discharge stage following ejection of all the debris. The Ishii entrainment model requires an estimate of both the liquid film flow rate (for Re_f) and the gas flow rate (for We); see Equations (19) and (20). However, the model given in Reference Ish91 for the film flow rate assumes that the vessel orifice is completely filled with liquid, and thus applies only to the first stage. The gas flow rates, however, are calculated assuming that the orifice is completely filled with gas, and therefore apply only to the third stage. Thus, contradictory assumptions are required to calculate the entrainment rate at any one time. Furthermore, this problem is not just a formality; physically, one expects the onset of gas blowdown to have a large effect upon film flow rates, and this effect is not modeled.

In the implementation for the assessment, this problem was largely shrugged off, if only out of necessity. It would be difficult to justify doing so in a CONTAIN implementation, however, especially in the case of an entrainment rate calculation that would have to embrace modeling assumptions which are logically incompatible at any one time in the entire process. Note that even in the implementation for assessment, no effort was made to numerically integrate a predicted rate over a blowdown history, as was done for the Tutu and Whalley-Hewitt correlations; instead, only rough estimates of "characteristic times" for dispersal and blowdown were made, and F_d was estimated from their ratio. It is believed that this approach was adequate to capture the dominant dependencies of the model and was useful for assessment, but it cannot be recommended for the CONTAIN code.

6. Conclusions

Candidate models and correlations describing entrainment and dispersal of core debris from reactor cavities in DCH events have been assessed against a data base of approximately 600 experiments performed at BNL and SNL in which dispersal of low-temperature corium simulants from scaled models of reactor cavities was studied. Cavity geometries considered are those of the Surry and Zion nuclear power plants and scale factors of 1/42 (at BNL) and 1/10 (at SNL) were studied for both geometries. Other parameters varied in the experiments include gas pressure driving the dispersal, identities of the driving gas and of the simulant fluid, orifice diameter in the pressure vessel, and volume of the gas pressure vessel. Correlations were assessed in terms of their ability to reproduce the observed trends in the fractions dispersed as these experimental parameters were varied.

It proved possible to systematize the data in a manner which permitted an analytical representation of the dependence of the dispersed fraction, F_d, upon the various experimental parameters. The analytical representations of the experimental trends are considered to be an important product of the present work because they permit one to make a fairly extensive assessment of many of the correlations considered without performing a direct comparison of the predicted and observed values of F_d for each data point, a process which is somewhat cumbersome. (A few correlations are sufficiently complex that this analytical approach is difficult to apply.) Using these analytical representations of the experimental trends, the candidate correlations were screened to eliminate those which would clearly be unsatisfactory. These analytical representations of the experimental trends could likewise be used to assess any additional correlations which may be proposed, if they are not excessively complex.

The correlations considered generally must be fit separately to the Surry and the Zion data in order to obtain good results, although the differences in the fitting constant, K_c, required was not large in some instances. The dependence of K_c upon cavity geometry was not surprising because it was not expected that the correlations could properly account for all the differences that would arise due to the different cavity geometries. However, it was also found that, with one partial exception, different values of K_c were also required to fit the BNL and the SNL data for the same cavity geometry. The partial exception was the modified Whalley-Hewitt correlation, which gave acceptable results for both the BNL and the SNL data for the Surry geometry with the same value of K_c; this was not true for the Zion data, however.

If the BNL-SNL differences are interpreted as scale effects, the results imply that the correlations may not adequately account for the effect of scale, which would mean that considerable caution is needed in using the correlations for analysis of DCH events in NPP. However, interpretation is complicated by the fact that the BNL and SNL experiments were scaled counterparts of one another only with respect to the cavity geometries; differences in other parts of the experimental systems may have distorted comparisons between the BNL and SNL data sets. Although some distortions have been identified, there is no conclusive evidence that they account for the differences between the BNL and the SNL data sets. If additional experiments are judged necessary to address the scaling question, it is strongly recommended

that the experimental design include proper scaling of all relevant portions of the experimental systems, not just the cavity.

For the fraction of the debris dispersed, the correlations recommended for inclusion in the CONTAIN code are the Tutu-Ginsberg correlations, the integral form of the correlation proposed by Levy and a modified form of the Whalley-Hewitt correlation. For entrainment rates, the recommended correlations are the time-dependent forms of the Levy correlation, a correlation suggested by Tutu, and the modified Whalley-Hewitt correlation. Once these correlations have been incorporated within CONTAIN, it is recommended that assessment be continued by comparing them with the results of the more realistic DCH experiments using thermitic melts.

References

Chu91. Moon-Hyun Chun at al., "A Parametric Study of the High Pressure Melt Ejection from Two Different Scale Reactor Cavity Models," Int. Comm. Heat Mass Transfer 18, pp. 619-628, 1991.

Ish91. Mamoru Ishii, "Scaling Study of Corium Dispersion in DCH," Appendix N of An Integrated Structure and Scaling Methodology for Severe Accident Technical Issue Resolution, NUREG/CR-5809 (EGG-2659), Draft Report for Comment, Idaho National Engineering Laboratory, November 1991.

Lev91. S. Levy, "Debris Dispersal from Reactor Cavity During Low Temperature Simulant Tests of Direct Containment Heating (DCH), Proc. Eighteenth Water Reactor Safety Information Meeting, NUREG/CP-0114, Vol. 2, April 1991.

Mac85. R. V. Macbeth and R. Trenberth, "Experimental Modelling of Core Debris Dispersion from the Vault Under a PWR Pressure Vessel," AEEW - R 1888 DRAFT, AEE Winfrith, UK, March 1985.

Mur89. K. K. Murata et al., "User's Manual for CONTAIN 1.1: A Computer Code for Severe Nuclear Reactor Accident Containment Analysis," NUREG/CR-5026, SAND87-2309, Sandia National Laboratories, November 1989.

Ost94. R. W. Ostensen et al., "Models and Correlations for Direct Containment Heating," Sandia National Laboratories, March 15 1991, to be published SAND94-0961.

Tut88. N. K. Tutu et al., "Debris Dispersal from Reactor Cavities During High-Pressure Melt Ejection Accident Scenarios," NUREG/CR-5146 (BNL-NUREG 52147), Brookhaven National Laboratory, July 1988.

Tut90a. N. K. Tutu et al., "Melt Dispersal Characteristics of the Watts Bar Cavity," Technical Report A-3024, 4/90, Brookhaven National Laboratory, April 1990.

Tut90b. N. K. Tutu and T. Ginsberg, "A Letter Report on the Results of Melt Dispersal Experiments with the Surry and Zion Cavity Models," Brookhaven National Laboratory, Letter Report to the U.S.NRC, Oct. 1990.

Tut91. N. K. Tutu, "An Idealized Transient Model for Melt Dispersal from Reactor Cavities During Pressurized Melt Ejection Accident Scenarios," BNL-46305 Informal Report, Brookhaven National Laboratory, June 1991.

Was91. K. E. Washington et al., "Reference Manual for the CONTAIN 1.1 Code for Containment Severe Accident Analysis," NUREG/CR-5715, SAND91-0835, Sandia National Laboratories, July 1991.

Wha78. P. B. Whalley and G. F. Hewitt, "The Correlation of Liquid Entrainment Fraction and Entrainment Rate in Annular Two-Phase Flow," AERE-R9187, HTFS RS237, AERE Harwell, England, July 1978.

Wil88. D. C. Williams and D. L. Y. Louie, "CONTAIN Analyses of Direct Containment Heating in the Surry Plant," Proceedings of the Thermal Hydraulics Division, 1988 ANS/ENS Winter Meeting, Washington, DC, October 31 - November 4 1988.

Wil92. D. C. Williams, "An Interpretation of the Results of Some Recent Direct Containment Heating (DCH) Experiments in the Surtsey Facility," Proceedings of the ANS Fifth International Topical Meeting on Nuclear Reactor Thermal Hydraulics (NURETH-5), Salt Lake City, Sept. 20-24 1992.

EXTERNAL DISTRIBUTION:

U.S. Nuclear Regulatory Commission (9)
Division of Reactor System Safety
Office of Nuclear Regulatory Research
ATTN: C. Ader, T-10K-8
E. Beckjord, 10-F-12
A. Drozd, 8-H-7
F. Eltawila, NLN-344
R. B. Foulds, NLN-344
C. G. Gingrich, NLN-344
W. Hodges, T10E-37
J. Kudrick, 8-H-7
R. Lee, T-10K-8
A. Malliakos, NLN-344
J. Monninger, OWFN 8-D
A. Notafrancesco, T-10K-8
A. Rubin, T-10K-8
L. M. Shotkin, NLN-353
T. Spies, T-10F-12

U.S. Nuclear Regulatory Commission (2)
Office of ACRS
ATTN: M. D. Houston, T-2E-26
T. Kress, T-2E-26
Washington, D.C. 20555-0001

U.S. Department of Energy (2)
Albuquerque Operations Office
Post Office Box 5400
ATTN: C. E. Garcia, Director
For: C. B. Quinn
R. L. Holton
Albuquerque, NM 87185

U.S. Department of Energy
Office of Nuclear Safety Coordination
ATTN: R. W. Barber
Washington, D.C. 20545

U.S. Department of Energy
Idaho Operations Office
850 Energy Drive
ATTN: S. W. Sorrell
Idaho Falls, ID 83401

U.S. Department of Energy
Office of Nuclear Energy
Division of IMRs and Breeders
Office of Advanced Reactor Programs
ATTN: N. Grossman, Director
Washington, D.C. 20585

U.S. Department of Energy
Scientific and Technical Information Center
Post Office Box 62
Oak Ridge, TN 37831

Argonne National Laboratory (4)
9700 South Cass Avenue
ATTN: J. Binder
C. Johnson
L. Baker, Jr.
B. Spencer

Battelle Columbus Laboratory (2)
505 King Avenue
ATTN: R. Denning
J. Gieseke
Columbus, OH 43201

Battelle Pacific Northwest Laboratory
Post Office Box 999
ATTN: M. Freshley
Richland, WA 99352

Brookhaven National Laboratory (4)
Building 130
32 Lewis
ATTN: R. Bari
T. Pratt
N. Tutu
H. Todosow
Upton, NY 11973

Ebasco Services Incorporated
Applied Physics Department
Two World Trade Center
Attn: J. J. Shin
New York, NY 10048

EG&G Idaho (2)
Post Office Box 1625/MS2508
ATTN: D. L. Knudson
C. Allison
Idaho Falls, ID 83415

Electric Power Research Institute (2)
3412 Hillview Avenue
ATTN: A. Michaels
M. Murillo
Palo Alto, CA 94303

Energy Research, Inc. (2)
Post Office Box 2034
ATTN: H. Esmali
M. Khatib-Rahbar
Rockville, MD 20852

Fauske & Associates, Inc. (5)
16W070 West 83rd Street
ATTN: M. Epstein
H. K. Fauske
R. Hammersley
R. Henry
M. G. Plys
Burr Ridge, IL 60952

General Electric Company (2)
Advanced Boiling Water Reactor Program
Nuclear Energy Business Operations
175 Curtner Avenue
ATTN: W. Holtzclaw
F. J. Moody
San Jose, CA 95125

Knolls Atomic Power Laboratory
Post Office Box 1072
ATTN: J. Connine, D2-221
K. Wells
J. McMullan
Schenectady, NY 12301

Lawrence Livermore National Laboratory
Post Office Box 808, MS-L390
Livermore, CA 94550

Levy & Associates
3880 South Bascom Avenue, Suite #112
ATTN: S. Levy
San Jose, CA 95124

Los Alamos National Laboratory (3)
Post Office Box 1663
ATTN: B. Boyack, K-551
D. G. Rose, C-925
M. Stevenson
Los Alamos, NM 87545

Massachusetts Institute of Technology (3)
ATTN: M. Golay
M. S. Kazimi (Bldg. 24-219)
N. E. Todreas (Bldg . 24-215)
Cambridge, MA 02139

Oak Ridge National Laboratory (5)
Post Office Box 2009
ATTN: S. R. Greene
S. A. Hodge
C. Hyman
D. B. Simpson
K. Smith, MS-8057
Oak Ridge, TN 37831-8057

Pennsylvania Power & Light Company
Two North Ninth Street
ATTN: T. S. Yih
Allentown, PA 18101

Purdue University
Heat Transfer Laboratory
School of Mechanical Engineering
ATTN: R. Viskanta
West Lafayette, IN 47907-1209

Purdue University
School of Nuclear Engineering
ATTN: M. Ishii
West Lafayette, IN 47907

Rennselaer Polytechnic Institute
Department of Nuclear Engineering &
Engineering Sciences
Tibbits Avenue, NES Building
ATTN: M. Podowski

Science Applications International Corp.
2109 Air Park Road, S.E.
ATTN: D. R. Bradley
Albuquerque, NM 87106

Stone & Webster Engineering (2)
Post Office B ox 2325
ATTN: J. Metcalf, MS245-2
E. Warman
Boston, MA 02107

Texas A&M University
Department of Nuclear Engineering
ATTN: Y. A. Hassan
College Station, TX 77843

Jack Tills & Associates
Post Office Box 549
ATTN: J. Tills
Sandia Park NM 87047

University of California
Department of Chemical and
Nuclear Engineering
ATTN: T. Theofanous
Santa Barbara, CA 93106

University of California at Los Angeles
Nuclear Energy Laboratory
405 Hilgaard Avenue
ATTN: I. Catton
Los Angeles, CA 90024

University of Evansville
Mechanical & Civil Engineering Dept.
1800 Lincoln Avenue
ATTN: Dr. Douglas W. Stamps
Evansville, Indiana 47722

University of Maryland
Department of Nuclear Engineering
ATTN: Professor K. Almenas
College Park, MD 20742

University of Missouri
Nuclear Engineering Department
ATTN: S. K. Loyalka
Columbia, MO 65211

University of New Mexico
Department of Chemistry and
Nuclear Engineering
ATTN: F. E. Haskin
Albuquerque, NM 87131

University of Wisconsin (2)
Department of Nuclear Engineering
153 Engineering Research Building
1500 Johnson Drive
ATTN: M. L. Corradini
G. A. Moses
Madison, WI 53706

Westinghouse Bettis Atomic Laboratory
Post Office Box 79
ATTN: J. W. Wolfe, ZAP 34N
West Mifflin, PA 15122

Westinghouse Savannah River (3)
Woodside Executive Park
1359 Silver Bluff Road
ATTN: K. O'Kula
W. Peebles
D. Sharp
Aiken, SC 29808

FOREIGN DISTRIBUTION:

IAEA
Division of Nuclear Reactor Safety
Wagranerstrasse 5
Post Office Box 100
A/1400 Vienna
ATTN: M. Jankowski
AUSTRIA

Belgonucleaire SA (2)
Rue du Champ de Mars 25
ATTN: H. Bairiot
J. Basselier
B-1050 Brussels
BELGIUM

Director, Research, Science Education CEC (2)
Rue de la Loi 2000
1049 Brussels
ATTN: W. Balz
B. Tolley
BELGIUM

Commission on the Use of Atomic Energy for
Peaceful Purposes - 69 Shipchenski
Prokhod Boulevard, 1574, Sofia
ATTN: Y. Yanev
BULGARIA

AECL CANDU
Sheridan Park Research Community
2251 Speakman Avenue
ATTN: V. J. Nath
Mississauga, Ontario L5K 1B2
CANADA

AECL Research (5)
Chalk River Research Laboratories
ATTN: B. H. McDonald
D. S. Cox
L. N. Carlucci
L. W. Dickson
R. S. Dickson
Chalk River, Ontario KOJ 1JO
CANADA

AECL Research (2)
Whitshell Laboratories
ATTN: S. R. Mulpuru
L. A. Simpson
Pinawa, Manitoba R0E 1L0
CANADA

Ontario Hydro (2)
700 University Avenue
ATTN: O. Akalin
F. C. Iglesias
Toronto, Ontario M5G 1X6
CANADA

Nuclear Research Institute (4)
250 68 Rez
ATTN: J. Kujal
F. Pazdera
CZECH REPUBLIC

State Office for Nuclear Safety
Slezska 9
ATTN: J. Stuller
120 00 Prague 2
CZECH REPUBLIC

RISO National Laboratory
Department of Energy Technology
Post Office Box 49
DK-4000 Roskilde
ATTN: P. B. Fynbo
DENMARK

Finnish Center Radiation & Nuclear Safety
Department of Nuclear Safety
Post Office Box 268
SF-00101 Helsinki
ATTN: J. V. Sandberg
FINLAND

Tech Research Centre of Finland (VTT) (2)
Nuclear Engineering Laboratory (YDI)
PL 169
00181 Helsinki
ATTN: L. Mattila
A. Silde
FINLAND

Cadarache Center for Nuclear Studies (7)
F-13108 Sait Paul-Lez-Durance Cedex
ATTN: B. Andre
P. Dumaz
M. Schwartz
F. Serre
A. Meyer-Heine
G. Hache
A. Tattegrain
FRANCE

Inst. de Protection et de Surete Nucleaire (6)
CEN/FAR-B.P. No. 6
F-92265, Fontenay-aux-Roses
ATTN: J. Bardelay
J. Duco
M. Gomolinski
M. LeComte
M. LiVolant
R. Pochard
Cedex
FRANCE

Battelle Institute e. V. (2)
Am Romerhof 35
D-6000 Frankfurt am Main 90
ATTN: D. T. Kanzleiter
L. Wolf
GERMANY

Gesellschaft fur Reaktorsicherheit (4)
Forschungsgelande
8046 Garching
ATTN: K. Trambauer
G. Weber
M. Sonnenkalb
M. Finnhaber
GERMANY

Gesellschaft fur Reaktorsicherheit mbH
Postfach 101650
Glockengasse 2
D-5000 Koln 1
ATTN: J. Langhans
GERMANY

Ruhr-University of Bochum
Department of Nuclear & New Energy System
ATTN: U. Brockmeier
GERMANY

University of Stuttgart (2)
IKE
Pfaffenwaldring 31
ATTN: U. Bieder
N. Kourti
D-7000 Stuttgart 80
GERMANY

Technische Universitat Munchen
Forschungsgelande
8046 Garching
ATTN: Professor Dr. I. H. Karwat
GERMANY

Kernforschungszentrum Karlsruhe (4)
Post Office Box 3640
ATTN: S. Hagen
P. Hoffman
B. Kuczera
V. Scholtyssek
75 Karlsruhe
GERMANY

Research Centre Rossendorf, Inc.
Forschungszentrum Rossendorf
Postfach 19
ATTN: Dr. H. Funke
DO-8051 Dresden
GERMANY

Institute for Electric Power Research (2)
Division of Nuclear & Power Engineering
Post Office Box 233
ATTN: Z. Techy
L. Voross
H-1368 Budapest
HUNGARY

Hungarian Atomic Energy Commission
H-1374 Budapest, Post Office Box 565
ATTN: S. Elo
Budapest
HUNGARY

CEC Joint Research Center (3)
I-21020 Ispra (Varese)
ATTN: P. Fasoli-Stella
A. Markovina
R. Ricchena
J. Capitao
Y. Drossinos
A. V. Jones
I. Shepherd
ITALY

Nucleare e della Protezione Sanitaria (3)
(DISP) (ENEA)
Ente Nazionale Energie Alternative
Viale Regina Margherita, 125
Cassella Postale M. 2358
ATTN: G. Petrangeli
M. Pezzilli
G. Saponaro
1-00144 Roma A.D.
ITALY

ENEL-CRTN
Via Monfalcone 15
ATTN: E. Borioli
20132 Milan
ITALY

Toshiba Corporation
Nuclear Safety Engineering Section
8, Shinsugita-Cho, Isogo-Ku
Yokohama 235
ATTN: M. Naito
JAPAN

Power Reactor Nuclear Fuel Development
Corporation (PNC)
9-13, 1-Chome
ATTN: H. Hiroi
Minato-Ku, Tokyo
JAPAN

Nuclear Power Engineering Center
Fujitakanko Building
17-1, 3-Chome, Toranomon, Minato-Ku
ATTN: Kenji Takumi
Tokyo, 105
JAPAN

Japan Atomic Energy Research Institute (4)
Tokai-mura
Naku-gun
ATTN: K. Soda
J. Sugimoto
Y. Maruyama
N. Yamano
Ibaraki-ken, 319-11
JAPAN

POSTECH
Department of Mechanical Engineering
Post Office Box 125
Kyungbuk 790-600
ATTN: M. H. Kim
KOREA

Korea Atomic Energy Research Institute
150 Dukjin-dong, Yoosung-gu
ATTN: Hee-Dong Kim
Taejon 305-353
KOREA

Korea Institute of Nuclear Safety
Safety Review and Assessment Division
Post Office Box 16, Daeduk-Danji
ATTN: J. J. Lee
Taejon, 305-353
KOREA

VATESI (2)
Gediminis Prospect 36
ATTN: A. Kaliaatka
P. Vaisnys
Vilnius
LITHUANIA

Com. Nacional de Seguridad Nucl. Salvag
Colonia Narvarte Delegation B. Juarez
ATTN: M. M. Vaillard
Dr. Abrtshsm #779
C.P. 03020
MEXICO

Atomic Energy Council (2)
67, Lane 144 Keelung Road
Section 4, Taipei, Taiwan
ATTN: Yi-Bin Chen
You-Shin Yang
S. J. Shieh
REPUBLIC OF CHINA

Institute of Nuclear Energy Research
Post Office Box 3
Lungtan, Taiwan 325
ATTN: S. I. Chang
REPUBLIC OF CHINA

Nuclear Safety Institute (4)
Russian Research Center KI
1 Kurchatov Square
ATTN: V. Asmolov
E. G. Basanski
V. Demin
S. B. Dorofeev
123182 Moscow
RUSSIA

Russian Academy of Sciences (3)
Nuclear Safety Institute
52, B. Tulskaya
ATTN: L. Bolshov
V. Chudanov
V. F. Strizhov
113191 Moscow
RUSSIA

Nuclear Regulatory Authority, Slovak Republic
Post Office Box 24
820 07 Bratislava 27
ATTN: J. Misak
SLOVAK REPUBLIC

Jozef Stefan Institute
Jamova 39
ATTN: B. Mavko
61111 Ljubljana
SLOVENIA

Catedra de Tecnologia Nuclear
E.T.S. Ingenieros Industriales
Universidad Politecnica
Jose Gutierrez Abascal, 2
28006-Madrid
ATTN: L. Herranz
SPAIN

Consejo de Seguridad Nuckan
SOR Angela de la Cruz No. 3
ATTN: J. Bagues
28056 Madrid
SPAIN

Consejo de Seguridad Nuclear (2)
Justo Dorado 11
ATTN: J. E. deCarlos
J. A. Martinez
28040 Madrid
SPAIN

E.T.S. Ingenieros Industriales
Jost Gutierrez Abascal, 2
ATTN: A. Alonso
28006 Madrid
SPAIN

Royal Institute of Technology
Nuclear Power Safety
S-100 44 Stockholm
ATTN: B. R. Sehgal
K. M. Becker
SWEDEN

Swedish Nuclear Power Inspectorate (2)
Post Office Box 27106
S-102 52 Stockholm
ATTN: W. Frid
L. Hammer
SWEDEN

Studsvik Nuclear
S-611 82, Nykoping
ATTN: K. O. Johansson
SWEDEN

Swiss Federal Nuclear Safety Inspectorate (2)
CH-5303 Wurenlingen
ATTN: S. Chakraborty
D. Sopheil
U. Schmocker
SWITZERLAND

Paul Scherrer Institute
ATTN: P. Hosemann
CH-5232 Villigen, PSI
SWITZERLAND

Institute of Nuclear Energy Research
Post Office Box 3
ATTN: Sen-I Chang
Lung-Tan
TAIWAN 325

Netherlands Energy Research
Foundation (ECN) (3)
Postbus 1
1755 ZG Petten
ATTN: K. J. Brinkman
P. M. Stoop
E. J. Velema
A. A. Booij
E. Cordfunke
M. E. Huntelaar
R. Konings
S. Spoelstra
P. Stoop
THE NETHERLANDS

N. V. Kema
Post Office Box 9035
ATTN: P. Kloeg
6800 ET Arnhem
THE NETHERLANDS

AEA Culham Laboratory (2)
Abingdon
Oxfordshire, OX14-3DB
ATTN: B. D. Turland
D. F. Fletcher
UNITED KINGDOM

AEA Winfrith (6)
Dorchester
Dorset DT2 8DH
ATTN: T. Butland
P. Ellicott
S. Kinnersley
P. N. Smith
D. W. Sweet
D. Williams 210/A32
B. Bowsher
T. Haste
S. Kinnersly
A. Mason
J. Lillington
R. O'Mahoney
UNITED KINGDOM

CEGB National Power
Barnett Way
Barnwood, Gloucestershire GL4 7RS
ATTN: S. J. Board
UNITED KINGDOM

Nuclear Electric (3)
Berkeley Nuclear Laboratory, Berkeley
ATTN: C. Chapman
J. Eccles
J. Gwyther
Gloucestershire GL 13 9PB
UNITED KINGDOM

CEGB, Booths Hall
Chelford Road, Knutsford
Cheshire WA16 8QG
ATTN: N. E. Buttery
UNITED KINGDOM

AERE Harwell (4)
Didcot
ATTN: R. G. J. Ball
N. E. Beatham
M. A. Mignanelli
A. L. Nichols
Oxfordshire OX11 ORA
UNITED KINGDOM

UKAEA, Risely Nuclear Laboratories (4)
Risley, Warrington
ATTN: A. T. D. Butland
I. H. Dunbar
G. F. Holford
C. D. Wheatley
Cheshire WA3-4NE
UNITED KINGDOM

INTERNAL DISTRIBUTION:

MS0100	Document Processing (7613-2) for DOE/OSTI (2)
MS0619	Print Media (12615)
MS0736	N. R. Ortiz (6400)
MS0739	K. D. Bergeron (6421)
MS0739	N. E. Bixler (6421)
MS0739	R. K. Cole, Jr. (6421)
MS0739	A. A. Elsbernd (6421)
MS0739	C. M. Erickson (6421)
MS0739	R. G. Gido (6421)
MS0739	R. O. Griffith (6421)
MS0739	S. W. Hong
MS0739	K. K. Murata (6421)
MS0739	R. C. Schmidt (6421)
MS0739	E. L. Tadios (6421)
MS0739	D. C. Williams (6421) (5 cys)
MS0742	J. E. Kelly (6414)
MS0744	D. A. Powers (6404)
MS0747	A. L. Camp (6412)
MS0747	S. E. Dingman (6412)
MS0748	F. T. Harper (6413)
MS0899	Tech Library (13414) (5 cys)
MS1137	M. D. Allen (6402)
MS1137	M. M. Pilch (6402)
MS1139	K. O. Reil (6423)
MS1139	T. K. Blanchat (6423)
MS1139	R. O. Gauntt (6423)
MS9018	Central Technical Files (8523-2)